Hybrid Beamforming Design for mmWave-Enabled Massie MIMO Systems

Guofeng Xu

U5491523

Supervised by Dr. Nan Yang

October 2018

A thesis submitted in part fulfilment of the degree of

Bachelor of Engineering (Research & Development) (Honors)

The Department of Engineering

Australian National University

Abstract

Massive (multiple-input multiple output) MIMO technology is emerged as one of the most promising technologies to deal with the increasing demand of data transmission in wireless communication networks. Traditional MIMO systems employs digital beamforming where each antenna is directly connected to a radio frequency (RF) chain. However, with the scale of antenna numbers in massive MIMO systems, hybrid beamforming technique is not a suitable choice due to its huge cost and power consumption. Thanks to the low cost and power consumption of phase shifters, hybrid beamforming has attracted a lot of interests as a cost effective approach to benefit the advantages of massive MIMO. It is now considered as an enabling technology to achieve a balance between analog beamforming and digital beamforming. However, the design of optimal hybrid beamformer in mmWave systems shows its challenge and complexity due to the non-convex nature of the problem. Therefore, this thesis will present three main strategies to relax this nonconvex problem such that a suboptimal solution can be found. The result of achievable rates for different hybrid beamforming designs in simulation illustrate a significant performance advantage over analog beamforming and a near-optimal performance compared with fully-digital beamforming.

Key words: Massive MIMO, mmWave, hybrid beamforming, phase shifter, non-convex

Acknowledgements

I would like to thank all the people who helped me for this project during my honors year. Especially, I would like to express my deepest gratitude for all the guidance and assistance provided from my supervisor Dr. Nan Yang. His technical help, patience and encouragement throughout this work are really great value for this project and for the rest career of my life. I also would like to thank Mr. Noman Akaba and Yuxin Liu for their personal suggestions and feedbacks for me. Lastly, the support and encourage from my family and friends are greatly appreciated during this journey.

Notations

In this thesis, the following notations are used: $\boldsymbol{A}$ is a matrix; $a$is a scalar; $\boldsymbol{a}$ is a vector; $\boldsymbol{A}^{(i)}$ is the i^{th} column of $\boldsymbol{A}$; $(*)^T$ and $(*)^H$ are the transpose and Hermitian (conjugate) transpose; $\mathrm{tr}(\boldsymbol{A})$ and $\|\boldsymbol{A}\|_F$ are trace and Fresenius form of $\boldsymbol{A}$; $|\boldsymbol{A}|$ and $(\boldsymbol{A})^{-1}$are the determinant and inverse of $\boldsymbol{A}$. $\|\boldsymbol{a}\|_p$ is the p-norm of $\boldsymbol{a}$; $\mathrm{diag}(\boldsymbol{A})$ is the diagonal elements of $\boldsymbol{A}$; $[\boldsymbol{A}|\boldsymbol{B}]$ is the form of vector/matrix concatenation in row; $\boldsymbol{I}_N$ is the $N \times N$ identity matrix; $\boldsymbol{A}_{MN}$ is the $M \times N$ dimensional matrix; $\mathcal{CN}(\boldsymbol{a}, \boldsymbol{A})$ is the complex Gaussian vector with mean $\boldsymbol{a}$ and covariance matrix $\boldsymbol{A}$; $\mathbb{E}[*]$ is the expectation; $\mathcal{R}\{*\}$ is the real part of a variable.

Table of Contents

List of Figures

Chapter 1

1. Introduction

The desire for higher data rates and reliability for the next generation of wireless communications has led many researchers and engineers in telecommunication industry towards development of new technologies [1]. One of the most promising candidates for future cellular communications is massive multiple-input multiple-output (MIMO) systems. Massive MIMO shows its various advantages over the current MIMO system by providing a much larger multiplexing and diversity gains. Millimeter wave (mmWave) communications has also emerged as one of the foreseen technologies for the fifth generation (5G) of cellular commination systems. The broad spectral carrier frequencies ranging from 30GHz to 300GHz is much larger than our current fourth generation (4G) of wireless communications, leading to a higher data rates [2]. Moreover, due to the short wavelength of mmWave, packing a large number of antenna elements in a sizable array is possible [3]. The large antenna arrays can then provide high directivity with the help of massive MIMO.

Hence, this project aims to study the fundamental characteristics of massive MIMO and mmWave and apply these two emerging technologies to design and analyze mmWave enabled massive MIMO systems. Especially, different hybrid beamforming design algorithms have been investigated and implemented. Simulation results using MATLAB are presented for system performance analysis.

1.1. Motivation and Objective

The motivation of this project is to raise the efficiency of cellular communication to keep up with the increasing demand of data in future networks. Three main factors, cell density, available spectrum and spectral efficiency, are the key parameters to realize higher cellular communication efficiency [4]. Thus, to increase the network throughput of an area, academia and industry are more concerned about exploring more available spectrum and higher spectral efficiency as it is quite expensive to deploy more base stations for higher cell density. The exploration of broader spectrum refers to the application of mmWave as the sub-6 GHz frequency bands or cellular communications are becoming more and more saturated [1]. The pursuit of higher spectral efficiency mainly relies on the upgrade of base station and more advanced signal processing techniques [5]. In other words, if we can upgrade our current based station with large antenna arrays, a much higher spectral efficiency will be expected to achieve in future networks. Thus, the aim of this project is mainly to use mmWave in massive MIMO systems for hybrid beamforming design for the next generation of wireless communication networks.

The main objectives (contributions) of this project involve:

1) Study and understand the fundamental knowledge of massive MIMO and mmWave required for hybrid beamforming design.
2) Investigate and explore different beamforming algorithms and designs.
3) Implement and simulate different beamforming algorithms in MATLAB.
4) Analyze and evaluate system performance for each system models.

1.2. Overview of the Thesis

This thesis is organized as following: Chapter 2 will discuss the background of massive MIMO and mmWave. The literature of different beamforming techniques will also be presented. Chapter 3 will discuss the spatially sparse precoding design in mmWave massive MIMO systems for single user. In Chapter 4, a two-stage multi user hybrid precoding algorithm will be presented and discussed. The performance of hybrid minimum mean square error (MMSE) beamforming design for mmWave multiuser systems will be evaluated and analyzed. Finally, the conclusion and future works will be shown in chapter 6.

Chapter 2

2. Background and Literature Review

The fifth generation network is expected to support a significantly large amount of mobile data traffic and a huge number of wireless connections with an even better cost, energy-efficiency and quality of service [6]. The capacity of a single-user communication system relies on the system bandwidth and signal to noise ratio (SNR). Specifically, it can be defined by Shannon capacity, which is the maximum data rate for which information that can be transmitted and received reliably over a communication channel. The Shannon limit is given by [7]

$$C = Blog_2\left(1 + \frac{P_R}{\sigma_n B}\right) > R \tag{2.1}$$

C denotes the channel capacity, B denotes the bandwidth, P_R denotes the received signal power, σ_n denotes power spectral density of noise, and R denotes the actual achievable rate. Particularly, $\frac{P_R}{\sigma_n B}$ can also be considered as a single parameter – SNR. Transmitting a high power signal over a large bandwidth will lead to a very high data rate. However, it is usually unpractical due to the limited bandwidth and high inter-cell and intra cell interference. Thus, to address these issues, the study of mmWave and multiple-input multiple-output (MIMO) has attracted a lot of interests for both academia and industry over the last decade. Therefore, some fundamental characteristics of these two emerging techniques and their related technology – beamforming will be mainly

presented in this section. In addition, several existing beamforming designs will be mentioned and discussed as well.

2.1. Fundamentals of Massive MIMO Systems

The massive MIMO term was firstly introduce by Tomas Marzetta in 2010 in [8]. It is an extension of MIMO and is typically referred as a large number of antennas being used at transmitter and receiver to provide higher throughput and spectral efficiency [1]. Since it is more practical to group more antennas at the base station rather than mobile station, massive MIMO is often referred to a scenario that the number of antennas at the base station is much larger than the number of user equipment. Practically, massive does not mean a massive scale on size but implies a massive number of antennas being packed on large antenna arrays at the base station.

Figure 1: Practical antenna installments in base station, 3 sectors, 8 antenna LTE-A [5]

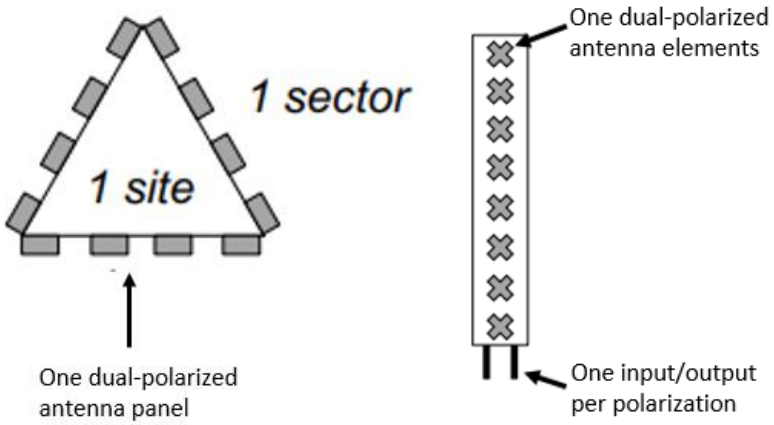

(a) Side view (b) Top view

Figure 2: Inside display of one dual-polarized antenna panel [5]

Figure 1 illustrates an 8 antenna LTE advanced base-station with three sectors and in each sector, there are four vertical panels and each of them has two polarizations. If we look inside the panel as shown in Figure 2 (b), there are eight antenna elements with dual polarizations. Therefore, with a simple calculation, there are 192 antennas in total for the base station shown in Figure 1. This means we can group around 200 antennas on the base station side of the same size of our current 4G system. With the same base station size as before, more number of connectors for input and output signals can realize a much higher spectral efficiency. There are already existing some massive MIMO testbed research which can refer in [5, 9, 10].

The purpose of this massive MIMO is to scale up with the benefits of conventional MIMO systems such that a much higher spectral efficiency can be achieved [11]. Fortunately, with the study of massive MIMO, people have found that small scale fading and interference vanishes thanks to the asymptotic orthogonality principle of massive MIMO. It can be clearly illustrated as follows.

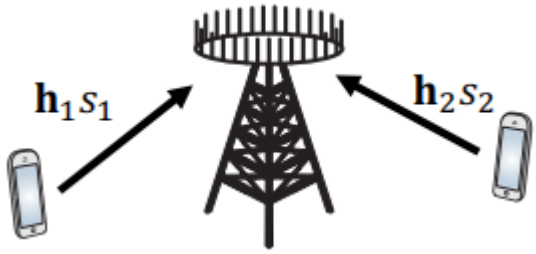

Figure 3: An example of demonstrating asymptotic orthogonality principle of massive MIMO [5]

As an example, Figure 3 shows an uplink process of two mobile users sending signals s_k to a base station. The channel is selected as i.i.d. Rayleigh fading channel for ease of formulating and demonstrating in this example. Therefore, we define $\boldsymbol{h}_k = [\boldsymbol{h}_{k1} \dots \boldsymbol{h}_{kM}]^T \sim \mathcal{CN}(0, \boldsymbol{I}_M)$, where M stands for the number of antennas. The noise can be defined as $\boldsymbol{n} \sim \mathcal{CN}(0, \boldsymbol{I}_M)$. Thus, the received signal y can be expressed as $\boldsymbol{y} = \boldsymbol{h}_1 s_1 + \boldsymbol{h}_2 s_2 + \boldsymbol{n}$. The base station now would like to separate the signals by combing. In this case, we use maximum ratio filter $\boldsymbol{v}_1 = \frac{1}{M}\boldsymbol{h}_1$ designed for user one. It takes the channel of user one and normalizes it with a number of antennas. After that, the processed receive signal

$$\tilde{\boldsymbol{y}}_1 = \boldsymbol{v}_1^H \boldsymbol{y} = \boldsymbol{v}_1^H \boldsymbol{h}_1 s_1 + \boldsymbol{v}_2^H \boldsymbol{h}_2 s_2 + \boldsymbol{v}_1^H \boldsymbol{n} \tag{2.2}$$

We can also evaluate each term in (2.2).

Signal remains:

$$\boldsymbol{v}_1^H \boldsymbol{h}_1 = \frac{1}{M} \|\boldsymbol{h}_1\|^2 \xrightarrow{M \to \infty} \mathbb{E}[|h_{11}|^2] = 1$$

Interference vanishes:

$$\boldsymbol{v}_1^H \boldsymbol{h}_2 = \frac{1}{M} \boldsymbol{h}_1^H \boldsymbol{h}_2 \xrightarrow{M \to \infty} \mathbb{E}[h_{11}^H h_{21}] = 0$$

Noise vanishes:

$$\boldsymbol{v}_1^H n = \frac{1}{M} \boldsymbol{h}_1^H \boldsymbol{n} \xrightarrow{M \to \infty} \mathbb{E}[h_{11}^H n_1] = 0$$

Hence, the asymptotically noise and interference both vanish if the number of antennas approaches to infinity due to the law of large numbers. Thanks to this principle, low complexity linear beamforming techniques such as zero forcing (ZF) can result in a near optimal performance in multiuser scenarios [11]. Chapter 4 will further detail the application of this principle in designing the baseband precoder at stage two. It is also worth mentioning that the performance of massive MIMO systems is highly dependent on the knowledge of channel state information (CSI) at the base station. Thus, in order to ensure the availability of CSI for the base station in massive MIMO systems, it is commonly assumed that the system operates in a time-division duplex (TDD) manner [1] with the help of channel reciprocity property. The frequency-division duplex (FDD) can also be used in massive MIMO systems, however is more challenging.

2.2. Fundamentals of Millimeter Wave Systems

The sub-6 GHz frequency bands for our current cellular communication systems are becoming more and more saturated due to the limited spectrum resources at such carrier frequencies. One approach to address the problem is to exploit more unlicensed spectrum at mmWave frequencies for access.

2.2.1. MmWave propagation characteristics

The main characteristics of mmWave propagation involve the following four aspects [1, 2, 4, 12].

(1) High free space propagation loss.
(2) Less multipath components (MPCs) compared to sub-6 GHz channels (e.g. Rayleigh fading channel).
(3) Severe vulnerability and sensitivity to signal blockage.
(4) High penetration losses in indoor-to-outdoor scenarios.

Hence, in order to address these issues for employing mmWave for the future networks, a few challenges need to be tackled. The scaling of high and directional antenna gains are one of the most efficient solution to deal with the high attenuation of mmWave due to its electromagnetic nature. Directional antennas can affect the observed effective channel at the baseband such that the delay spread of the channel can be reduced [1]. Therefore, the inter-symbol-interference (ISI) could be reduced, resulting in a better system performance.

2.2.2. MmWave channel models

MmWave channels are expected to have limited number of scatters in its propagation path. Thus, to incorporate such effect, an extended Saleh-Valenzuela geometric channel model [13-15] can be used for mmWave system. Concretely, the channel $\boldsymbol{H}_i \in \mathbb{C}^{N\times M}$ from the base station (BS) to each mobile station (MS_i) can be modeled as

$$\boldsymbol{H}_i = \sqrt{\frac{N_t N_r}{L_i}} \sum_{l=1}^{L_i} \alpha_{i,l} \mathbf{a}_{\mathrm{r}}\left(\phi_{i,l}^r, \theta_{i,l}^r\right) \mathbf{a}_{\mathrm{t}}^H\left(\phi_{i,l}^t, \theta_{i,l}^t\right) \tag{2.3}$$

This clustered channel model is assumed to be a summation of all the contributions of each ray in each cluster. Thus, the total number of propagation paths is defined as $L_i = N_{ray} N_{cl}$.

In (2.3), N_t and N_r stand for the number of antennas at BS and each MS, $\left(\phi_{i,l}^r, \theta_{i,l}^r\right)$ and $(\phi_{i,l}^t, \theta_{i,l}^t)$ are its azimuth/elevation angles of arrival and departure respectively (AOA, AOD). The steering vector $\mathbf{a}_{\mathrm{r}}\left(\phi_{i,l}^r, \theta_{i,l}^r\right)$ and $\mathbf{a}_{\mathrm{t}}^H\left(\phi_{i,l}^t, \theta_{i,l}^t\right)$with AOA/AODs are the normalized receive and transmit array response vectors respectively. The complex gain of the l^{th} path $\alpha_{i,l}$ is assumed to be i.i.d. Gaussian distributed. Finally, a normalization factor is added to ensure $\mathbb{E}[\|\boldsymbol{H}_i\|_F^2] = N_t N_r$.

Based on the beam-space system representation introduced in [2], the channel $\boldsymbol{H}$ can be reformulated to a more compact form as

$$\boldsymbol{H}_i = A_{i,r} D_i A_{i,t}^H, \tag{2.4}$$

where

$$\boldsymbol{A}_{i,r} = [\mathbf{a}_{\mathrm{r}}\left(\phi_{i,1}^r, \theta_{i,1}^r\right), \ldots, \mathbf{a}_{\mathrm{r}}\left(\phi_{i,L_i}^r, \theta_{i,L_i}^r\right)]$$

$$\boldsymbol{A}_{i,t} = [\mathbf{a}_{\mathrm{t}}\left(\phi_{i,1}^t, \theta_{i,1}^t\right), \ldots, \mathbf{a}_{\mathrm{t}}\left(\phi_{i,L_i}^t, \theta_{i,L_i}^t\right)]$$

$$\boldsymbol{D}_i = diag(\alpha_{i,1}\sqrt{\frac{N_t N_r}{L_i}}, \dots, \alpha_{i,L_i}\sqrt{\frac{N_t N_r}{L_i}})$$

It is noted that the array response vectors $\mathbf{a}_{\mathrm{t}}^{H}(\phi_{i,l}^{t}, \theta_{i,l}^{t})$ and $\mathbf{a}_{\mathrm{r}}(\phi_{i,l}^{r}, \theta_{i,l}^{r})$ are functions of transmit and receive antenna array structures only. Two commonly used antenna arrays are uniform linear array (ULA) and uniform planar array (UPA). Concretely, for an N-element ULA on the y-axis, the array response vector can be written as

$$\mathbf{a}_{\mathrm{ULAy}}(\phi) = \frac{1}{\sqrt{N}}\left[1, e^{jkdsin(\phi)}, \dots, e^{j(N-1)kdsin(\phi)}\right]^T, \tag{2.5}$$

where $k = \frac{2\pi}{d}$ and d is the inter-element spacing.

For a UPA in the yz-plane with W (width) and H (height) on the y and z axes, the array response vector can be written as

$$\mathbf{a}_{\mathrm{UPA}}(\phi, \theta) = \frac{1}{\sqrt{N}}\left[1, \dots, e^{jkd(msin\phi sin\theta + ncos\theta)}, \dots, e^{jkd((W-1)sin\phi sin\theta + (H-1)cos\theta)}\right]^T, \tag{2.6}$$

where $0 \le m \le W$ and $0 \le n \le H$ are the y and z indices of an antenna element respectively and the antenna array size is $N = WH$. Uniform planar arrays is usually of more interest in mmWave beamforming since they have the following three benefits [15].

(1) UPA yields smaller antenna array dimensions.
(2) UPA facilitates to pack more antenna elements in a reasonably-sized array.
(3) UPA enables beamforming in the elevation domain (also known as 3D beamforming)

Thus, the UPA will be mainly used for all three system models in this thesis. Also, considering the number of antennas simulated for all three system models in this thesis is assumed as a square integer, accordingly, the author will adopt UPA with $W = H$ for channel realizations in Chapter 3, 4 and 5.

2.3. Beamforming in Massive MIMO Systems

While massive MIMO with high degrees of freedom provides higher energy and data rates, mmWave frequency bands provide larger bandwidth. Thus, thanks to the much shorter wavelength of mmWaves, large antenna arrays can be packed into highly directional beamforming, making massive MIMO practical and applicable. At the same time, due to the increased free-space path-

loss at mmWave frequencies, using high gain and directional antennas (beamforming) is crucial to compensate for the severe path loss. Hence, in this section, an overview of the beamforming techniques for massive MIMO system will be discussed.

2.3.1. Beamforming principles

Beamforming is generally defined as a signal processing technique used in sensor arrays for directional signal transmission or reception [1]. In simple words, by constructively or deconstructively adding different signals, a desired directional signal with very high power is expected to be obtained. This is achieved by manipulating the change of phase or amplitude for different signals from different antennas. Based on the degrees of freedom for phase and amplitude manipulation of signals, the hardware architecture of beamforming can be divided into three main categories: analog, digital, and hybrid beamforming [1].

It is noted that the term ‘beamforming’ and ‘precoding/combining’ will be often used interchangeably in this thesis as they both refer to the signal processing techniques designed for exploiting spatial multiplexing at the transmitter and receiver side. To keep the expression of existing work from literature clearly, the original term was maintained for demonstration in this thesis.

2.3.2. Analog Beamforming

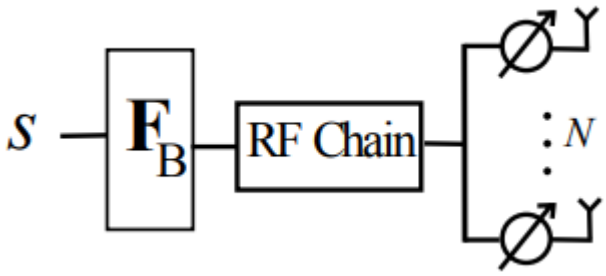

Figure 4: Hardware architecture of analog beamforming [1]

Analog beamforming, also known as Radio Frequency (RF) beamforming, is the simplest and cheapest approach to realize directional signal transmission. As can be seen from Figure 4, each antenna is equipped with a phase shifter to form one angular beam and whole phase array antenna is then connected to a single RF chain. By manipulating the phase of each antenna element, it is possible to attenuate the interference and increase the SNR. Analog beamforming is already being used for short range mmWave communications such as in IEEE 802.15 standard [16].The main drawback of analog beamforming is due to the constant modulus constraint imposed by the phase

shifters [1]. More concretely, constant modulus constraint means the phase shifters can only change the phase but not the amplitude. Thus, analog beamforming cannot achieve full spatial multiplexing gains. This limitation will also be elaborated in the following chapters.

2.3.3. Digital Beamforming

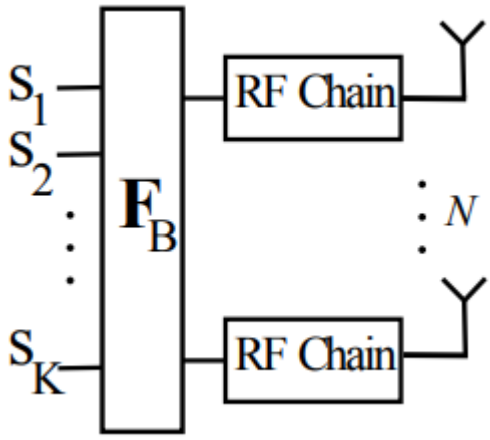

Figure 5: Hardware architecture of digital beamforming [1]

Digital beamforming is capable of providing the highest level of flexibility regarding to the implementation of beamforming as it allows for both magnitude and phase adjustment for each antenna element [1]. Figure 5 demonstrates a block diagram of the digital beamforming architecture, where each antenna in the array is connected to baseband through a dedicated RF chain. It is the ideal beamforming method which can lead to a full spatial multiplexing gain. However, in practical, the implementation of digital beamforming for massive MIMO systems is challenging and extremely expensive. This is because RF chains are expensive and have a high power consumption. When the number of antennas are greatly scaled in massive MIMO, the number of RF chains also scaled up massively. Hence, implementing and realizing digital beamforming is unpractical for mmWave massive MIMO systems [17].

2.3.4. Hybrid Beamforming

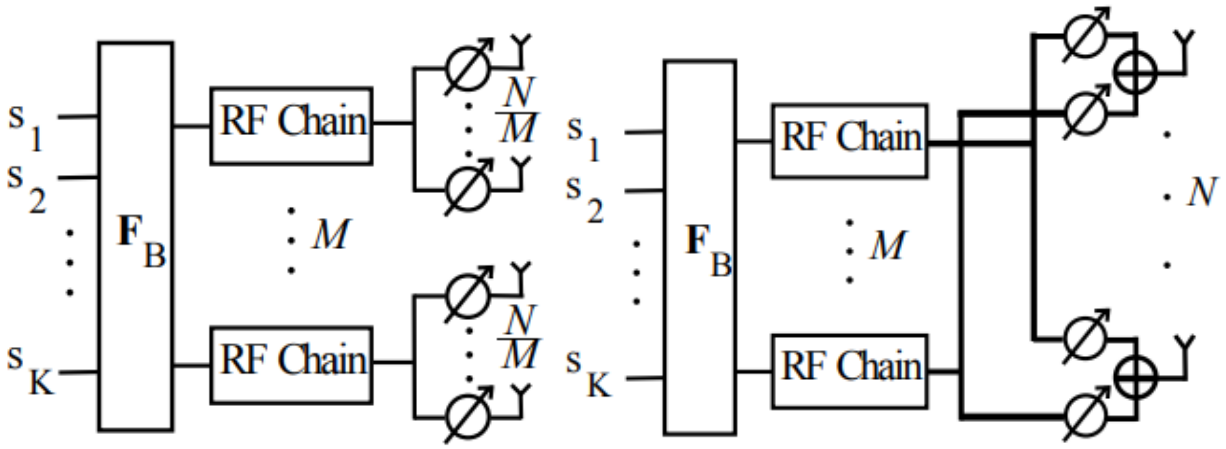

(a) Sub-connected structure (b) Fully connected structure

Figure 6: Hardware architectures of two types of hybrid beamforming [1]

To reduce the number of RF chains while achieving a better multiplexing gains than analog beamforming, hybrid beamforming has attracted a lot of research attentions over the last decade by providing a tradeoff between cost and performance [1]. It also has two main types based on the configuration of the structure. Figure 6 (a) shows a sub-connected hybrid beamforming structure, where each antenna is connected to a phase shifter and a subset of antennas is then connected to a RF chain. As shown in Figure 6 (b), each RF chain is connected to all the antenna elements through a complex phase shifter configuration networks for fully-connected hybrid beamforming. As a comparison, full connected structure can provider higher beamforming gain and spectral efficiency as each RF chain is linked with all antennas. Thus, a narrower and more directional beam can be generated. However, it is easy to observe that fully-connected structure requires higher power consumption and more RF paths. Therefore, fully-connected phase shifter network model is more often used in theoretical work while sub-connected hybrid beamforming is more suitable in practice [1]. The design challenges rise dramatically with the consideration of constant modulus constraint and discrete resolution of the phase shifters. The constraints make the optimization design of hybrid beamforming non-convex and very difficult to solve. The joint design of analog and digital (baseband) beamformers are completely different from the traditional MIMO design. This is because the traditional MIMO design only relies on analog or digital beamforming rather than the combination of both. Hence, how to effectively and jointly design the baseband beamformer and RF beamformer for hybrid precoding will be the main concern that the author will present and discuss in this thesis.

2.4. Review of Beamforming Designs

Hybrid beamforming has been studied over the last decade. In the following, an overview of the existing works on hybrid beamforming is presented.

Hybrid beamforming provides a tradeoff between system performance and hardware complexity. Below are the main directions of designing the precoder/combiners.

(1) Iterative Coordinated Beamforming Designs

The general idea of this design is to iterate between the design of the precoder and combiners in multi-user MIMO systems, with the aim of converging to a good solution [12, 18, 19]. However, it is not suitable for mmWave channel as the feeding of large mmWave channel matrix back to BS requires a huge feedback overhead.

(2) AltMin (MO-AltMin) Hybrid Beamforming Design

This algorithm proposed in [20] was based on a manifold optimization. This algorithm does not require any pre-determined RF codebooks for the analog precoder. It is the first time of research to solve the hybrid precoder design problem under the unit modulus constraints. However, due to the high prerequisite knowledge of geometry and advanced mathematics in Riemannian manifold, the author is not able to fully understand this algorithm.

(3) Single-user Spatially Sparse Beamforming Design

This algorithm mainly decouples the joint optimization problem into two separate optimization problems for precoding and combing. As an example, [15] formulates the precoding problem as a sparse reconstruction problem. The solution can be found via the principle of orthogonal matching pursuit. Same procedure applies for combing. Chapter 3 will detail and elaborate this algorithms from all aspects.

(4) Two-stage Multiuser Hybrid ZF Beamforming

This algorithm was proposed in [12] to demonstrate its low-complexity and good performance for multi-user millimeter wave systems. In the first stage, the BS RF precoder and MS RF combiner were jointly designed to maximize the desired signal power for each user regardless of the interference between users. In the second stage, a ZF baseband precoder was designed to tackle the multi-user interference. Chapter 4 will detail this algorithm with complete sum rate expression and implementation.

(5) MMSE-based Hybrid Beamforming

This algorithm was proposed based on minimizing the sum mean-squared error (MSE) of the data streams for each user [3, 17]. Different from two-stage multiuser hybrid ZF beamforming, this algorithm allows for the joint design of both baseband and RF precoders for all the users. Based on the rules of thumb of this algorithm, three MMSE designs will be introduced and detailed in Chapter 5.

There are some other algorithms proposed in the last few years regarding to hybrid beamforming, which also illustrate their unique advantages and benefits on some aspects. Due to the time limitation of this thesis, the author will explore more hybrid beamforming algorithms in future works.

Chapter 3

3. Spatially Sparse Beamforming in Millimeter Wave Massive MIMO Systems

This chapter will mainly exploit the sparse-scattering nature of mmWave channel to formulate the hybrid beamforming design problem into a sparsity constrained matrix reconstruction problem.

3.1. System Model

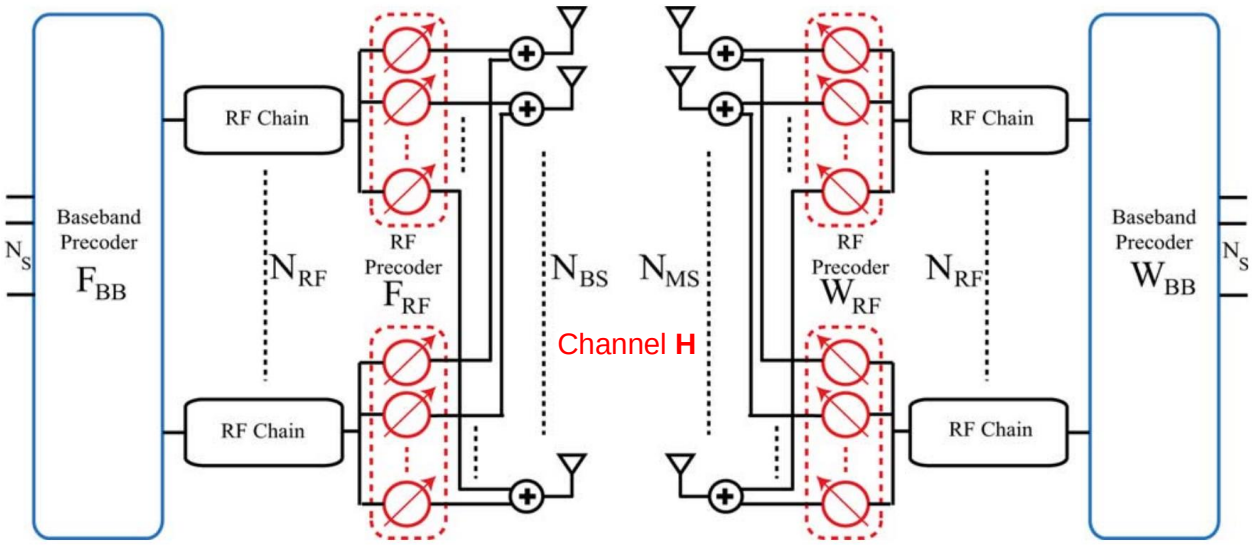

Figure 7: Single-user mmWave Massive MIMO architecture based on hybrid analog-digital precoding and combining [21]

Consider a single-user mmWave system shown in Figure 7, a BS (transmitter) with N_t antennas transmits N_s data streams to a MS (receiver) with N_r antennas. To transmit multi-stream communication practically, the base station is quipped with N_t^{RF} radio frequency (RF) chains such that $N_s \leq N_t^{RF} \leq N_t$. This beamforming architecture enables the BS to apply an $N_t^{RF} \times N_s$ baseband precoder $\boldsymbol{F}_{BB}$ using its N_t^{RF} transmit RF chains, followed by an RF precoder $\boldsymbol{F}_{RF}$ using analog circuitry with a $N_t \times N_t^{RF}$ dimention. The discrete-time transmitted signal is therfore given by $\boldsymbol{x} = \boldsymbol{F}_{RF}\boldsymbol{F}_{BB}\boldsymbol{s}$ where $\boldsymbol{s}$ is the $N_s \times 1$symbol vector such that $\mathbb{E}[\boldsymbol{s}\boldsymbol{s}^{\boldsymbol{H}}] = \frac{1}{N_s}\boldsymbol{I}_{Ns}$. The elements of the RF precoder $\boldsymbol{F}_{RF}$ are either analog or digital B-bits resolution phase shifters. It can be represented by

$$\boldsymbol{F}_{RF} = \begin{pmatrix} e^{j\theta_{11}} & \cdots & e^{j\theta_{1N_t^{RF}}} \\ \vdots & \ddots & \vdots \\ e^{j\theta_{N_t1}} & \cdots & e^{j\theta_{N_tN_t^{RF}}} \end{pmatrix}, \tag{3.1}$$

where $\Theta = [0,2\pi]$ for analog phase shifters and $\Theta = [0, \frac{2\pi}{2^B}, \ldots, \frac{(2^B-1)2\pi}{2^B}]$ for digital phase shifters. Thus, we can observe from (3.1) that, each entry in $\boldsymbol{F}_{RF}$ has equal norm, which means $\left(\boldsymbol{F}_{RF}^{i}{\boldsymbol{F}_{RF}^{i}}^{H}\right)_{l,l} = N_t^{-1}$. The transmitter's total power constraint is enforced by normalizing $\boldsymbol{F}_{BB}$ such that $\|\boldsymbol{F}_{RF}\boldsymbol{F}_{BB}\|_F^2 = N_s$.

The channel for mmWave propagation shown in Figure 7 is a narrowband clustered channel model that described in 2.2.2. The only difference is in this case, the channel is only two dimensional due to single-user. The channel formulation is also mentioned in section2.2.2.

Therefore, the received signal before combing can be expressed as

$$\boldsymbol{y} = \sqrt{\rho}\boldsymbol{H}\boldsymbol{F}_{RF}\boldsymbol{F}_{BB}\boldsymbol{s} + n, \tag{3.2}$$

where $\boldsymbol{y}$ is the $N_r \times 1$ received vector and ρ standards for the average received power. $\boldsymbol{H}$ is the $N_r \times N_t$ channel matrix described in section 2.2.2 such that $\mathbb{E}[\|\boldsymbol{H}\|_F^2] = N_tN_r$. Also, a noise vector $\boldsymbol{n}$ with i.i.d complex Gaussian (i.e. $n \sim \mathcal{CN}(0, \sigma_n^2)$) is also considered. Here, in this case, the channel knowledge is assumed to be perfectly and instanteously known to both BS (transmitter) and MS (receiver). In practical systems, CSI at the receiver can be obtained through training and subsequently shared with the transmitter through limited feedback. The influence of limited

feedback due to the quantization constraint of RF precoder $\boldsymbol{F}_{RF}$ for this model will be discussed in section 3.4.

The receiver will use N_r^{RF} ($N_s \leq N_r^{RF} \leq N_r$) RF chains and analog phase shifters to decode the received signal. Thus, the received signal after combing as illustrated in the right part of Figure 7 will become the processed received signal

$$\tilde{y} = \sqrt{\rho}\boldsymbol{W}_{BB}^{\mathrm{H}}\boldsymbol{W}_{RF}^{\mathrm{H}}\boldsymbol{H}\boldsymbol{F}_{RF}\boldsymbol{F}_{BB}\boldsymbol{s} + \boldsymbol{W}_{BB}^{\mathrm{H}}\boldsymbol{W}_{RF}^{\mathrm{H}}, \tag{3.3}$$

where $\boldsymbol{W}_{RF}$ is the $N_r \times N_r^{RF}$ RF combining matrix and $\boldsymbol{W}_{RF}$ is the $N_r^{RF} \times N_s$ baseband combining matrix. Similar to RF precoder $\boldsymbol{F}_{RF}$, each element in $\boldsymbol{W}_{RF}$ share the same norm due to the use of phase shifters.

If Gaussian symbols are transmitted through mmWave channels, based on (2.1), the spectral efficiency can be derived as

$$R = \log_2\left(\left|\boldsymbol{I}_{N_s} + \frac{\rho}{N_S}\boldsymbol{R}_n^{-1}\boldsymbol{W}_{BB}^{H}\boldsymbol{W}_{RF}^{H}\boldsymbol{H}\boldsymbol{F}_{RF}\boldsymbol{F}_{BB}\boldsymbol{F}_{BB}^{H}\boldsymbol{F}_{RF}^{H}\boldsymbol{H}^{H}\boldsymbol{W}_{RF}\boldsymbol{W}_{BB}\right|\right), \tag{3.4}$$

where $\boldsymbol{R}_n = \sigma_n^2\boldsymbol{W}_{BB}^{H}\boldsymbol{W}_{RF}^{H}\boldsymbol{W}_{RF}\boldsymbol{W}_{BB}$ is the noise covariance matrix after combining.

3.2. Problem Statement

We attempt to find the optimal design of precoders ($\boldsymbol{F}_{RF}, \boldsymbol{F}_{BB}$) and combiners ($\boldsymbol{W}_{RF}, \boldsymbol{W}_{BB}$) that can maximize the outcome of (3.4). One general and direct approach is to maximize the mutual information by jointly optimizing four different matrix variables ($\boldsymbol{F}_{RF}, \boldsymbol{F}_{BB}, \boldsymbol{W}_{RF}, \boldsymbol{W}_{BB}$).

$$I(\boldsymbol{F}_{RF}, \boldsymbol{F}_{BB}, \boldsymbol{W}_{RF}, \boldsymbol{W}_{BB}) = \log_2\left(\left|\boldsymbol{I}_{N_s} + \frac{\rho}{N_S}\boldsymbol{R}_n^{-1}\boldsymbol{W}_{BB}^{H}\boldsymbol{W}_{RF}^{H}\boldsymbol{H}\boldsymbol{F}_{RF}\boldsymbol{F}_{BB}\boldsymbol{F}_{BB}^{H}\boldsymbol{F}_{RF}^{H}\boldsymbol{H}^{H}\boldsymbol{W}_{RF}\boldsymbol{W}_{BB}\right|\right) \tag{3.5}$$

However, due to the constant modulus constraint of phase shifters, finding the global optimal solution for all four variables is found to be impeccable and impractical. Hence, to simply the optimization process, we can decouple the joint transceiver optimization problem and only focus on the optimal design of precoders ($\boldsymbol{F}_{RF}, \boldsymbol{F}_{BB}$). This is due to the fact that, same design algorithms can be applied on both transmitter and receiver side. Therefore, in this way, we can neglect the impact of combiners ($\boldsymbol{W}_{RF}, \boldsymbol{W}_{BB}$) to find optimal design of precoders ($\boldsymbol{F}_{RF}, \boldsymbol{F}_{BB}$) first and operate the similar process for combiners after that.

3.3. Formulation of the Spatially Sparse Beamforming Algorithm

As stated in section 3.2, the optimal design of precoders $(\boldsymbol{F}_{RF}, \boldsymbol{F}_{BB})$ can be found by maximize the mutual information achieved by Gaussian signaling over the mmWave channel.

$$I(\boldsymbol{F}_{RF}, \boldsymbol{F}_{BB}) = \log_2 \left(\left| \boldsymbol{I}_{N_s} + \frac{\rho}{N_S \sigma_n^2} \boldsymbol{H} \boldsymbol{F}_{RF} \boldsymbol{F}_{BB} \boldsymbol{F}_{BB}^H \boldsymbol{F}_{RF}^H \boldsymbol{H}^H \right| \right), \tag{3.6}$$

Note that the difference between (3.5) and (3.6) is the removal of the optimization of combiners $(\boldsymbol{W}_{RF}, \boldsymbol{W}_{BB})$.

Proceeding with the design of $(\boldsymbol{F}_{RF}, \boldsymbol{F}_{BB})$, the optimal design of precoders can be simplified as

$$(\boldsymbol{F}_{RF}^{opt}, \boldsymbol{F}_{BB}^{opt}) = \underset{\boldsymbol{F}_{RF}, \boldsymbol{F}_{BB}}{\operatorname{argmax}} \; I(\boldsymbol{F}_{RF}, \boldsymbol{F}_{BB}), \tag{3.7}$$

$$s.t. \;\; \boldsymbol{F}_{RF} \in \mathcal{F}_{RF},$$

$$\|\boldsymbol{F}_{RF} \boldsymbol{F}_{BB}\|_F^2 = N_s,$$

where $\mathcal{F}_{RF}$ is a set of pre-defined RF codebooks for $\boldsymbol{F}_{RF}$.

However, solving (3.7) is still a very difficult problem. Therefore, we need to adopt some approximations to find practical near-optimal solution for precoders $(\boldsymbol{F}_{RF}, \boldsymbol{F}_{BB})$ that can be implemented in Figure 7.

Firstly, the optimal unconstrained precoder matrix $\boldsymbol{F}_{opt}$ is defined as the singular value decomposition (SVD) of channel matrix $\boldsymbol{H}$. Specifically,

$$svd(\boldsymbol{H}) = \boldsymbol{U} \boldsymbol{\Sigma} \boldsymbol{V}^{\boldsymbol{H}}, \tag{3.8}$$

where $\boldsymbol{U}$ is an $N_r \times rank(\boldsymbol{H})$ unitary matrix; $\boldsymbol{\Sigma}$ is an $rank(\boldsymbol{H}) \times rank(\boldsymbol{H})$ diagonal matrix of singular values in decreasing order; and V is an $N_t \times rank(\boldsymbol{H})$ unitary matrix. Therefore, combine (3.6) and (3.8), we have

$$I(\boldsymbol{F}_{RF}, \boldsymbol{F}_{BB}) = \log_2 \left(\left| \boldsymbol{I}_{N_s} + \frac{\rho}{N_S \sigma_n^2} \boldsymbol{\Sigma}^{\boldsymbol{2}} \boldsymbol{V}^{\boldsymbol{H}} \boldsymbol{F}_{RF} \boldsymbol{F}_{BB} \boldsymbol{F}_{BB}^H \boldsymbol{F}_{RF}^H \boldsymbol{V} \right| \right), \tag{3.9}$$

Also, define the two partitions of $\boldsymbol{\Sigma}$ **and** $\boldsymbol{V}$ as follows.

$$\boldsymbol{\Sigma} = \begin{bmatrix} \boldsymbol{\Sigma_1} & \boldsymbol{0} \\ \boldsymbol{0} & \boldsymbol{\Sigma_2} \end{bmatrix}, \qquad \boldsymbol{V} = [\boldsymbol{V}_1 \;\; \boldsymbol{V}_2]. \tag{3.10}$$

In (3.10), $\boldsymbol{\Sigma_1}$ is in dimension $N_s \times N_s$ and $\boldsymbol{V}_1$ is in dimension $N_t \times N_s$. Therefore, the optimal unconstrained precoder $\boldsymbol{F}_{opt}$ will be equal to the $\boldsymbol{V}_1$. Also, it is noted that the precoder $\boldsymbol{V}_1$ is generally unable to be expressed as the product of RF precoder $\boldsymbol{F}_{RF}$ and baseband precoder $\boldsymbol{F}_{BB}$ with $\boldsymbol{F}_{RF} \in \mathcal{F}_{RF}$ and therefore cannot be applied in mmWave channel models. However, if we can make $\boldsymbol{F}_{RF}\boldsymbol{F}_{BB}$ sufficiently close to the optimal precoder $\boldsymbol{V}_1$, the mutual information expressed in (3.9) can become comparable.

Hence, the following assumption is adopted for figure out the above concern.

Approximation 1: Assume that the mmWave system parameters $(N_t, N_r, N_t^{RF}, N_r^{RF})$ and mmWave propagation channel parameters $(N_{cl}, N_{ray}, \phi_{i,l}^r, \theta_{i,l}^r, \phi_{i,l}^t, \theta_{i,l}^t)$ described in section 2.2.2 are such that the hybrid precoder $\boldsymbol{F}_{RF}\boldsymbol{F}_{BB}$ can become sufficiently close to the optimal precoder $\boldsymbol{V}_1$. To be exact, the constraint of close can be defined as follows.

$$\begin{aligned} \boldsymbol{V}_2^* \boldsymbol{F}_{RF}\boldsymbol{F}_{BB} &\approx 0 \\ \boldsymbol{V}_1^* \boldsymbol{F}_{RF}\boldsymbol{F}_{BB} &= \boldsymbol{I}_{Ns} \end{aligned} \tag{3.11}$$

Here, the two conditions in (3.11) have been verified using MATLAB in further implementing the algorithm.

To make a comparison, *Approximation 1* is similar to the assumption for unlimited size of RF codebooks such that a near optimal unquantized precoder can be achieved. Particularly, the following three conditions can guarantee a validation of *Approximation 1*.

i) A sufficiently larger number of antennas at base station.

ii) A reasonable number of RF chains at base station satisfied for $N_s < N_t^{RF} \leq N_t$.

iii) Correlated channel matrix $\boldsymbol{H}$.

Therefore, with the above assumption, the key part expression $(\boldsymbol{V^H F}_{RF}\boldsymbol{F}_{BB}\boldsymbol{F}_{BB}^H\boldsymbol{F}_{RF}^H\boldsymbol{V})$ in (3.9) can be expanded and rearranged as

$$\boldsymbol{V^H F}_{RF}\boldsymbol{F}_{BB}\boldsymbol{F}_{BB}^H\boldsymbol{F}_{RF}^H\boldsymbol{V} = \begin{bmatrix} \boldsymbol{V_1^H F}_{RF}\boldsymbol{F}_{BB}\boldsymbol{F}_{BB}^H\boldsymbol{F}_{RF}^H\boldsymbol{V_1} & \boldsymbol{V_1^H F}_{RF}\boldsymbol{F}_{BB}\boldsymbol{F}_{BB}^H\boldsymbol{F}_{RF}^H\boldsymbol{V_2} \\ \boldsymbol{V_2^H F}_{RF}\boldsymbol{F}_{BB}\boldsymbol{F}_{BB}^H\boldsymbol{F}_{RF}^H\boldsymbol{V_1} & \boldsymbol{V_2^H F}_{RF}\boldsymbol{F}_{BB}\boldsymbol{F}_{BB}^H\boldsymbol{F}_{RF}^H\boldsymbol{V_2} \end{bmatrix} = \begin{bmatrix} \boldsymbol{Q}_{11} & \boldsymbol{Q}_{12} \\ \boldsymbol{Q}_{21} & \boldsymbol{Q}_{22} \end{bmatrix} \tag{3.12}$$

Thus, combine (3.12) and (3.9), we can further simplify the mutual information as

$$I(\boldsymbol{F}_{RF}, \boldsymbol{F}_{BB}) = \log_2\left(\left|\boldsymbol{I}_{N_s} + \frac{\rho}{N_S\sigma_n^2}\boldsymbol{\Sigma^2 V^H F}_{RF}\boldsymbol{F}_{BB}\boldsymbol{F}_{BB}^H\boldsymbol{F}_{RF}^H\boldsymbol{V}\right|\right)$$

$$= \log_2\left(\left|\boldsymbol{I}_{N_s} + \frac{\rho}{N_S\sigma_n^2}\begin{bmatrix}\boldsymbol{\Sigma_1^2} & \boldsymbol{0}\\ \boldsymbol{0} & \boldsymbol{\Sigma_2^2}\end{bmatrix}\begin{bmatrix}\boldsymbol{Q}_{11} & \boldsymbol{Q}_{12}\\ \boldsymbol{Q}_{21} & \boldsymbol{Q}_{22}\end{bmatrix}\right|\right) \quad (3.13)$$

According to the Schur complement for matrix determinants [22], (3.13) can be rearranged as

$$\begin{aligned} I(\boldsymbol{F}_{RF}, \boldsymbol{F}_{BB}) &= \log_2\left(\left|\begin{pmatrix}\frac{\rho}{N_S\sigma_n^2}\boldsymbol{\Sigma_1^2} + \boldsymbol{I} & \frac{\rho}{N_S\sigma_n^2}\boldsymbol{\Sigma_1^2}\boldsymbol{Q}_{12}\\ \frac{\rho}{N_S\sigma_n^2}\boldsymbol{\Sigma_2^2}\boldsymbol{Q}_{21} & \frac{\rho}{N_S\sigma_n^2}\boldsymbol{\Sigma_2^2}\boldsymbol{Q}_{22} + \boldsymbol{I}\end{pmatrix}\right|\right) \\ &= \log_2\left(\left|\boldsymbol{I}_{N_s} + \frac{\rho}{N_S\sigma_n^2}\boldsymbol{\Sigma_1^2}\boldsymbol{Q}_{11}\right|\right) \\ &+ \log_2\left(\left|\boldsymbol{I} + \frac{\rho}{N_S\sigma_n^2}\boldsymbol{\Sigma_2^2}\boldsymbol{Q}_{22} - \frac{\rho^2}{N_S^2\sigma_n^4}\boldsymbol{\Sigma_2^2}\boldsymbol{Q}_{21}\left(\boldsymbol{I}_{N_s} + \frac{\rho}{N_S\sigma_n^2}\boldsymbol{\Sigma_1^2}\boldsymbol{Q}_{11}\right)^{-1}\boldsymbol{\Sigma_1^2}\boldsymbol{Q}_{12}\right|\right) \quad (3.14) \end{aligned}$$

This is obtained by assuming

$$\begin{cases} A = \frac{\rho}{N_S\sigma_n^2}\boldsymbol{\Sigma_1^2} + \boldsymbol{I} \\ B = \frac{\rho}{N_S\sigma_n^2}\boldsymbol{\Sigma_1^2}\boldsymbol{Q}_{12} \\ C = \frac{\rho}{N_S\sigma_n^2}\boldsymbol{\Sigma_2^2}\boldsymbol{Q}_{21} \\ D = \frac{\rho}{N_S\sigma_n^2}\boldsymbol{\Sigma_2^2}\boldsymbol{Q}_{22} + \boldsymbol{I} \end{cases},$$

And apply

$$\begin{vmatrix} A & B \\ C & D \end{vmatrix} = |A||D - CA^{-1}B|$$

According to (3.10), (3.14) can be further simplified to

$$I(\boldsymbol{F}_{RF}, \boldsymbol{F}_{BB}) \approx \log_2\left(\left|\boldsymbol{I}_{N_s} + \frac{\rho}{N_S\sigma_n^2}\boldsymbol{\Sigma_1^2}\boldsymbol{V}_1^H\boldsymbol{F}_{RF}\boldsymbol{F}_{BB}\boldsymbol{F}_{BB}^H\boldsymbol{F}_{RF}^H\boldsymbol{V}_1\right|\right) \quad (3.15)$$

Apply the Schur complement identity for matrix determinants [22] again on (3.15), we have

$$\begin{aligned} I(\boldsymbol{F}_{RF}, \boldsymbol{F}_{BB}) &\approx \log_2\left(\left|\boldsymbol{I}_{N_s} + \frac{\rho}{N_S\sigma_n^2}\boldsymbol{\Sigma_1^2}\right|\right) \\ &+ \log_2\left(\left|\boldsymbol{I} - \left(\boldsymbol{I}_{N_s} + \frac{\rho}{N_S\sigma_n^2}\boldsymbol{\Sigma_1^2}\right)^{-1}\frac{\rho}{N_S\sigma_n^2}\boldsymbol{\Sigma_1^2}(\boldsymbol{I}_{N_s} - \boldsymbol{V}_1^H\boldsymbol{F}_{RF}\boldsymbol{F}_{BB}\boldsymbol{F}_{BB}^H\boldsymbol{F}_{RF}^H\boldsymbol{V}_1)\right|\right) \quad (3.16) \end{aligned}$$

Apply (3.10) on (3.16), we have

$$I(\boldsymbol{F}_{RF}, \boldsymbol{F}_{BB}) \approx \log_2\left(\left|\boldsymbol{I}_{N_s} + \frac{\rho}{N_S\sigma_n^2}\boldsymbol{\Sigma_1^2}\right|\right) - \mathrm{tr}\left(\left(\boldsymbol{I}_{N_s} + \frac{\rho}{N_S\sigma_n^2}\boldsymbol{\Sigma_1^2}\right)^{-1} \times \frac{\rho}{N_S\sigma_n^2}\boldsymbol{\Sigma_1^2}(\boldsymbol{I}_{N_s} - \boldsymbol{V}_1^H\boldsymbol{F}_{RF}\boldsymbol{F}_{BB}\boldsymbol{F}_{BB}^H\boldsymbol{F}_{RF}^H\boldsymbol{V}_1)\right) \quad (3.17)$$

If we adopt a high effective-SNR approximation with condition $\left(\boldsymbol{I}_{N_s} + \frac{\rho}{N_S\sigma_n^2}\boldsymbol{\Sigma_1^2}\right)^{-1}\frac{\rho}{N_S\sigma_n^2}\boldsymbol{\Sigma_1^2} \approx \boldsymbol{I}_{Ns}$, the expression of mutual information from (3.17) can be finalize as

$$I(\boldsymbol{F}_{RF}, \boldsymbol{F}_{BB}) \approx \log_2\left(\left|\boldsymbol{I}_{N_s} + \frac{\rho}{N_S\sigma_n^2}\boldsymbol{\Sigma_1^2}\right|\right) - \mathrm{tr}\left(\left(\boldsymbol{I}_{N_s} - \boldsymbol{V}_1^H\boldsymbol{F}_{RF}\boldsymbol{F}_{BB}\boldsymbol{F}_{BB}^H\boldsymbol{F}_{RF}^H\boldsymbol{V}_1\right)\right)$$

$$= \log_2\left(\left|\boldsymbol{I}_{N_s} + \frac{\rho}{N_S\sigma_n^2}\boldsymbol{\Sigma_1^2}\right|\right) - (N_s - \|\boldsymbol{V}_1^H\boldsymbol{F}_{RF}\boldsymbol{F}_{BB}\|_F^2) \quad (3.18)$$

Here, in (3.18), we find out that the second term$(N_s - \|\boldsymbol{V}_1^H\boldsymbol{F}_{RF}\boldsymbol{F}_{BB}\|_F^2)$ is the squared chordal distance between the two points $\boldsymbol{F}_{opt} = \boldsymbol{V}_1$ and $\boldsymbol{F}_{RF}\boldsymbol{F}_{BB}$ on the Grassmann manifold [15]. Since Approximation 1 states that these two points are really close, hence we can exploit the manifold's locally Euclidean property to replace the chordal distance by the Euclidean distance $\left\|\boldsymbol{F}_{opt} - \boldsymbol{F}_{RF}\boldsymbol{F}_{BB}\right\|_F$ [15, 23]. Therefore, near-optimal hybrid precoders that maximize $I(\boldsymbol{F}_{RF}, \boldsymbol{F}_{BB})$ with the above approximations can be obtained by minimizing $\left\|\boldsymbol{F}_{opt} - \boldsymbol{F}_{RF}\boldsymbol{F}_{BB}\right\|_F$ instead. From another perspective, instead of maximizing $\|\boldsymbol{V}_1^H\boldsymbol{F}_{RF}\boldsymbol{F}_{BB}\|_F^2$ (or equivalently minimizing$\left(\boldsymbol{I}_{N_s} - \boldsymbol{V}_1^H\boldsymbol{F}_{RF}\boldsymbol{F}_{BB}\boldsymbol{F}_{BB}^H\boldsymbol{F}_{RF}^H\boldsymbol{V}_1\right)$) which is described in approximation 1, we can rather minimize $\left\|\boldsymbol{F}_{opt} - \boldsymbol{F}_{RF}\boldsymbol{F}_{BB}\right\|_F$ to construct a new problem.

The precoder design problem can be rewritten as

$$(\boldsymbol{F}_{RF}^{opt}, \boldsymbol{F}_{BB}^{opt}) = \underset{\boldsymbol{F}_{RF}, \boldsymbol{F}_{BB}}{\mathrm{argmin}}\left\|\boldsymbol{F}_{opt} - \boldsymbol{F}_{RF}\boldsymbol{F}_{BB}\right\|_F, \quad (3.19)$$

$$s.t.\ \ \boldsymbol{F}_{RF} \in \mathcal{F}_{RF},$$

$$\|\boldsymbol{F}_{RF}\boldsymbol{F}_{BB}\|_F^2 = N_s.$$

Now, the original problem in (3.5) is reformulated into finding the maximum project of $\boldsymbol{F}_{opt}$ onto the set of hybrid precoders of the form $\boldsymbol{F}_{RF}\boldsymbol{F}_{BB}$ with $\boldsymbol{F}_{RF} \in \mathcal{F}_{RF}$. To provide a near-optimal solution, we shall exploit the structure of mmWave massive MIMO channels. Note that the optimal precoder $\boldsymbol{F}_{opt} = \boldsymbol{V}_1$ such that the columns of the unitary matrix $\boldsymbol{V}$ form an orthonormal basis for

the channel's row space. In other words, the array response vectors $\mathbf{a}_{\mathrm{t}}\left(\phi_{i,l}^{t},\theta_{i,l}^{t}\right)$ form a finite span of the channel's row space. Also, due to the random nature of array response vectors, if we only select N_t^{RF} columns of $\mathbf{a}_{\mathrm{t}}\left(\phi_{i,l}^{t},\theta_{i,l}^{t}\right)$, then these columns are linearly independent.

Thus, by exploiting the structure of channel matrix $\boldsymbol{H}$, we can further simplify (3.19) by adding the restriction that the of RF precoder $\boldsymbol{F}_{RF}$ are from the array response vector $\mathbf{a}_{\mathrm{t}}\left(\phi_{i,l}^{t},\theta_{i,l}^{t}\right)$. In other words, each column of $\boldsymbol{F}_{RF}$ should be one of the basis vector from $\mathbf{a}_{\mathrm{t}}\left(\phi_{i,l}^{t},\theta_{i,l}^{t}\right)$.

$$\begin{aligned}(\boldsymbol{F}_{RF}^{opt},\boldsymbol{F}_{BB}^{opt}) &= \operatorname{argmin}\left\|\boldsymbol{F}_{opt}-\boldsymbol{F}_{RF}\boldsymbol{F}_{BB}\right\|_{F},\\ s.t.\ \ \boldsymbol{F}_{RF}^{i} &\in \{\mathbf{a}_{\mathrm{t}}\left(\phi_{i,l}^{t},\theta_{i,l}^{t}\right),\forall i,l\},\\ \|\boldsymbol{F}_{RF}\boldsymbol{F}_{BB}\|_{F}^{2} &= N_s\end{aligned} \tag{3.20}$$

In (3.20), we aim to find the best low dimensional representation of $\boldsymbol{F}_{opt}$ using the basis vectors from $\mathbf{a}_{\mathrm{t}}\left(\phi_{i,l}^{t},\theta_{i,l}^{t}\right)$. Under any circumstances, the optimization of precoding problem is to firstly select the 'best' N_t^{RF} array response vectors and thereafter compute the optimal baseband precoder $\boldsymbol{F}_{BB}$ as a local optimal (also can be deemed as globally sub-optimal) solution.

Accordingly, the constraint of $\boldsymbol{F}_{RF}$ can be further embedded into the optimization objective in (3.20) to form the final equivalent problem which can be deemed as a classic compressed sensing problem.

$$\begin{aligned}\widetilde{\boldsymbol{F}}_{BB}^{opt} &= \underset{\widetilde{\boldsymbol{F}}_{BB}}{\operatorname{argmin}}\left\|\boldsymbol{F}_{opt}-\boldsymbol{A}_t\widetilde{\boldsymbol{F}}_{BB}\right\|_{F},\\ s.t.\ \left\|\operatorname{diag}\left(\widetilde{\boldsymbol{F}}_{BB}\widetilde{\boldsymbol{F}}_{BB}^{H}\right)\right\|_{0} &= N_t^{RF}\\ \left\|\boldsymbol{A}_t\widetilde{\boldsymbol{F}}_{BB}\right\|_{F}^{2} &= N_s,\end{aligned} \tag{3.21}$$

where $\boldsymbol{A}_t = [\,\mathbf{a}_{\mathrm{t}}\left(\phi_{1,1}^{t},\theta_{1,1}^{t}\right),\ldots,\mathbf{a}_{\mathrm{t}}\left(\phi_{N_{cl},N_{ray}}^{t},\theta_{N_{cl},N_{ray}}^{t}\right)]$ is an $N_t \times N_{cl}N_{ray}$ matrix of array response vectors and $\widetilde{\boldsymbol{F}}_{BB}$ is an $N_{cl}B_{ray} \times N_s$ matrix. The sparsity constraint $\left\|\operatorname{diag}\left(\widetilde{\boldsymbol{F}}_{BB}\widetilde{\boldsymbol{F}}_{BB}^{H}\right)\right\|_{0} = N_t^{RF}$ means that $\widetilde{\boldsymbol{F}}_{BB}$ can only have at most N_t^{RF} non-zero rows; or equivalently, only N_t^{RF} columns of the matrix $\boldsymbol{A}_t = [\,\mathbf{a}_{\mathrm{t}}\left(\phi_{1,1}^{t},\theta_{1,1}^{t}\right),\ldots,\mathbf{a}_{\mathrm{t}}\left(\phi_{N_{cl},N_{ray}}^{t},\theta_{N_{cl},N_{ray}}^{t}\right)]$ can be effectively selected.

Concretely, the final purpose of this precoding optimization problem is to jointly design the RF precoder $\boldsymbol{F}_{RF}$ and baseband precoder $\boldsymbol{F}_{BB}$ with a sparsity constraint. Namely, we possess the optimal precoder $\boldsymbol{F}_{opt}$ and a set of basis for $\boldsymbol{F}_{RF}$ such that we need to select the best N_t^{RF} basis from $\boldsymbol{A}_t$ and their corresponding coefficient matrix $\boldsymbol{F}_{BB}$ to reconstruct the optimal precoder as close as possible. Then, to find the best N_t^{RF} basis and to compute the corresponding baseband precoder $\boldsymbol{F}_{BB}$, a classic basis pursuit algorithm can be applied for its low complexity and satisfying result. The algorithm is stated as follows.

Algorithm 1 Spatially Sparse Precoding via Orthogonal Matching Pursuit [15]

Input: $\boldsymbol{F}_{opt}$

Output: $\boldsymbol{F}_{RF}, \boldsymbol{F}_{BB}$

1. $\boldsymbol{F}_{RF} = Empty\ Matrix$
2. $\boldsymbol{F}_{res} = \boldsymbol{F}_{opt}$
3. **For** $i \leq N_t^{RF}$ **do**
4. $\quad \boldsymbol{\psi} = \boldsymbol{A}_t^H \boldsymbol{F}_{res}$
5. $\quad k = argmax_{l=1,\dots,N_{cl}N_{ray}} (\boldsymbol{\psi}\boldsymbol{\psi}^{\boldsymbol{H}})_{l,l}$
6. $\quad \boldsymbol{F}_{RF} = [\, \boldsymbol{F}_{RF} | \boldsymbol{A}_t^{(k)}]$
7. $\quad \boldsymbol{F}_{BB} = (\, \boldsymbol{F}_{RF}^H \boldsymbol{F}_{RF})^{-1} \boldsymbol{F}_{RF}^H \boldsymbol{F}_{opt}$
8. $\quad \boldsymbol{F}_{res} = \frac{\boldsymbol{F}_{opt} - \boldsymbol{F}_{RF} \boldsymbol{F}_{BB}}{\| \boldsymbol{F}_{opt} - \boldsymbol{F}_{RF} \boldsymbol{F}_{BB} \|_F}$
9. **End for**
10. $\boldsymbol{F}_{BB} = \sqrt{N_s} \frac{\boldsymbol{F}_{BB}}{\| \boldsymbol{F}_{RF} \boldsymbol{F}_{BB} \|_F}$
11. **Return** $\boldsymbol{F}_{RF}, \boldsymbol{F}_{BB}$

To sum up, the algorithm starts to select the best basis vector $\mathbf{a}_t(\phi_{k,k}^t, \theta_{k,k}^t)$ by finding the maximum project of the basis onto the optimal precoder $\boldsymbol{F}_{opt}$. The selection process can be determined by comparing the inner product $\boldsymbol{\psi}$ and choosing the one which has the largest project. Then, the selected column of the basis vector is appended to the RF precoder $\boldsymbol{F}_{RF}$. After that, the corresponding baseband precoder $\boldsymbol{F}_{BB}$ can be computed by solving a least square solution. The contribution from the largest basis vector will be removed and the algorithm will then iterate and continue to find the column vector that has the largest projection onto the residual ($\boldsymbol{F}_{opt}$ minus the

previous basis vectors' contribution). The algorithm will continue to find N_t^{RF} number of column vectors (beamforming vectors) for $\boldsymbol{F}_{RF}$ and calculate the related $\boldsymbol{F}_{BB}$ which can jointly reconstruct the signal to the utmost extent.

To design the optimal combiner, we assume that the hybrid precoders ($\boldsymbol{F}_{RF}$, $\boldsymbol{F}_{BB}$) are fixed and apply the mean square error (MSE) between transmit and receive symbols such that the optimal combiners ($\boldsymbol{W}_{RF}$, $\boldsymbol{W}_{BB}$) should minimize the error.

To make it clear, the problem can be stated as

$$(\boldsymbol{W}_{RF}^{opt}, \boldsymbol{W}_{BB}^{opt}) = \underset{\boldsymbol{W}_{RF}, \boldsymbol{W}_{BB}}{\operatorname{argmin}} \ \mathbb{E}[\|\boldsymbol{s} - \boldsymbol{W}_{BB}^H \boldsymbol{W}_{RF}^H \boldsymbol{y}\|_2^2] \quad , \tag{3.22}$$

$$s.t. \ \ \boldsymbol{W}_{RF} \in \mathcal{W}_{RF},$$

where $\boldsymbol{W}_{RF}$ is a set of pre-defined RF combiners.

The MMSE solution to a MSE problem is well known and has a closed form solution.

The basic MMSE estimator with per-antenna is

$$\boldsymbol{W} = \boldsymbol{H}^{\mathrm{H}}(\boldsymbol{H}\boldsymbol{H}^{\boldsymbol{H}} + N_0 \boldsymbol{I}_{Nr})^{-1} \tag{3.23}$$

By replacing channel $\boldsymbol{H}$ by effective channel $\boldsymbol{H}\ \boldsymbol{F}_{RF}\ \boldsymbol{F}_{BB}$ in (3.23) with some rearrangements, we shall get the optimal MMSE precoder as

$$\begin{aligned} \boldsymbol{W}_{MMSE}^{*} &= \mathbb{E}[\boldsymbol{s}\boldsymbol{y}^{\boldsymbol{H}}]\mathbb{E}[\boldsymbol{y}\boldsymbol{y}^{H}]^{-1} \\ &= \frac{\sqrt{\rho}}{N_s}\ \boldsymbol{F}_{BB}^H\ \boldsymbol{F}_{RF}^H \boldsymbol{H}^H \left(\frac{\rho}{N_s}\boldsymbol{H}\boldsymbol{F}_{RF}\boldsymbol{F}_{BB}\boldsymbol{F}_{BB}^H\boldsymbol{F}_{RF}^H\boldsymbol{H}^*\right)^{-1} \\ &= \frac{1}{\sqrt{\rho}}\left(\boldsymbol{F}_{BB}^H\boldsymbol{F}_{RF}^H\boldsymbol{H}^{\boldsymbol{H}}\boldsymbol{H}\boldsymbol{F}_{RF}\boldsymbol{F}_{BB} + \frac{\sigma_n^2 N_s}{\rho}\boldsymbol{I}N_s\right)^{-1} \boldsymbol{F}_{BB}^H\boldsymbol{F}_{RF}^H\boldsymbol{H}^{\boldsymbol{H}} \end{aligned} \tag{3.24}$$

Similar with $\boldsymbol{F}_{opt}$ mentioned in (3.23), $\boldsymbol{W}_{MMSE}$ cannot be decomposed into the product of $\boldsymbol{W}_{RF}$ and $\boldsymbol{W}_{BB}$ with $\boldsymbol{W}_{RF} \in \mathcal{W}_{RF}$. Thus, we need to find the optimal RF combiner $\boldsymbol{W}_{RF}$ and baseband combiner $\boldsymbol{W}_{BB}$ to reconstruct $\boldsymbol{W}_{MMSE}$ as much as possible.

To do so, the expectation of MSE in (3.22) can be firstly reformulated as

$$\begin{aligned} \mathbb{E}[\|\boldsymbol{s} - \boldsymbol{W}_{BB}^H\boldsymbol{W}_{RF}^H\boldsymbol{y}\|_2^2] &= \mathbb{E}[(\boldsymbol{s} - \boldsymbol{W}_{BB}^H\boldsymbol{W}_{RF}^H\boldsymbol{y})^H(\boldsymbol{s} - \boldsymbol{W}_{BB}^H\boldsymbol{W}_{RF}^H\boldsymbol{y})] \\ &= \mathbb{E}[tr((\boldsymbol{s} - \boldsymbol{W}_{BB}^H\boldsymbol{W}_{RF}^H\boldsymbol{y})(\boldsymbol{s} - \boldsymbol{W}_{BB}^H\boldsymbol{W}_{RF}^H\boldsymbol{y})^H)] \end{aligned}$$

$$= \mathrm{tr}(\mathbb{E}[\mathbf{s}\mathbf{s}^{\mathrm{H}}]) - 2\mathcal{R}\{\mathrm{tr}(\mathbb{E}[\mathbf{s}\mathbf{y}^{\mathrm{H}}]\, \boldsymbol{W}_{RF}\boldsymbol{W}_{BB})\} + \mathrm{tr}(\boldsymbol{W}_{BB}^{H}\boldsymbol{W}_{RF}^{H}\mathbb{E}[\boldsymbol{y}\boldsymbol{y}^{H}]^{-1}\, \boldsymbol{W}_{RF}\boldsymbol{W}_{BB}) \quad (3.25)$$

We can further add a constant term $\{\mathrm{tr}\big(\boldsymbol{W}_{MMSE}^{\mathrm{H}}\mathbb{E}[\mathbf{y}\mathbf{y}^{\mathrm{H}}]\boldsymbol{W}_{MMSE}\big) - \mathrm{tr}(\mathbb{E}[\mathbf{s}\mathbf{s}^{\mathrm{H}}])\}$ on (3.25) such that a new function can be obtained:

$$\begin{aligned}\mathcal{J}(\boldsymbol{W}_{RF}, \boldsymbol{W}_{BB}) &= \mathrm{tr}(\mathbb{E}[\mathbf{s}\mathbf{s}^{\mathrm{H}}]) - 2\mathcal{R}\{\mathrm{tr}(\mathbb{E}[\mathbf{s}\mathbf{y}^{\mathrm{H}}]\, \boldsymbol{W}_{RF}\boldsymbol{W}_{BB})\} + \mathrm{tr}(\boldsymbol{W}_{BB}^{H}\boldsymbol{W}_{RF}^{H}\mathbb{E}[\boldsymbol{y}\boldsymbol{y}^{H}]^{-1}\, \boldsymbol{W}_{RF}\boldsymbol{W}_{BB}) \\ &+ \mathrm{tr}\big(\boldsymbol{W}_{MMSE}^{\mathrm{H}}\mathbb{E}[\mathbf{y}\mathbf{y}^{\mathrm{H}}]\boldsymbol{W}_{MMSE}\big) - \mathrm{tr}(\mathbb{E}[\mathbf{s}\mathbf{s}^{\mathrm{H}}]) \\ &= \mathrm{tr}\big(\boldsymbol{W}_{MMSE}^{\mathrm{H}}\mathbb{E}[\mathbf{y}\mathbf{y}^{\mathrm{H}}]\boldsymbol{W}_{MMSE}\big) - 2\mathcal{R}\{\mathrm{tr}(\mathbb{E}[\mathbf{s}\mathbf{y}^{\mathrm{H}}]\, \boldsymbol{W}_{RF}\boldsymbol{W}_{BB})\} \\ &+ \mathrm{tr}(\boldsymbol{W}_{BB}^{H}\boldsymbol{W}_{RF}^{H}\mathbb{E}[\boldsymbol{y}\boldsymbol{y}^{H}]\, \boldsymbol{W}_{RF}\boldsymbol{W}_{BB}) \quad (3.26)\end{aligned}$$

Since

$$\mathrm{tr}(\mathbb{E}[\mathbf{s}\mathbf{y}^{\mathrm{H}}]\, \boldsymbol{W}_{RF}\boldsymbol{W}_{BB}) = \mathrm{tr}(\mathbb{E}[\mathbf{s}\mathbf{y}^{\mathrm{H}}]\mathbb{E}[\boldsymbol{y}\boldsymbol{y}^{H}]^{-1}\mathbb{E}[\boldsymbol{y}\boldsymbol{y}^{H}]\, \boldsymbol{W}_{RF}\boldsymbol{W}_{BB}), \quad (3.27)$$

$$\boldsymbol{W}_{MMSE}^{\mathrm{H}} = \mathbb{E}[\boldsymbol{s}\boldsymbol{y}^{H}]\mathbb{E}[\boldsymbol{y}\boldsymbol{y}^{H}]^{-1} \quad (3.28)$$

By combining (3.27) and (3.28), we can rewrite $\mathrm{tr}(\mathbb{E}[\mathbf{s}\mathbf{y}^{\mathrm{H}}]\, \boldsymbol{W}_{RF}\boldsymbol{W}_{BB})$ as

$$\mathrm{tr}(\mathbb{E}[\mathbf{s}\mathbf{y}^{\mathrm{H}}]\, \boldsymbol{W}_{RF}\boldsymbol{W}_{BB}) = \mathrm{tr}\big(\, \boldsymbol{W}_{MMSE}^{\mathrm{H}}\mathbb{E}[\mathbf{y}\mathbf{y}^{\mathrm{H}}]\boldsymbol{W}_{RF}\boldsymbol{W}_{BB}\big) \quad (3.29)$$

Thus, by inserting (3.29) back to (3.26), we can obtain

$$\begin{aligned}\mathcal{J}(\boldsymbol{W}_{RF}, \boldsymbol{W}_{BB}) &= \mathrm{tr}\big(\boldsymbol{W}_{MMSE}^{\mathrm{H}}\mathbb{E}[\mathbf{y}\mathbf{y}^{\mathrm{H}}]\boldsymbol{W}_{MMSE}\big) - 2\mathcal{R}\big\{\mathrm{tr}\big(\, \boldsymbol{W}_{MMSE}^{\mathrm{H}}\mathbb{E}[\mathbf{y}\mathbf{y}^{\mathrm{H}}]\boldsymbol{W}_{RF}\boldsymbol{W}_{BB}\big)\big\} \\ &+ \mathrm{tr}(\boldsymbol{W}_{BB}^{H}\boldsymbol{W}_{RF}^{H}\mathbb{E}[\boldsymbol{y}\boldsymbol{y}^{H}]\, \boldsymbol{W}_{RF}\boldsymbol{W}_{BB}) \quad (3.30)\end{aligned}$$

Apply factorization for (3.30), we have

$$\mathcal{J}(\boldsymbol{W}_{RF}, \boldsymbol{W}_{BB}) = \mathrm{tr}\big((\boldsymbol{W}_{MMSE} - \boldsymbol{W}_{BB}^{H}\boldsymbol{W}_{RF}^{H})\mathbb{E}[\boldsymbol{y}\boldsymbol{y}^{H}] \times (\boldsymbol{W}_{MMSE} - \boldsymbol{W}_{BB}^{H}\boldsymbol{W}_{RF}^{H})^{H}\big) \quad (3.31)$$

Finally, use the trace-norm conversion property on (3.31), it becomes

$$\mathcal{J}(\boldsymbol{W}_{RF}, \boldsymbol{W}_{BB}) = \left\|\mathbb{E}[\boldsymbol{y}\boldsymbol{y}^{H}]^{\frac{1}{2}}(\boldsymbol{W}_{MMSE} - \boldsymbol{W}_{RF}\boldsymbol{W}_{BB})\right\|_{F}^{2} \quad (3.32)$$

Thus, the MMSE estimation problem described in (3.22) becomes

$$(\boldsymbol{W}_{RF}^{opt}, \boldsymbol{W}_{BB}^{opt}) = \underset{\boldsymbol{W}_{RF}, \boldsymbol{W}_{BB}}{\mathrm{argmin}} \left\|\mathbb{E}[\boldsymbol{y}\boldsymbol{y}^{H}]^{\frac{1}{2}}(\boldsymbol{W}_{MMSE} - \boldsymbol{W}_{RF}\boldsymbol{W}_{BB})\right\|_{F} \quad (3.33)$$

$$s.t.\ \boldsymbol{W}_{RF} \in \mathcal{W}_{RF},$$

This is equivalent to find the optimal ($\boldsymbol{W}_{RF}\boldsymbol{W}_{BB}$) which achieves the minimum distance from the unconstrained MMSE combiner$\boldsymbol{W}_{MMSE}$. The solution algorithm is therefore close to the design of hybrid precoder. However, one difference worth mentioning is that the projection is measured by using an $\mathbb{E}[\boldsymbol{y}\boldsymbol{y}^H]^{\frac{1}{2}}$-weighted Fresenius form rather than a standard norm$\|*\|_F^2$. Similarly, by further embedded the constraint of $\boldsymbol{W}_{RF}$ in (3.33) thanks to the structure of clustered mmWave channels, a near-optimal baseband combiner $\widetilde{\boldsymbol{W}}_{BB}^{opt}$ can be found as

$$\widetilde{\boldsymbol{W}}_{BB}^{opt} = \underset{\widetilde{\boldsymbol{W}}_{BB}}{\operatorname{argmin}} \left\| \mathbb{E}[\boldsymbol{y}\boldsymbol{y}^H]^{\frac{1}{2}} \left(\boldsymbol{W}_{MMSE} - \boldsymbol{A}_r \widetilde{\boldsymbol{W}}_{BB} \right) \right\|_F \tag{3.34}$$

$$s.t.\ \left\| \operatorname{diag}\left(\widetilde{\boldsymbol{W}}_{BB} \widetilde{\boldsymbol{W}}_{BB}^H \right) \right\|_0 = N_r^{RF},$$

where $\boldsymbol{A}_r = [\, \mathbf{a}_{\mathrm{r}}(\phi_{1,1}^r, \theta_{1,1}^r), \ldots, \mathbf{a}_{\mathrm{r}}\left(\phi_{N_{cl},N_{ray}}^r, \theta_{N_{cl},N_{ray}}^r\right)]$ is an $N_r \times N_{cl}N_{ray}$ matrix of array response vectors and $\widetilde{\boldsymbol{W}}_{BB}$ is an $N_{cl}B_{ray} \times N_s$ matrix.

Hence, the detailed algorithm can be described as follows.

Algorithm 2 Spatially Sparse MMSE Combining via Orthogonal Matching Pursuit [15]

Input: $\boldsymbol{W}_{MMSE}$

Output: $\boldsymbol{W}_{RF}, \boldsymbol{W}_{BB}$

1. $\boldsymbol{W}_{RF} = Empty\ Matrix$
2. $\boldsymbol{W}_{res} = \boldsymbol{W}_{MMSE}$
3. **For** $i \leq N_r^{RF}$ **do**
4. $\boldsymbol{\psi} = \boldsymbol{A}_r^H \mathbb{E}[yy^H] \boldsymbol{F}_{res}$
5. $k = argmax_{l=1,\ldots,N_{cl}N_{ray}} (\boldsymbol{\psi}\boldsymbol{\psi}^*)_{l,l}$
6. $\boldsymbol{W}_{RF} = [\, \boldsymbol{W}_{RF} | \boldsymbol{A}_r^{(k)}]$
7. $\boldsymbol{W}_{BB} = (\, \boldsymbol{W}_{RF}^H\, \mathbb{E}[yy^H] \boldsymbol{W}_{RF})^{-1}\, \boldsymbol{W}_{RF}^H\, \mathbb{E}[yy^H] \boldsymbol{W}_{MMSE}$
8. $\boldsymbol{F}_{res} = \frac{\boldsymbol{W}_{MMSE} - \boldsymbol{W}_{RF}\boldsymbol{W}_{BB}}{\| \boldsymbol{W}_{MMSE} - \boldsymbol{W}_{RF}\boldsymbol{W}_{BB} \|_F}$
9. **End for**
10. **Return** $\boldsymbol{F}_{RF}, \boldsymbol{F}_{BB}$

Based on number of RF chains at transmitter or receiver, we shall also define the following order for determining the precoder or combiner since we calculate one of them with the assumption of fixing the other.

Hence, the rule [15] is

$$N_t^{RF} \leq N_r^{RF} \begin{cases} 1.\ \text{Solve for } \boldsymbol{F}_{RF}\boldsymbol{F}_{BB} \text{ using Algorithm 1.} \\ 2.\ \text{Given } \boldsymbol{F}_{RF}\boldsymbol{F}_{BB}, \text{solve for } \boldsymbol{W}_{RF}\boldsymbol{W}_{BB} \text{ using Algorithm 2.} \end{cases}$$

$$N_t^{RF} > N_r^{RF} \begin{cases} 1.\ \text{Solve for } \boldsymbol{W}_{RF}\boldsymbol{W}_{BB} \text{ using Algorithm 2 assuming } \boldsymbol{F}_{RF}\boldsymbol{F}_{BB} = \boldsymbol{F}_{opt}. \\ 2.\ \text{Solve for } \boldsymbol{F}_{RF}\boldsymbol{F}_{BB} \text{ for the effective channel } \boldsymbol{W}_{BB}^{*}\boldsymbol{W}_{RF}^{*}\boldsymbol{H}. \end{cases}$$

In other words, starting by solving the more constrained side which has smaller number of RF chains (basis vectors) and then solve the remaining precoding/combining process with the assumption of fixed precoding/combining which has already been solved previously.

It is also noted that the channel knowledge may not be perfectly available in practical systems. Thus, in the simulation of this system, the author will consider a quantization on the RF precoder $\boldsymbol{F}_{RF}$. The detailed quantization process is stated as follows.

Since $\boldsymbol{F}_{RF}$ has N_t^{RF}columns of the steering vector $\mathbf{a}_{\mathrm{t}}(\phi, \theta)$, meaning that $\boldsymbol{F}_{RF}$ admits the natural parametrization regarding to the N_t^{RF} used azimuth and elevation angles. Thus, if we define B_{RF} as the number of quantization bits, then range of azimuth or elevation angles can be quantized by $2^{B_{RF}}$ blocks. For example, if the range of elevation angle is $[0, \pi]$, the codebook for elevation angle at receiver can be constructed with a uniform distribution such that

$$\theta = \left[0, \frac{\pi}{2^{B_{RF}}}, \frac{2\pi}{2^{B_{RF}}}, \frac{3\pi}{2^{B_{RF}}}, \dots, \frac{(2^{B_{RF}} - 1)\pi}{2^{B_{RF}}}\right] \tag{3.35}$$

The actual generated elevation angle ate receiver will be quantized to the nearest block in the codebook and then the selected angle in the codebook with the closest distance to the actual elevation angle will be deemed as the quantized elevation angle. The index of the selected angle in the codebook will also be recorded and fed back to the transmitter.

The quantized azimuth or elevation (AOA/AOD) at transmitter or receiver side will build up the corresponding array response vectors. Further, the quantized array response vectors would construct the channel matrix. System with changing channel matrix will certainly have different rates. Hence, we can clearly see how the quantization of RF precoder will affect the system performance.

The quantization of baseband precoder $\boldsymbol{F}_{BB}$ should be based on the Grassmann manifold [24, 25]. Appropriate codebooks for $\boldsymbol{F}_{BB}$ can be designed using Lloyd's algorithm on a training set of baseband precoders and using the chordal distance as a distance measure [26]. However, due to the fundamental knowledge constraint and high complexity of the algorithm, the author cannot derive the approach for the quantization of baseband precoder.

3.4. Simulation Results and Performance Analysis

In this section, different simulation results will be presented for this spatially sparse beamforming design (**Algorithm 1** & **Algorithm 2**). The system parameters are setup as follows. The mmWave propagation channel has $\mathrm{N_{cl}} = 8$ clusters and $\mathrm{N_{ray}} = 10$ rays for each cluster with Laplacian distributed azimuth and elevation AOA/AODs [14, 27]. For simplicity of exposition, all clusters have the same power and angle spread for all azimuth and elevation angles are the same (i.e.$\sigma_{\phi}^{t} = \sigma_{\phi}^{r} = \sigma_{\theta}^{t} = \sigma_{\theta}^{r}$). For receiver, since the location and orientation are random, an Omni-directional antenna array elements are required, leading to a full 360° angle range for both azimuth and elevation. Whereas for transmitter, we assume a narrower transmission range to form a more directional signal due to the high pass-loss in the propagation environment of mmWave system. The space among antennas arrays is assumed to be half-wavelength. Two common configuration are mainly adopted in this section unless stated otherwise.

1. $N_t = 64, N_r = 16, N_t^{RF} = 4, N_r^{RF} = 4$;
2. $N_t = 256, N_r = 64, N_t^{RF} = 6, N_r^{RF} = 6$.

The detailed reason for such selections will be illustrated with the simulation results. Due to the limitation of simulation time, most simulation settings will adopt the first configuration which has a much shorter simulation time than configuration 2 but still possesses the property of massive MIMO.

The performance of spatially sparse beamforming, analog-only beamforming and unconstrained precoding solved by using SVD will be compared for each plot in this section. The same total power constraint is enforced for all three beamforming strategies. The signal to noise ratio (SNR) is defined as $\frac{\rho}{\sigma_n^2}$ which is the same in (2.1). In Figure 8, Figure 9, Figure 10, Figure 11, and Figure

12, perfect channel knowledge is assumed to be available at transmitter while Figure 13, Figure 14 will investigate the limited feedback of spatially sparse beamforming due to quantization impact.

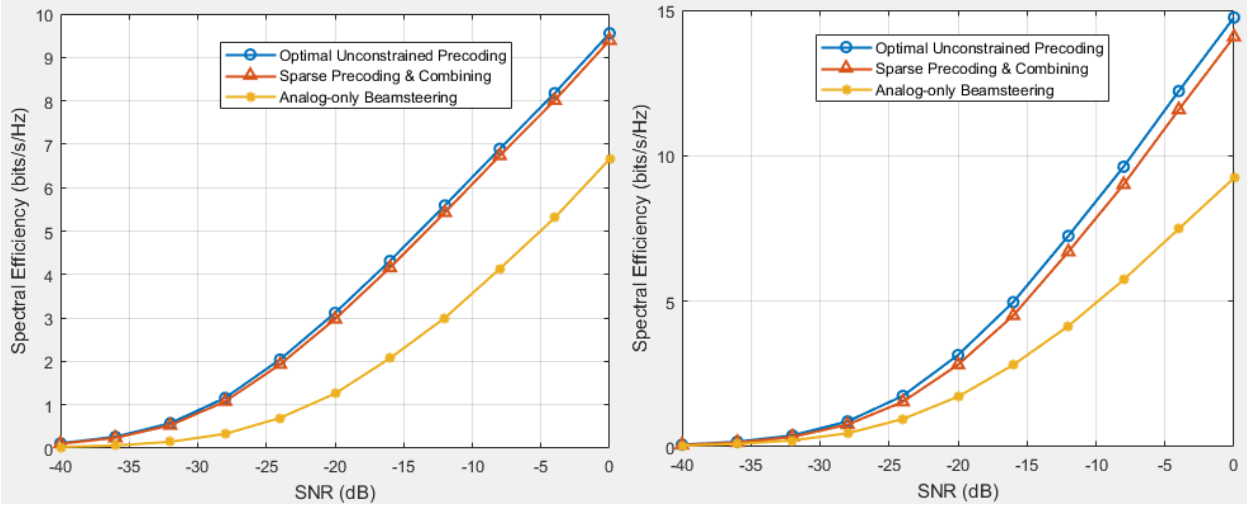

(a) $N_s = 1$ (b) $N_s = 2$

Figure 8: Spectral efficiency vs. SNR by using spatially sparse beamforming for a 64×16 mmWave system with square planar arrays at transmitter and receiver and, with $N_t^{RF} = N_r^{RF} = 4$. The number of clusters is assumed as $N_{cl} = 8$ with $N_{ray} = 10$. The angular spread is set as 7.5°. The number of RF chains assumed at transmitter and receiver are both four in the system. Two cases are shown for single data stream in (a) and two data streams in (b).

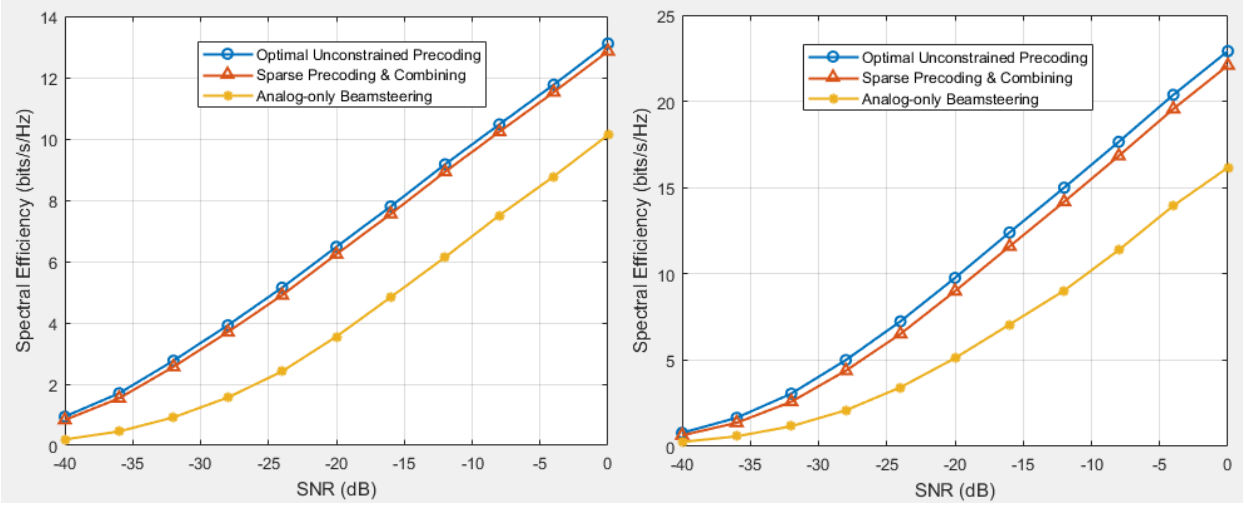

(a) $N_s = 1$ $N_s = 2$

Figure 9: Spectral efficiency vs. SNR by using spatially sparse beamforming for a 256×64 mmWave system with square planar arrays at transmitter and receiver and, with $N_t^{RF} = N_r^{RF} = 4$. The number of clusters is assumed as $N_{cl} = 8$ with $N_{ray} = 10$. The angular spread is set as 7.5°. The number of RF chains assumed at transmitter and receiver are both six in the system. Two cases are shown for single data stream in (a) and two data streams in (b).

Figure 8 shows the spectral efficiency achieved for a mmWave massive MIMO system with 64 BS antennas and 16 MS antennas with square planar arrays. In both (a) and (b), the sparse precoding

& combining design achieves a near-optimal spectral efficiency compared with the optimal unconstrained precoding using SVD. This implies that the spatially sparse hybrid beamforming design can approximate the channel's dominant singular vectors accurately as a combination of four steering vectors. The sparse hybrid beamforming significantly outperforms than analog-only beamforming for any cases. The rate gap between sparse hybrid beamforming and optimal unconstrained precoding (fully digital beamforming) is narrower when $N_s = 1$ compared with $N_s = 2$. This is because more data streams can incur rate difference accumulation when sum up the achievable rate. It is noted that to the number of RF chains should be twice larger than the number of data streams to achieve a fully-digital beamforming performance [1]. Thus, the number of data streams in this section can only be 1 or 2 if 4 RF chains are used.

Similarly, Figure 9 plots the performance with same system settings but with a much larger antenna arrays. In this case, $N_t = 256, N_r = 64, N_t^{RF} = 6, N_r^{RF} = 6$. The performance of sparse hybrid beamforming design stills shows its huge advantage over analog-only beamforming even for a very large antenna arrays. The rate gap shares the similar characteristics described for Figure 8.

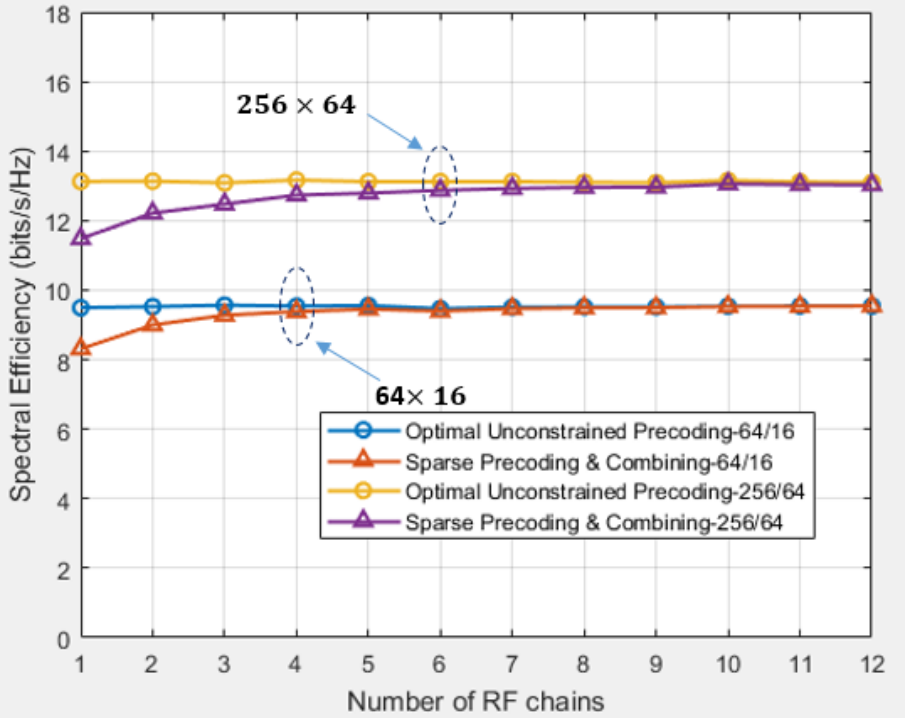

Figure 10: Spectral efficiency vs. Number of RF chains by using spatially sparse beamforming for (64×16) *and* (256×64)*mmWave systems with square planar arrays at transmitter and receiver. The number of clusters is assumed as* $N_{cl} = 8$ *with* $N_{ray} = 10$*. The angular spread is set as 7.5°. The number of RF chains assumed at transmitter and receiver are set equally in the system. Two data stream* $N_s = 1$ *are assumed for both scenarios.*

Figure 10 investigates the impact of RF chains for two different configurations. It is shown that with the increase of RF chain amounts, the spectral efficiency experiences a significant growth in the beginning while remains the same when $\mathrm{N_t^{RF}} = \mathrm{N_r^{RF}}$reaches to 6. The figure indicates that only a few number of RF chains are needed for a near-optimal system performance for both scenarios. This is because the most dominant beamsteering vectors imposed by the mmWave channel's dominant physical directions are sufficient to reconstruct the optimal precoder. More RF chains than the required number can only provide very minor growth on the rate and which can be negligible. In addition, RF chains are expensive hardware devices. Hence, we should reduce its quantity as much as possible while maintain the same level of achievable rate. Hence, to satisfy a near-optimal spectral efficiency, we select the minimum number of RF chains that meet this requirement, where $\mathrm{N_t^{RF}} = \mathrm{N_r^{RF}} = 4$ for $N_t = 64, N_r = 16$ and $\mathrm{N_t^{RF}} = \mathrm{N_r^{RF}} = 6$ for $N_t = 256, N_r = 64$.Thus, the extra RF chains over the minimum require number are redundant.

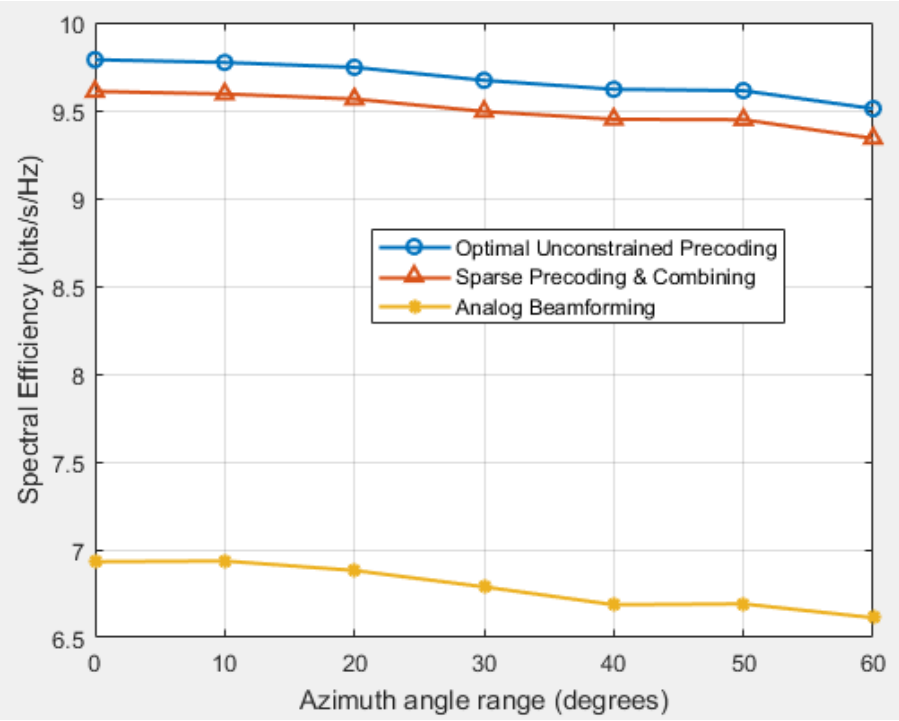

Figure 11: Spectral efficiency vs. Number of RF chains by using spatially sparse beamforming for a (64×16)*mmWave system with square planar arrays at transmitter and receiver at SNR=0, and with* $N_t^{RF} = N_r^{RF} = 4$*. The number of clusters is assumed as* $N_{cl} = 8$ *with* $N_{ray} = 10$*. The angular spread is set as 7.5°. Data stream* $N_s = 1$*.*

Figure 11 investigates the impact of azimuth angle range at BS on the system performance. The default azimuth angle range setting is $[0 - 60°]$ for all other simulation scenarios in this section. However, by restricting the azimuth angle within a narrower range, we can clearly see a growth of spectral efficiency. This is because the BS antenna arrays are expected to form more directional

beamsteering vectors if the azimuth angle range shrinks. The bigger shrinkage will lead to a smaller range which can subsequently generate more directional beams. The more directional and narrower beam will ultimately increase the spectral efficiency. However, the growth at low azimuth angle range is limited compared with the default setting (less than 10%). This is because azimuth angle is only one dimension for beams in transmission, the elevation angle also plays an important role in forming the beamsteering vectors. Also, there is an angle spread (7.5°) added for each angle and then all AOAs and AODs will be generated based on Laplacian distribution. All these variables explains the limited rate increase with even a very small range of azimuth angle.

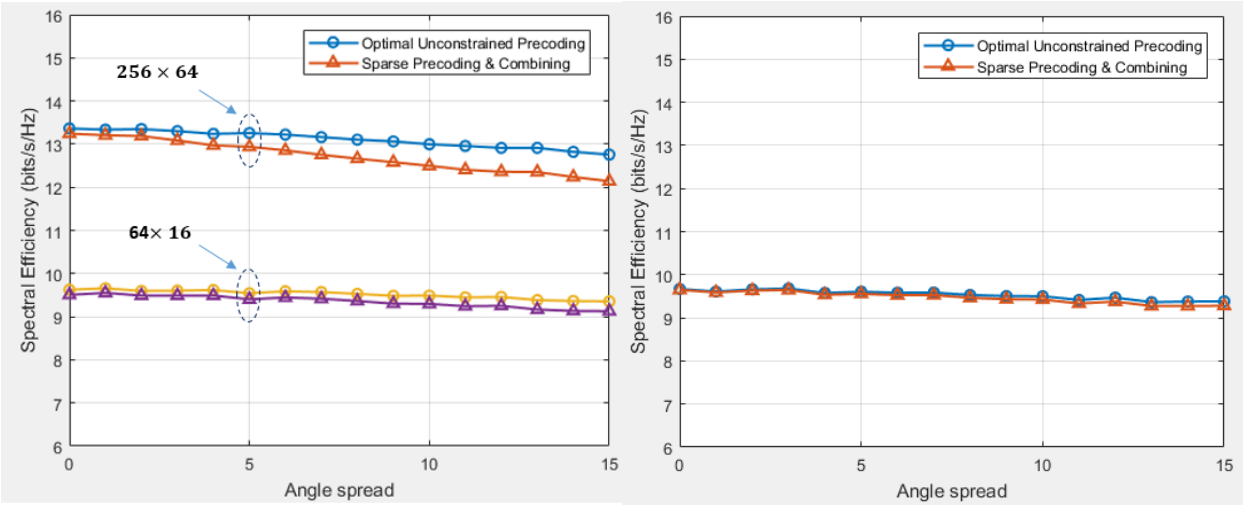

(a) $N_t^{RF} = N_r^{RF} = 4$ (b) $N_t^{RF} = N_r^{RF} = 6$

Figure 12: Spectral efficiency vs. Number of RF chains by using spatially sparse beamforming for a (64×16)*mmWave system with square planar arrays at transmitter and receiver at SNR=0. The number of clusters is assumed as* $N_{cl} = 8$ *with* $N_{ray} = 10$*. Data stream* $N_s = 1$*.*

Figure 12 illustrates the impact of angle spread on the system performance. For simplicity of exposition, the angle spread of all azimuth/elevation angles are equal (i.e.$\sigma_\phi^t = \sigma_\phi^r = \sigma_\theta^t = \sigma_\theta^r$). It is observed that as angle spread increases, the system performance degrades due to richer scattering in mmWave channel. However, the rate gap remains below 10% even for a significant angle spread such as $15°$. For smaller angle spread such as $5°$ for 64×16 massive MIMO system, the degradation is negligible. For a larger antenna arrays configuration such as 256×64. Angle spread can have a larger impact on the rate gap between optimal unconstrained precoding and sparse hybrid beamforming although it is still within an acceptable range.

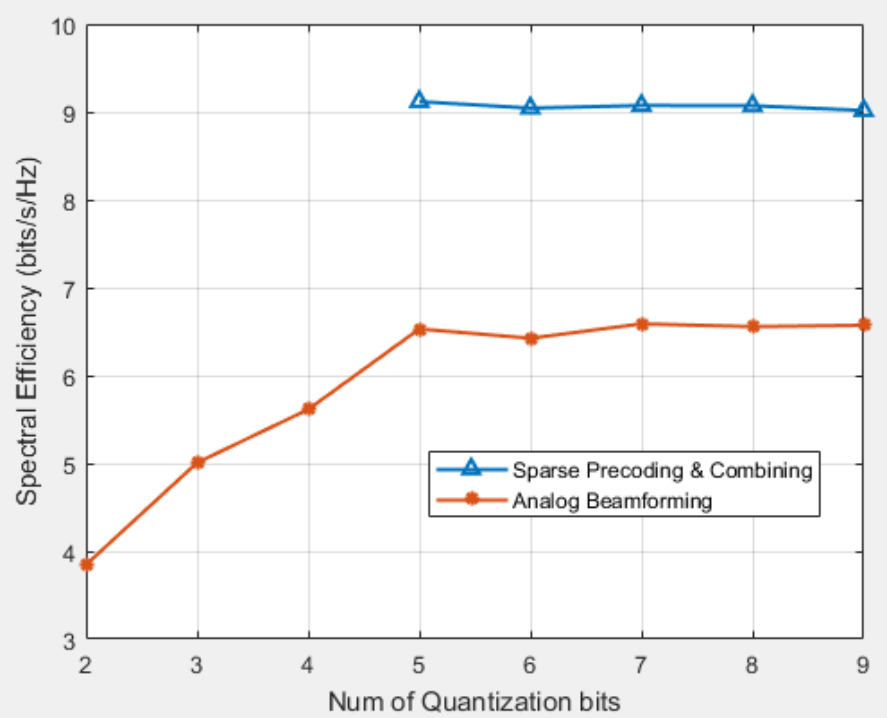

Figure 13: Spectral efficiency vs. Number of RF chains by using spatially sparse beamforming for a (64×16) *mmWave system with square planar arrays at transmitter and receiver at SNR=0, and with* $N_t^{RF} = N_r^{RF} = 4$*. Data stream* $N_s = 1$*. Quantized AOA/AODs are used using the approach depicted in 3.3.*

Figure 13 investigates the impact of quantization bits on the system performance. The approach to build the codebook of azimuth or elevation AOA/AODs are presented in 3.3. It is founded that there is a minimum quantization bits requirement to implement the sparse precoding combing design algorithm. This finding to some extent coincides with the statement in [1] (Section 3.3). Once the number of quantization bits reaches to 5, larger bits are not needed for higher spectral efficiency. This is because 5 quantization bits are sufficient to give accurate feedbacks. For analog-beamforming, there is a dramatic increase as the number of quantization bits grows from 2 to 5. If 2 bits are used, then 4 possible choices cannot describe the actual direction of beamsteering vector accurately. However, if the quantization bits become 5, then 32 options are sufficient to quantize the dominant paths in mmWave channel. This outcome differs from the simulation results in [15] to some extent, however, is still reasonable according to the settings in this system model. Besides, under any circumstances, the sparse precoding & combining design outperforms at least 30% than analog beamforming in this simulation plot.

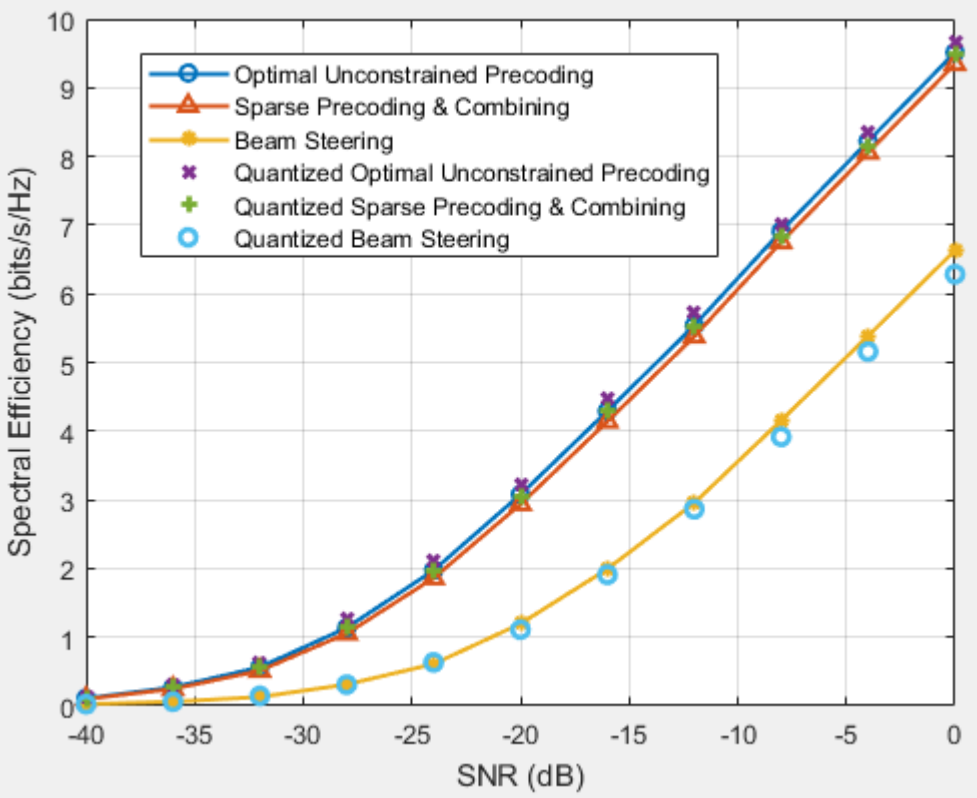

Figure 14: Spectral efficiency vs. Number of RF chains by using spatially sparse beamforming for a (64×16) *mmWave system with square planar arrays at transmitter and receiver and with* $N_t^{RF} = N_r^{RF} = 4$*. Data stream* $N_s = 1$*. Quantized AOA/AODs are used using the approach depicted in 3.3 with a quantization bits of 5.*

Figure 14 illustrates the system performance for a particular scenario. The system parameter settings are the same with Figure 8. However, the spectral efficiencies achieved with 5 quantization bits per angle are also plotted. It is found that achievable rates using quantized angles have almost no change compared with infinite-resolution quantization (perfect channel knowledge). Thus, this figure also validate the finding from Figure 13 from another point of view.

3.5. Summary

In this chapter, a spatially sparse hybrid beamforming design is investigated and simulated. The design of optimal precoder is reformulated as a sparsity-constrained signal recovery problem. The solution to the problem is to use orthogonal matching pursuit (OMP). The same problem can be applied for finding the sub-optimal combiner. The performance that this algorithm achieved is near-optimal and can also be suitable for limited feedback systems by quantizing the RF precoders. A future work that mainly involves an investigation to the baseband precoder quantization is needed.

Chapter 4

4. Two-stage Multi-user Hybrid Beamforming Design in Millimeter Wave Massive MIMO Systems

In this chapter, a low-complexity hybrid analog/digital precoding for downlink multiuser mmWave systems are presented.

4.1. System Model

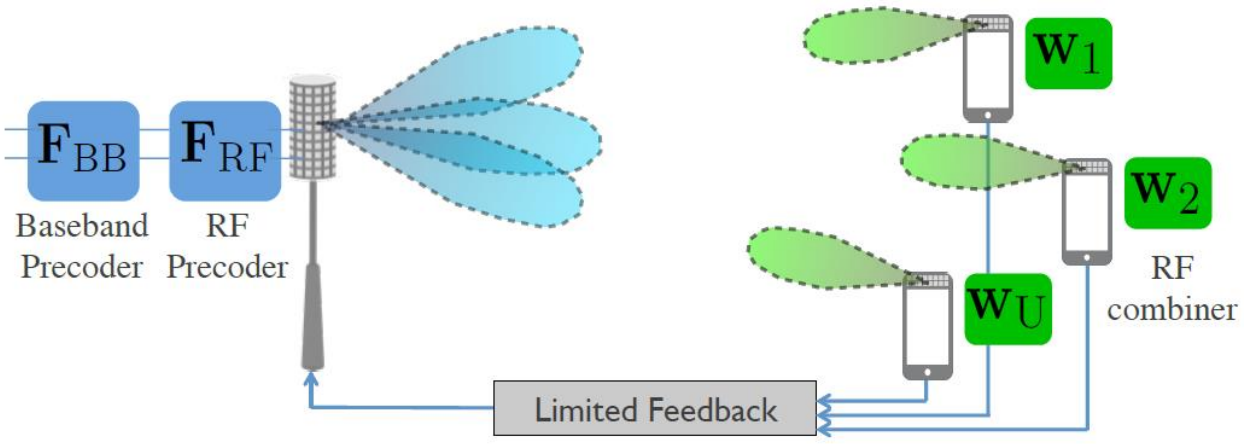

Figure 15: A multi-user mmWave downlink system model, in which a BS uses hybrid analog/digital precoding and a large antenna array to serve U MSs. Each MS employs analog-only combining and has a limited feedback channel to the BS [12].

A multi-user mmWave system shown in Figure 15 illustrates the simplified hybrid beamforming architecture that with analog-combining only. A base station with N_t antennas and N_t^{RF} RF chains

is assumed to communicate with U mobile stations (users). Each MS is equipped with N_r antennas as depicted in Figure 16. In this system, we focus on the multi-user beamforming where the BS communicates with each MS by only one data stream, $i.e. N_s = 1$. Hence, the total number of streams equal to the number of MS. Since for a multi-user hybrid precoding system with $N_t > N_t^{RF}$, its spatial multiplexing gain is limited by $\min(N_t^{RF}, U)$, we assume that the maximum quantity of users that can be served simultaneously by the BS equals to N_t^{RF}. In other words, if $N_t^{RF} > U$, this model will only use U out of N_t^{RF} RF chains to serve U users.

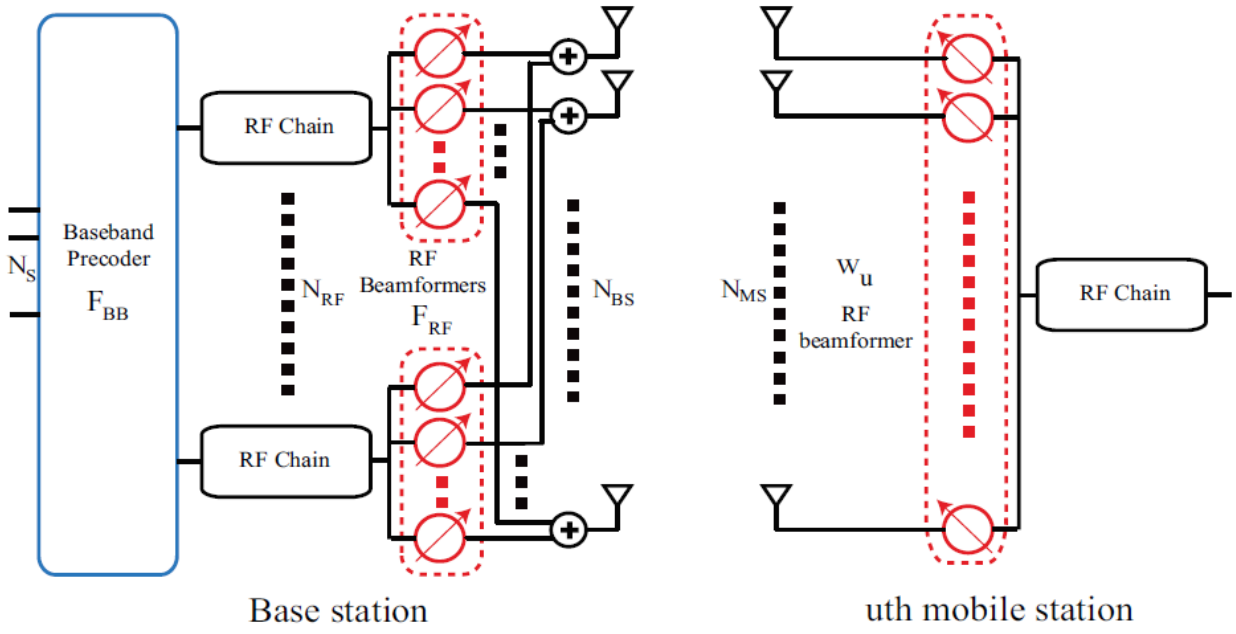

Figure 16: A hybrid beamforming architecture for multi-user MIMO system with hybrid precoding and analog-only combining [21]

In the downlink process, the transmitted symbol signal after precoding will become

$$\boldsymbol{x} = \boldsymbol{F}_{RF}\boldsymbol{F}_{BB}\boldsymbol{s}, \tag{4.1}$$

where $\boldsymbol{s} = [s_1, s_2, \dots, s_U]^T$ is a $U \times 1$vector with $\mathbb{E}[\boldsymbol{s}\boldsymbol{s}^H] = \frac{P}{U}\boldsymbol{I}_U$. P is the average total transmission power and an equal power allocation strategy will be applied for all different user streams. Note that as this is a multi-user system, the symbols are transmitted to multi-users in parallel, which is different from the single-user transmission MIMO system in chapter 3. The baseband precoder $\boldsymbol{F}_{BB} = [\boldsymbol{f}_1^{BB}, \boldsymbol{f}_2^{BB}, \dots, \boldsymbol{f}_U^{BB}]$ is of dimension $U \times U$ and $\boldsymbol{F}_{RF} = [\boldsymbol{f}_1^{RF}, \boldsymbol{f}_2^{RF}, \dots, \boldsymbol{f}_U^{RF}]$ is of dimension $N_t \times U$. Similar with the constraint in chapter 3, each element in $\boldsymbol{F}_{RF}$ must satisfy $\left|[\boldsymbol{F}_{RF}]_{ij}\right|^2 = N_t^{-1}$. This is due to the constant modulus constraint of phase shifters. The total power constraint is enforced by normalizing $\boldsymbol{F}_{BB}$ such that $\|\boldsymbol{F}_{RF}\boldsymbol{F}_{BB}\|_F^2 = U$.

The channel for mmWave propagation for this system is a narrowband clustered channel model that described in section 2.2.2. Since this is a multi-user system, the extended Saleh-Valenzuela geometric channel model described in 2.2.2 perfectly illustrates the channel model.

Therefore, the received signal before combing can be expressed as

$$\boldsymbol{y}_u = \boldsymbol{H}_u \sum_{\boldsymbol{i=1}}^{\boldsymbol{U}} \boldsymbol{F}_{RF} \boldsymbol{f}_n^{BB} \boldsymbol{s}_n + \boldsymbol{n}_u, \tag{4.2}$$

where $\boldsymbol{H}_u$ is the mmWave transmission channel from base station to the u^{th} mobile station, and noise vector $\boldsymbol{n}$ with i.i.d complex Gaussian (i.e. $n \sim \mathcal{CN}(0, \sigma_n^2)$) along with the channel during signal transmission is also considered.

The received signal $\boldsymbol{y}_u$ will then experience RF combining at the u^{th} mobile station to obtain the processed receiver signal

$$\tilde{y} = \boldsymbol{w}_u^H \boldsymbol{H}_u \sum_{\boldsymbol{n=1}}^{\boldsymbol{U}} \boldsymbol{F}_{RF} \boldsymbol{f}_n^{BB} \boldsymbol{s}_n + \boldsymbol{w}_{\boldsymbol{u}}^{\boldsymbol{H}} \boldsymbol{n}_u, \tag{4.3}$$

where $\boldsymbol{w}_u$ share the similar constant modulus constraint of $\boldsymbol{f}_U^{RF}$. In this chapter, we assume the same condition that depicted in [12] that only analog (RF) beamforming is used at the MS's. This is because MSs are likely to require cheaper hardware as well as lower power consumptions.

4.2. Problem Statement

The main objective of the problem is to design the baseband precoder $\boldsymbol{F}_{BB}$ and RF precoder $\boldsymbol{F}_{RF}$ at the BS as well as RF combiner $\boldsymbol{W}_{RF}$ at the MS to maximize the sum-rate produce in the system.

The total achievable rate can be calculated based on Shannon limit theorem [7] given the processed received signal described in (4.3).

$$R_{sum} = \sum_{u=1}^{U} \log_2 \left(1 + \frac{\frac{P}{U} |\boldsymbol{w}_u^H \boldsymbol{H}_u \boldsymbol{F}_{RF} \boldsymbol{f}_{\boldsymbol{n}}^{BB}|^2}{\frac{P}{U} \sum_{n \neq u} |\boldsymbol{w}_u^H \boldsymbol{H}_u \boldsymbol{F}_{RF} \boldsymbol{f}_{\boldsymbol{n}}^{BB}|^2 + \sigma^2} \right) \tag{4.4}$$

If the sum rate in the system is adopted as a performance metric for designing the hybrid beamformers, then the precoding design problem is to find the optimal RF precoder $\boldsymbol{F}_{RF}$, baseband precoder for each user $[\boldsymbol{f}_u^{BB}]_{u=1}^U$ and RF combiner $[\boldsymbol{w}_u]_{u=1}^U$.

Therefore, we need to solve

$$\left\{ \boldsymbol{F}_{RF}^{opt}, [\, \boldsymbol{f}_u^{BB,opt}]_{u=1}^{U}, [\, \boldsymbol{w}_u^{opt}]_{u=1}^{U} \right\} = \text{argmax} \sum_{u=1}^{U} \log_2 \left(1 + \frac{\frac{P}{U} |\boldsymbol{w}_u^H \boldsymbol{H}_u \boldsymbol{F}_{RF} \boldsymbol{f}_{\boldsymbol{n}}^{BB}|^2}{\frac{P}{U} \sum_{n \neq u} |\boldsymbol{w}_u^H \boldsymbol{H}_u \boldsymbol{F}_{RF} \boldsymbol{f}_{\boldsymbol{n}}^{BB}|^2 + \sigma^2} \right) \quad (4.5)$$

$$s.t. \quad [\, \boldsymbol{F}_{RF}]_{:,u} \in \mathcal{F}_{RF}, u = 1,2, \dots, U$$

$$\boldsymbol{w}_u \in \mathcal{W}_{RF}, u = 1,2, \dots, U,$$

$$\| \boldsymbol{F}_{RF} [\boldsymbol{f}_1^{BB}, \boldsymbol{f}_2^{BB}, \dots, \boldsymbol{f}_U^{BB}] \|_F^2 = U$$

Again, this is a non-convex and combinatorial problem which requires $(\mathcal{F}_{RF})^U \times (\mathcal{W}_{RF})^U$ number of searches for $\boldsymbol{F}_{RF}$ and $[\, \boldsymbol{w}_u]_{u=1}^{U}$. Furthermore, in order to jointly design $\boldsymbol{F}_{BB}$ for the optimal system performance, a large training and feedback overhead are needed, which makes the optimization problem unpractical and almost impossible to solve for the global optimal solution. Therefore, we introduce a two-stage multi-user hybrid precoding design which is presented in 4.3 for sub-optimal solution.

4.3. Two-stage Multi-user Hybrid Precoding Algorithm

The main idea of this algorithm is to split the beamforming process into two stages, each with separate constraints and domains. Since it is a simple and low-complexity algorithm, hence the general procedure is illustrated as follows.

In the first stage, the BS RF precoder $\boldsymbol{F}_{RF}$ and MS RF combiner $[\, \boldsymbol{w}_u]_{u=1}^{U}$ for each user are jointly designed to maximize the desired signal power, neglecting any interference incurred among the different users. Then, in the second stage, the baseband precoder $[\, \boldsymbol{f}_u^{BB}]_{u=1}^{U}$ can be designed for each user to manage the multi-user interference.

Therefore, based on this general idea, the 'two-stage multi-user hybrid precoder' algorithm was proposed by [12] as follows.

Algorithm 3 Two-Stage Multi-User Hybrid Precoders [21]

Input: $\mathcal{F}_{RF}$ BS RF beamforming codebook, $|\mathcal{F}_{RF}| = 2^{B_{RF}^{BS}}$

$\mathcal{W}_{RF}$ MS RF beamforming codebook, $|\mathcal{W}_{RF}| = 2^{B_{RF}^{MS}}$

Output: $\boldsymbol{F}_{RF}, \boldsymbol{F}_{BB}, [\, \boldsymbol{w}_u]_{u=1}^{U}$

First stage: Single-user RF precoding /combining design

1. **For** each MS $u, u = 1,2, \dots, U$
2. The BS and MS u select $\boldsymbol{v}_u^{opt}$ and $\boldsymbol{g}_u^{opt}$ that solve
3. $\{\boldsymbol{g}_u^{opt}, \boldsymbol{v}_u^{opt}\} = \underset{\substack{\forall \boldsymbol{g}_u \in \mathcal{W}_{RF} \\ \forall \boldsymbol{v}_u \in \mathcal{F}_{RF}}}{\operatorname{argmax}} \| \boldsymbol{g}_u^H \boldsymbol{H}_u \boldsymbol{v}_u \|$
4. MS u sets $\boldsymbol{w}_u = \boldsymbol{g}_u^{opt}$
5. BS sets $\boldsymbol{F}_{RF} = [\boldsymbol{v}_1^{opt}, \boldsymbol{v}_2^{opt}, .., \boldsymbol{v}_u^{opt}]$
6. **End for**

Second stage: Multi-user digital precoding design

7. **For** each MS $u, u = 1,2, \dots, U$
8. MS u estimates its effective channel $\bar{\boldsymbol{h}}_u^H = \boldsymbol{w}_u^H \boldsymbol{H}_u \boldsymbol{F}_{RF}$
9. MS u quantizes $\bar{\boldsymbol{h}}_u$ using a codebook $\mathcal{H}$ of size $2^{B_{BB}}$ and feeds back $\hat{\boldsymbol{h}}_u$ where
10. $\hat{\boldsymbol{h}}_u = \underset{\hat{\boldsymbol{h}}_u \in \mathcal{H}}{\operatorname{argmax}} \|\bar{\boldsymbol{h}}_u^H \hat{\boldsymbol{h}}_u\|$
11. BS design $\boldsymbol{F}_{BB} = \hat{\boldsymbol{H}}^H \left(\hat{\boldsymbol{H}} \hat{\boldsymbol{H}}^H\right)^{-1}, \hat{\boldsymbol{H}} = \left[\hat{\boldsymbol{h}}_1, \dots, \hat{\boldsymbol{h}}_U\right]^{\boldsymbol{H}}$
12. BS normalizes $\boldsymbol{f}_u^{BB} = \frac{\boldsymbol{f}_u^{BB}}{\| \boldsymbol{F}_{RF} \boldsymbol{f}_u^{BB} \|_F}, u = 1,2, \dots, U$
13. **End for**

Note that the codebook for RF precoder $\mathcal{F}_{RF}$ and combiner $\mathcal{W}_{RF}$ are defined as the same approach adopted in 3.3. The codebook $\mathcal{H}$ for the effective channel $\bar{\boldsymbol{h}}_u$ is based on a random vector quantization (RVQ) codebook. However, in the simulation section 4.5, the author will assume perfect channel knowledge (no quantization) of the effective channel due to the lack of research on the construction of a RVQ codebook. The limited feedback is only evaluated due to the quantization of $\boldsymbol{F}_{RF}$. The investigation on how to construct and quantize the effective channel to the corresponding RVQ codebook will be an important future work of this research project.

4.4. Performance Analysis with Infinite-Resolution Codebooks

In this section, the achievable rate analysis is based on a perfect channel knowledge assumption. In other words, the codebooks $\mathcal{F}_{RF}, \mathcal{W}_{RF}$, and $\mathcal{H}$ adopted in **Algorithm 3** are of infinite size, which allows continuous values for the AOA/AODs. The lower bound for single-path channel (Theorem 1 in [12]) will be derived. Since mmWave owns the characteristic of sparse scattering for

propagation, the most dominant beamsteering vector will be used for deriving this lower bound for single-path scenario. The simulation results of this lower bound will be shown in 4.5.

Consider the following assumptions:

(1) All channels have only one path in propagation, i.e., the $L_i = 1$ in (2.3).
(2) The RF precoding vectors $\boldsymbol{f}_u^{BB}$ and RF combining vectors $\boldsymbol{w}_u$ are beamsteering vectors with continuous angles.
(3) For receiver, each MS $u, u = 1,2, \dots, U$ possesses the perfect channel knowledge $\boldsymbol{H}_u$.
(4) For transmitter, each BS perfectly possesses the effective channel knowledge $\bar{\boldsymbol{h}}_u$ $u = 1,2, \dots, U$.

Then, we start with the derivation by reconsider step 3 (stage 1) in **Algorithm 3** that $\boldsymbol{H}_u$ has only one path

$$\{\boldsymbol{g}_u^{opt}, \boldsymbol{v}_u^{opt}\} = \underset{\substack{\forall \boldsymbol{g}_u \in \mathcal{W}_{RF} \\ \forall \boldsymbol{v}_u \in \mathcal{F}_{RF}}}{\operatorname{argmax}} \| \boldsymbol{g}_u^H \boldsymbol{H}_u \boldsymbol{v}_u \| \tag{4.6}$$

Then, the optimal RF precoding and combining vectors are

$$\boldsymbol{g}_u^{opt} = \mathbf{a}_{\mathrm{r}}(\theta_u)$$

$$\boldsymbol{v}_u^{opt} = \mathbf{a}_{\mathrm{r}}(\phi_u)$$

As described the step 4 and 5 (stage 1) in **Algorithm 3**, the MS then sets $\boldsymbol{w}_u = \boldsymbol{g}_u^{opt} = \mathbf{a}_{\mathrm{r}}(\theta_u)$ and BS sets $\boldsymbol{f}_u^{RF} = \boldsymbol{v}_u^{opt} = \mathbf{a}_{\mathrm{t}}(\phi_u)$. Concatenate all beamforming vectors for U users, the RF beamforming precoding matrix is $\boldsymbol{F}_{RF} = \left[\boldsymbol{v}_1^{opt}, \boldsymbol{v}_2^{opt}, .., \boldsymbol{v}_u^{opt}\right] = [\mathbf{a}_{\mathrm{t}}(\phi_1), \mathbf{a}_{\mathrm{t}}(\phi_2), \dots, \mathbf{a}_{\mathrm{t}}(\phi_u)] = \boldsymbol{A}_t$. For each user u, the effective channel after determining the RF precoder and combiner is

$$\bar{\boldsymbol{h}}_u^H = \boldsymbol{w}_u^H \boldsymbol{H}_u \boldsymbol{F}_{RF} \tag{4.7}$$

By substituting $\boldsymbol{w}_u = \boldsymbol{g}_u^{opt} = \mathbf{a}_{\mathrm{r}}(\theta_u)$ and $\boldsymbol{H}_u$ modelled in 2.2.2,

$$\begin{aligned} \bar{\boldsymbol{h}}_u^H &= \mathbf{a}_{\mathrm{r}}^H(\theta_u) \sqrt{\frac{N_t N_r}{1}} \alpha_u \mathbf{a}_{\mathrm{r}}(\theta_u) \mathbf{a}_{\mathrm{t}}^H(\phi_u) \boldsymbol{F}_{RF} \\ &= \sqrt{N_t N_r} \alpha_u \mathbf{a}_{\mathrm{t}}^H(\phi_u) \boldsymbol{F}_{RF} \end{aligned} \tag{4.8}$$

Now we define an integrated matrix to concatenate all effective channels by

$$\overline{\boldsymbol{H}} = \left[\overline{\boldsymbol{h}}_1, \overline{\boldsymbol{h}}_2, \dots, \overline{\boldsymbol{h}}_u\right]^H \tag{4.9}$$

Since the RF combiner has been determined, (4.8) can be rewritten as

$$\overline{\boldsymbol{H}} = \boldsymbol{D}\boldsymbol{A}_t^H \boldsymbol{A}_t, \tag{4.10}$$

where D is a $U \times U$ diagonal matrix and $[\boldsymbol{D}]_{u,u} = \sqrt{N_t N_r}\alpha_u$.

Based on step 11 in **Algorithm 3**, the digital baseband precoder can be derived by using Zero-Forcing (ZF)

$$\boldsymbol{F}_{BB} = \overline{\boldsymbol{H}}^H \left(\overline{\boldsymbol{H}\boldsymbol{H}^H}\right)^{-1} \boldsymbol{T}, \tag{4.11}$$

Where $\boldsymbol{T}$ is a diagonal matrix to satisfy the power constraints $\| \boldsymbol{F}_{RF}\, \boldsymbol{f}_u^{BB}\|^2 = 1, u = 1,2,\dots,U$.

The diagonal elements of $\boldsymbol{T}$ equals to

$$\boldsymbol{T}_{u,u} = \sqrt{\frac{N_t N_r}{(\boldsymbol{A}_t^H \boldsymbol{A}_t)^{-1}_{u,u}}}\,|\alpha_u|, u = 1,2,\dots,U \tag{4.12}$$

The proof of this condition is as follows:

By expanding $\| \boldsymbol{F}_{RF}\, \boldsymbol{f}_u^{BB}\|^2$ with the help of (4.9) and (4.10), it shows that

$$\begin{aligned}
\| \boldsymbol{F}_{RF}\, \boldsymbol{f}_u^{BB}\|^2 &= \left([T]_{u,:}\left(\overline{\boldsymbol{H}\boldsymbol{H}^H}\right)^{-1}\overline{\boldsymbol{H}_u}\right)(\boldsymbol{F}_{RF}^H\, \boldsymbol{F}_{RF})\left(\overline{\boldsymbol{H}_u^H}\left(\overline{\boldsymbol{H}\boldsymbol{H}^H}\right)^{-1}[T]_{u,:}\right) \\
&= [T]_{u,:}(\boldsymbol{D}^H)^{-1}(\boldsymbol{A}_t^H\boldsymbol{A}_t\boldsymbol{A}_t^H\boldsymbol{A}_t)^{-1}(\boldsymbol{A}_t^H\boldsymbol{A}_t\boldsymbol{A}_t^H\boldsymbol{A}_t\boldsymbol{A}_t^H\boldsymbol{A}_t)(\boldsymbol{A}_t^H\boldsymbol{A}_t\boldsymbol{A}_t^H\boldsymbol{A}_t)^{-1}(\boldsymbol{D})^{-1}[T]_{u,:} \\
&= [T]_{u,:}(\boldsymbol{D}^H)^{-1}(\boldsymbol{A}_t^H\boldsymbol{A}_t)(\boldsymbol{A}_t^H\boldsymbol{A}_t\boldsymbol{A}_t^H\boldsymbol{A}_t)^{-1}(\boldsymbol{D})^{-1}[T]_{u,:} \\
&= [T]_{u,:}(\boldsymbol{D}^H)^{-1}(\boldsymbol{A}_t^H\boldsymbol{A}_t)^{-1}(\boldsymbol{D})^{-1}[T]_{u,:} \\
&= [T]_{u,u}^2(\boldsymbol{D})^{-2}_{u,u}(\boldsymbol{A}_t^H\boldsymbol{A}_t)^{-1}_{u,u} \\
&= \frac{N_t N_r}{(\boldsymbol{A}_t^H\boldsymbol{A}_t)^{-1}_{u,u}}\alpha_u^2((N_t N_r)^{-1}\alpha_u^{-2})(\boldsymbol{A}_t^H\boldsymbol{A}_t)^{-1}_{u,u} \\
&= 1
\end{aligned}$$

Therefore, by setting $\boldsymbol{T}_{u,u} = \sqrt{\frac{N_t N_r}{(\boldsymbol{A}_t^H\boldsymbol{A}_t)^{-1}_{u,u}}}\,|\alpha_u|, u = 1,2,\dots,U$, the power constraint condition meet.

Then the achievable rate for each user u is

$$
\begin{aligned}
R &= \log\left(1+\frac{SNR}{U}\left|\bar{\boldsymbol{h}}_u^H \boldsymbol{f}_u^{BB}\right|^2\right) \\
&= \log\left(1+\frac{SNR}{U}\left|\bar{\boldsymbol{h}}_u^H \bar{\boldsymbol{h}}_u^H \left(\overline{\boldsymbol{h}_u \boldsymbol{h}_u^H}\right)^{-1} \boldsymbol{T}_{u,u}\right|^2\right) \\
&= \log\left(1+\frac{SNR}{U}\left|\boldsymbol{T}_{u,u}\right|^2\right) \\
&= \log\left(1+\frac{SNR}{U}\frac{N_t N_r|\alpha_u|^2}{(\boldsymbol{A}_t^H \boldsymbol{A}_t)_{u,u}^{-1}}\right) \qquad (4.13)
\end{aligned}
$$

As we know, the beamsteering vectors $[\mathbf{a}_\mathrm{t}(\phi_1), \mathbf{a}_\mathrm{t}(\phi_2), \dots, \mathbf{a}_\mathrm{t}(\phi_u)]$ are linearly independent and the probability of two AOAs $\phi_m = \phi_n, 1 \le m, n \le n$ exactly the same is zero since we assume a continuous angle selection. Thus, the matrix $\boldsymbol{P} = \boldsymbol{A}_t^H \boldsymbol{A}_t$ is positive definite (PD). This property is also validated in MATLAB.

Hence, based on [12] (Lemma 3), for any $n \times n$ Hermitian and PD matrix $\boldsymbol{P}$, with descending eigenvalues $1 < \lambda_{min} \le \lambda_1 \le \cdots \le \lambda_{max}$, the element $(\boldsymbol{P})_{u,u}^{-1}, u = 1,2, \dots, n$ satisfies

$$
(\boldsymbol{P})_{u,u}^{-1} \le \frac{1}{4[\boldsymbol{P}]_{u,u}}\left(\frac{\lambda_{max}(\boldsymbol{P})}{\lambda_{min}(\boldsymbol{P})}+\frac{\lambda_{min}(\boldsymbol{P})}{\lambda_{max}(\boldsymbol{P})}+2\right) \qquad (4.14)
$$

Since $(\boldsymbol{A}_t^H \boldsymbol{A}_t)_{u,u} = 1$, we have $\lambda_{max}(\boldsymbol{A}_t^H \boldsymbol{A}_t) = \sigma_{max}^2(\boldsymbol{A}_t)$ and $\lambda_{min}(\boldsymbol{A}_t^H \boldsymbol{A}_t) = \sigma_{min}^2(\boldsymbol{A}_t)$.

Therefore, by combining (4.13) and (4.14), the lower bound for the achievable rate is

$$
\begin{aligned}
R_u &\ge \log\left(1+\frac{SNR}{U}N_t N_r|\alpha_u|^2\frac{4}{\left(\frac{\lambda_{max}(\boldsymbol{P})}{\lambda_{min}(\boldsymbol{P})}+\frac{\lambda_{min}(\boldsymbol{P})}{\lambda_{max}(\boldsymbol{P})}+2\right)}\right) \qquad (4.15) \\
&= \log\left(1+\frac{SNR}{U}N_t N_r|\alpha_u|^2\frac{4}{\left(\frac{\sigma_{max}^2(\boldsymbol{A}_t)}{\sigma_{min}^2(\boldsymbol{A}_t)}+\frac{\sigma_{min}^2(\boldsymbol{A}_t)}{\sigma_{max}^2(\boldsymbol{A}_t)}+2\right)}\right), SNR = \frac{P}{\sigma^2}
\end{aligned}
$$

This lower bound rate for single path will be a benchmark for evaluating the system performance in 4.5.

4.5. Simulation Results and Performance Analysis

In this section, the performance of two-stage hybrid precoding design described in 4.4 will be presented and analyzed. The performance is evaluated by the average achievable rate over all users, measured by bits/s/Hertz. The azimuth AOD/AODs is uniformly distributed in $[0,2\pi]$ and the elevation AOD/AODs' range is within $[-\frac{\pi}{2},\frac{\pi}{2}]$ with the same distribution. In MATLAB, they are generated by using rand to distribute pseudo random numbers uniformly. The antenna array employed in BS is UPA with size 8×8. Four MSs employed by a 4×4 UPA each is also assumed. These assumptions are used in this section universally unless stated otherwise. The single user rate will be a benchmark for comparison for all other performance measurements. All simulations are run over 500 or 1000 times depending on the system settings to ensure a relatively short simulation time but reliable performances.

Firstly, Figure 17 shows achievable rates against signal to noise ratio for the system model in 4.1. A clear advantage of proposed hybrid precoding (Two-stage multi-user hybrid precoding design) than analog-only beamsteering regarding to spectral efficiency can be observed. The rate achieved by proposed hybrid precoding is also very close to the single-user rate thanks to the cancellation of multi-user interference using zero-forcing in stage 2 in **Algorithm 3**. As SNR increases from -20 dB to 10 dB, all rate values increase. This is easy to understand and can be directly referred to (2.1). It is also noted that with the growth of SNR, the performance gap between analog beamforming and hybrid beamforming increases, meaning that hybrid beamforming is more preferred to use in low noise scenario.

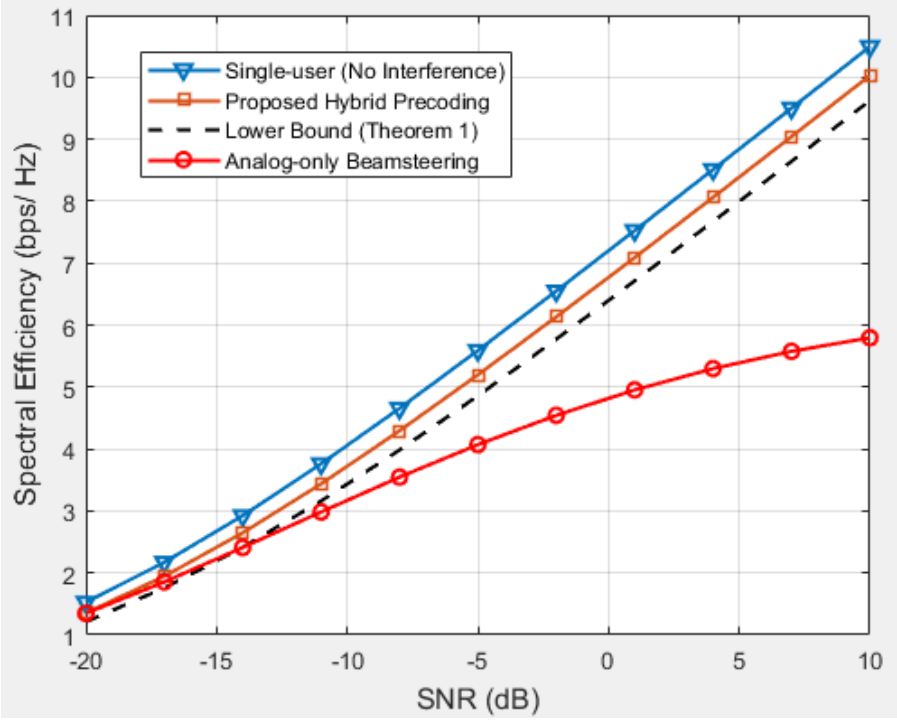

Figure 17: Achievable rates using two-stage multi-user hybrid beamforming design with perfect channel knowledge on both transmitter and receiver. Single path is assumed in propagation. Four users are served in the system. BS antennas are of the size 8×8 *and MS antennas are of the size* 4×4.

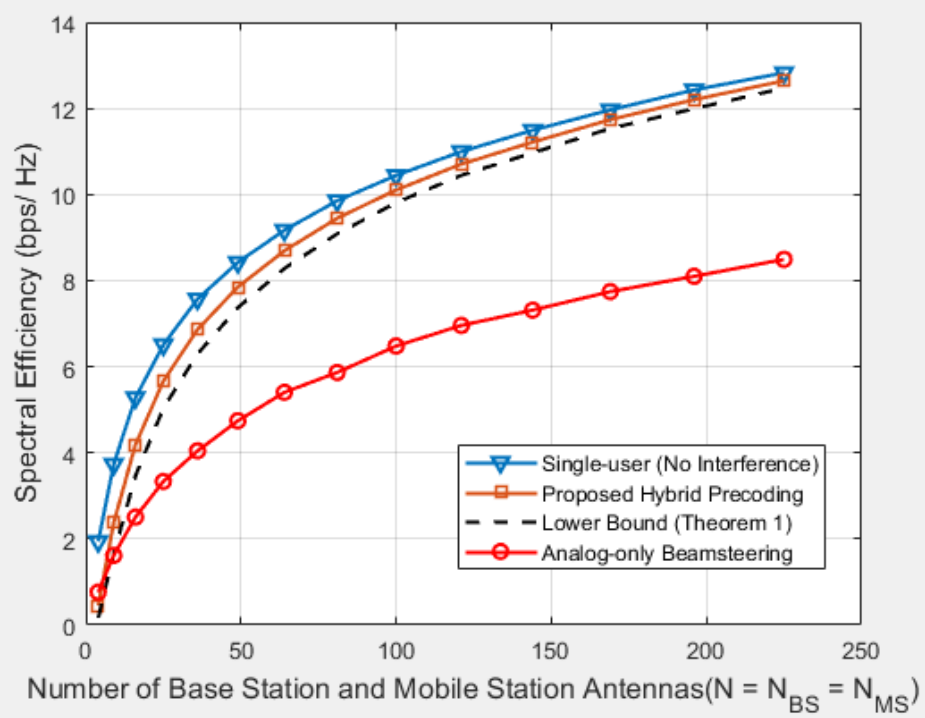

Figure 18: Achievable rates using two-stage multi-user hybrid beamforming design with perfect channel knowledge on both transmitter and receiver. Single path is assumed in propagation. Four users are served in the system. BS and MS are assumed to have the same number of antennas using UPA. The size of both BS and MS UPA changes from 2×2 *to* 15×15. *SNR is set to be 0 dB.*

In Figure 18, we consider the same setup described above, but set the number of antennas at BS and MS equal and change it from 4 to 225. The rate grows with the increase of antenna numbers. The increasing trend of single-user rate and hybrid precoding rate are almost the same and the gap between two lines even shrinks when at larger number of antennas.

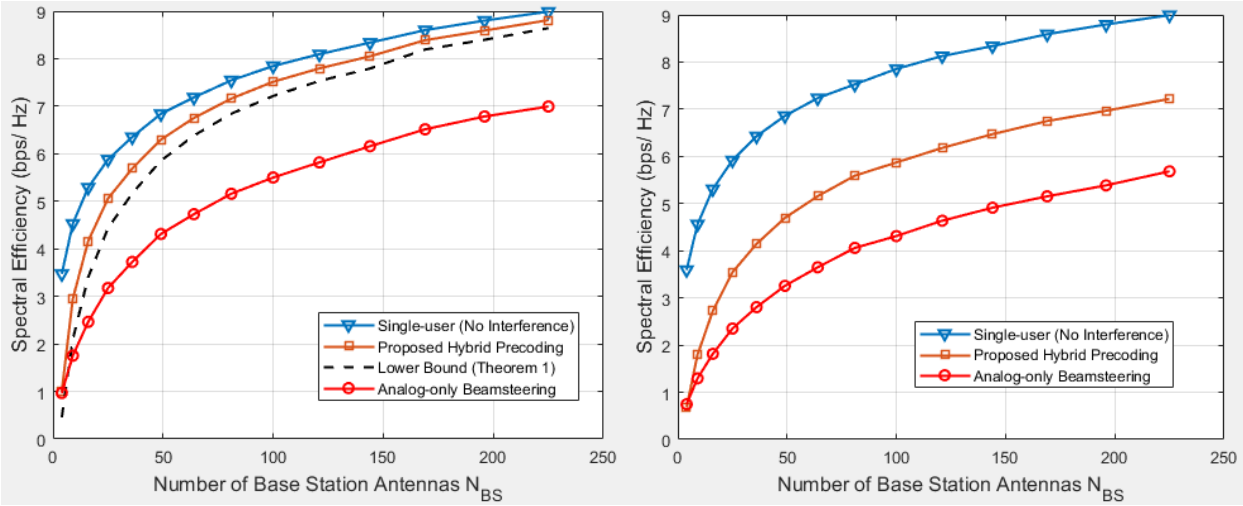

(a) $L = 1$ (b) $L = 3$

Figure 19: Achievable rates using two-stage multi-user hybrid beamforming design with perfect channel knowledge on both transmitter and receiver. Different paths are set for (a) and (b). Four users are served in the system. BS UPA has a square shape and the side length changes from 2 to 15; MS antennas are of the size 4×4. *SNR is set to be 0 dB.*

Figure 19 uses almost the same setup with Figure 18 but only allows the increase of base station antennas. The MS antennas remains by a configuration of 4×4. Also, in (b), the number of path during propagation in mmWave system changes to 3 to compare with $L = 1$ case. It can be clearly seen that both (a) and (b) in Figure 19 share a significant increasing trend for all achievable rates. This also demonstrates the multiplexing gain of massive MIMO. According to [4], there is no theoretical capacity limit and in practice, increasing the number of antennas in BS is one of the most efficient way if a higher spectral efficiency is required. It is interesting to find that compared with (a), when the number of paths increases to 3 rather than single path scenario, both analog beamforming rate and hybrid beamforming rate degrades approximately 20%. This is possibly because the randomness of channel will increase with more multipath components (MPCs).

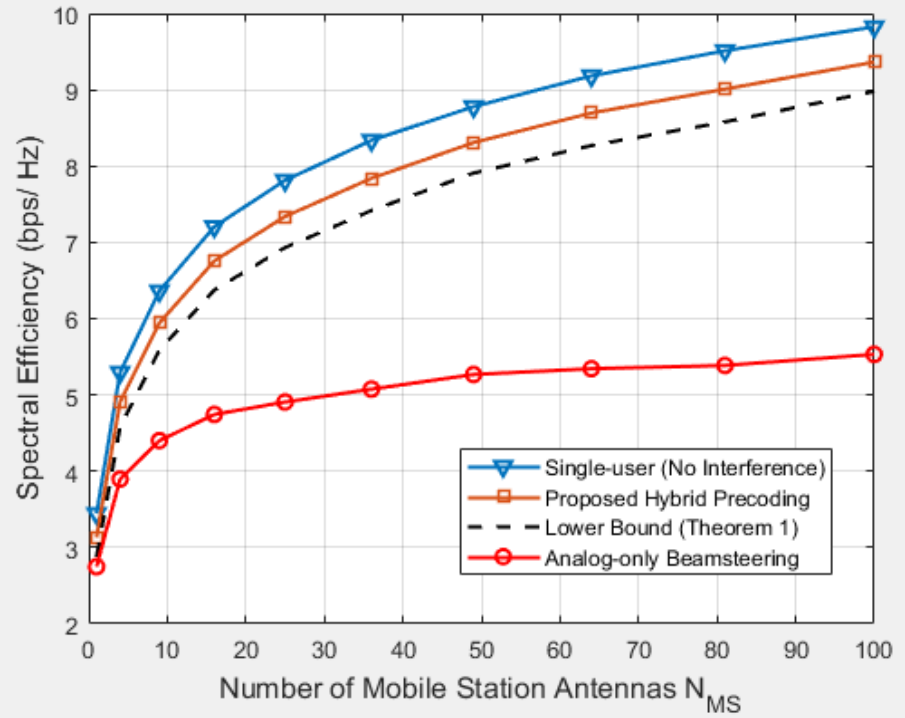

Figure 20: Achievable rates using two-stage multi-user hybrid beamforming design with perfect channel knowledge on both transmitter and receiver. Single path is assumed in propagation. Four users are served in the system. MS UPA has a square shape and the side length changes from 1 to 10; BS antennas are of the size 8×8. *SNR is set to be 0 dB.*

In Figure 20, the same set up is considered but to change the number of antennas at MS. This figure illustrates that the when a large number of antennas are used at MS, the spectral efficiency for analog beamforming nearly saturates while hybrid beamforming still possesses a significant increasing trend. The performance gap between then will be infinity if infinite number of MS antennas are used. The detailed prove according to this finding is shown in [12]. This property implies that when large antenna arrays are employed at the MS, hybrid beamforming in this system model is a more preferred approach and has a higher gain over analog beamforming in mmWave systems.

Figure 21 and Figure 22 will illustrate the impact of RF quantization in terms of the system performance for hybrid and analog-only beamforming. The RF codebook construction approach is presented in 3.3. Also, as stated at the end of 4.3, the quantization of effective channel was not able to be investigated by the author, the system simulated in this section still applies infinite-resolution for the effective channels. Therefore, to compensate for the lack of quantization of effective channel, a relatively high resolution are applied for the finite-resolution case for comparison in Figure 21 and Figure 22.

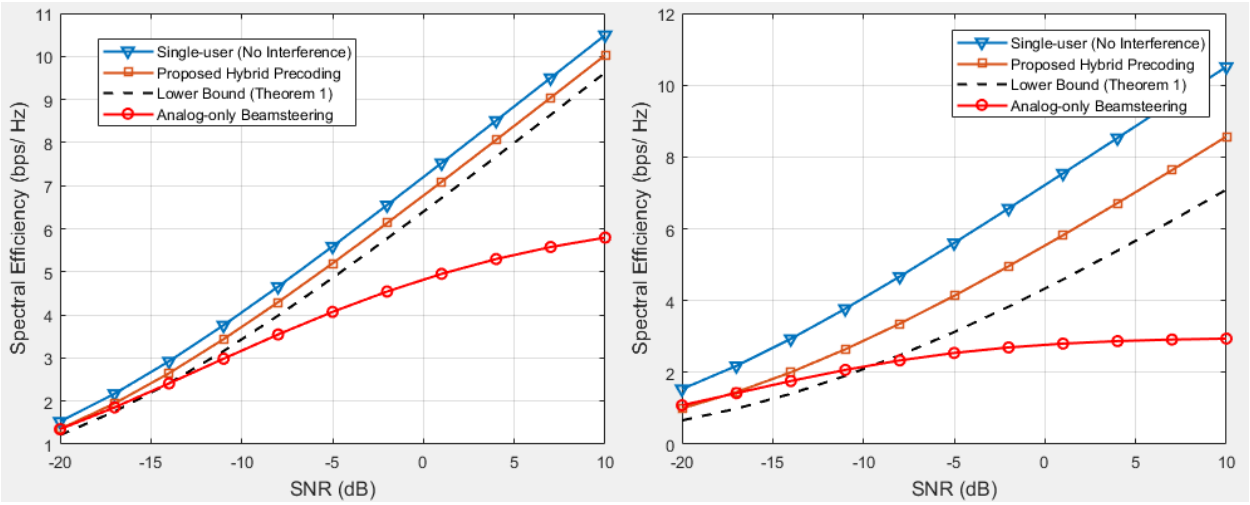

(b) Without quantization (b) With quantization (8 bits)

Figure 21: Achievable rates using two-stage multi-user hybrid beamforming design with perfect channel knowledge on both transmitter and receiver. Single path is assumed in propagation. Four users are served in the system. BS antennas are of the size 8×8 *and MS antennas are of the size* 4×4*. Both RF precoder and combiner have a quantization bits of 8.*

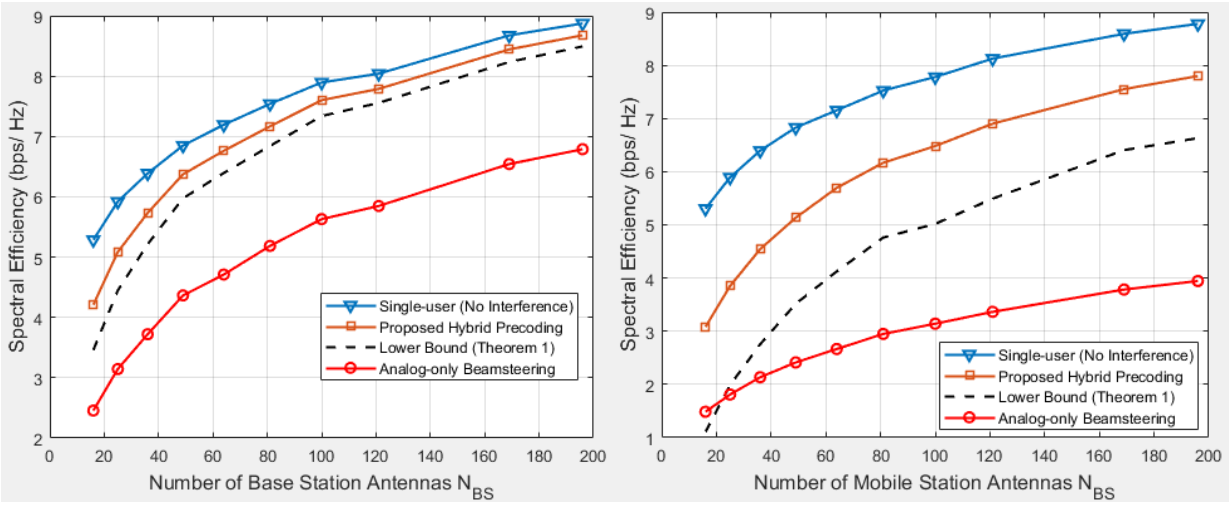

(a) Without quantization (b) With quantization (8 bits)

Figure 22: Achievable rates using two-stage multi-user hybrid beamforming design with perfect channel knowledge on both transmitter and receiver. Single path is assumed in propagation. Four users are served in the system. BS UPA has a square shape and the side length changes from 4 to 14; MS antennas are of the size 4×4*. SNR is set to be 0 dB. Both RF precoder and combiner have a quantization bits of 8.*

Figure 21 sets up the same system parameters with Figure 17. It is clearly seen in (b) that both hybrid precoding and analog-only beersteering (and the corresponding lower bound calculated for single-path scenario) have a performance degradation compared with the spectral efficiency

achieved in (a). Since analog-only beamforming is purely dependent on the beamsteering vectors, the quantization of RF precoder will definitely affect analog beamforming most.

Figure 23: Architecture of Multi-user mmWave system with hybrid precoding and combining illustrates the quantization effect with respect to spectral efficiency when different number of BS antennas are used. Since RF quantization is applied, the number of BS antennas should be greater than or equal to the number of MS antennas. From the figure, we can observe that there are significant rate loss due to the quantization of RF precoder and combiner. The gap difference between hybrid beamforming and lower bound also increases as the number of quantized variables used for calculating (Equation 4.15) the rate is 4, which is larger than 2 quantized variables for calculating (Equation 4.4) the rate of the proposed two-stage hybrid precoding. However, when the number of antenna reaches to a relatively large quantity (e.g. '60' in Figure 21), the gap among each rate maintains at a fixed level. This characteristic is valid for both (a) and (b).

4.6. Summary

In this chapter, a two-stage hybrid beamforming design for downlink multi-user system is investigated and presented. The design is of low-complexity and can leverage the sparse nature of mmWave channel. The performance of single-user, theoretical lower bound for single path scenario, hybrid beamforming and analog-only beamforming are presented and analyzed. Both infinite and finite resolution codebook cases are investigated. However, due to the lack of knowledge on constructing random vector quantization (RVQ) codebooks, the author omits the step of quantization for effective channels instead by assuming a larger resolution bits for RF precoder and combiner. The quantization of effective channels using RVQ codebook will be an important work in the future.

Chapter 5

5. Hybrid MMSE Beamforming Designs for mmWave Multiuser Massive MIMO Systems

5.1. System Model

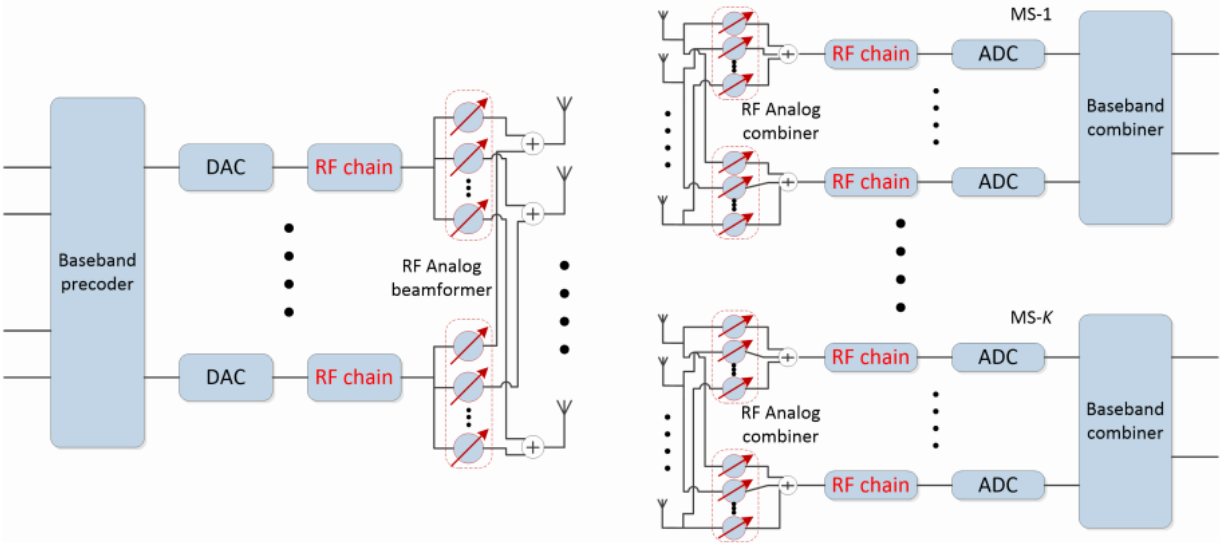

Figure 23: Architecture of Multi-user mmWave system with hybrid precoding and combining

Consider an mmWave massive MIMO system as shown in Figure 23. A BS equipped with N_t antennas and N_t^{RF} RF chains can communicate with K MSs. Similar with the setting in chapter 2, each MS has N_r antennas and only one RF chain. Therefore, each MS can support for one data stream. This assumption is justified in practice because the real MS is assumped to be simple, low

cost and with low power consumption. On the other side, if $K \leq N_t^{RF}$ the BS is able to support multiple data streams to *K* MSs in parallel due to its complex DSP capability.

We mainly focus on the downlink transmission and for downlink, the transmitted symbol $\boldsymbol{s}$ will first be processed by a $N_t^{RF} \times K$ baseband precoder $\boldsymbol{F}_{BB} = [\boldsymbol{f}_1^{BB}, \boldsymbol{f}_2^{BB}, \dots, \boldsymbol{f}_K^{BB}]$ followed by a $N_r \times N_t^{RF}$ RF precoder $\boldsymbol{F}_{RF}$ to become the transmit signal. Given $\boldsymbol{f_i} = \boldsymbol{F}_{RF}\boldsymbol{f}_{BB_i}$ as the combined BS precoding vector for ith MS, in mathematical formulation, the transmitted symbol signal after precoding will become

$$\boldsymbol{x} = \boldsymbol{F}_{RF}\boldsymbol{F}_{BB}\boldsymbol{s} = \sum_{\boldsymbol{i=1}}^{\boldsymbol{K}} \boldsymbol{f_i s_i}\,, \tag{5.1}$$

where $\boldsymbol{s} = [s_1, s_2, \dots, s_U]^T$ is a $U \times 1$ vector. The information symbols are transmitted independently that for each MS it possess the unit power, which means $\mathbb{E}[s_i s_j] = 0, i \neq j$ and $\mathbb{E}[|s_i|^2] = 1$. If the channel $\boldsymbol{H}_i \in \mathcal{C}^{Nr \times N_t}$ represents the propagation channel from the BS the ith MS, then the received signal at ith MS equals to

$$y_i = \boldsymbol{H}_i \boldsymbol{f}_i \boldsymbol{s}_i + \boldsymbol{H}_i \sum_{j \neq i}^{K} \boldsymbol{f}_j \boldsymbol{s}_j + \boldsymbol{n}_i, \tag{5.2}$$

where the noise vector $\boldsymbol{n}$ with i.i.d complex Gaussian (i.e. $n \sim \mathcal{CN}(0, \sigma_n^2)$).

The received signal $\boldsymbol{y}_i$ will then be processed by combining $\boldsymbol{w}_i^H = \boldsymbol{w}_{RF_i}^H \boldsymbol{w}_{BB_i}^H$ at the i^{th} mobile station to obtain the processed received signal

$$\widetilde{\boldsymbol{y}}_{\boldsymbol{\iota}} = \boldsymbol{w}_i^H \boldsymbol{H}_i \boldsymbol{f}_i \boldsymbol{s}_i + \boldsymbol{w}_i^H \boldsymbol{H}_i \sum_{j \neq i}^{\boldsymbol{K}} \boldsymbol{f}_j \boldsymbol{s}_j + \boldsymbol{w}_i^{\boldsymbol{H}} \boldsymbol{n}_i \tag{5.3}$$

Similar with the constrained described in chapter 3 and 4, both $\boldsymbol{F}_{RF}$ and $\boldsymbol{w}_{RF_i}$ have the constant modulus due to the characteristic of phase shifters.

The channel for mmWave propagation for this system is a narrowband clustered channel model that described in section 2.2.2. Since this is a multi-user system, the extended Saleh-Valenzuela geometric channel model described in 2.2.2 perfectly depicts the channel model.

5.2. Problem Statement

Given the processed received signal in (5.3), the signal to interference and noise ratio (SINR) at i^{th} MS is given by

$$SINR_i = \frac{\left|\boldsymbol{w}_i^H \boldsymbol{H}_i \boldsymbol{f}_i\right|^2}{\sum_{j\neq i}^{K}\left|\boldsymbol{w}_i^H \boldsymbol{H}_i \boldsymbol{f}_i\right|^2 + \sigma^2 \|\boldsymbol{w}_i\|^2} \tag{5.4}$$

If the transmit signal can be characterized as Gaussian signaling, the achievable data rate from BS to each MS-*i* is

$$R_i = \log(1 + SINR_i) \tag{5.5}$$

If we combine (5.4) and (5.4), then in this model, our main objective is to jointly design the optimal baseband/RF precoder and baseband /RF combiner at the same time to maximize the achievable sum rate. This optimization problem can be expressed as

$$\underset{\boldsymbol{F}_{RF,}\boldsymbol{F}_{BB},\boldsymbol{w}_{RF_i}\boldsymbol{w}_{BB_i}}{\text{maximize}} \sum_{i=1}^{K} \log\left(1 + \frac{\left|\boldsymbol{w}_i^H \boldsymbol{H}_i \boldsymbol{f}_i\right|^2}{\sum_{j\neq i}^{K}\left|\boldsymbol{w}_i^H \boldsymbol{H}_i \boldsymbol{f}_i\right|^2 + \sigma^2 \|\boldsymbol{w}_i\|^2}\right)$$

$$\text{subject to} \quad \boldsymbol{F}_{RF,} \in \mathcal{F}_{RF}$$

$$\boldsymbol{w}_{RF_i} \in \mathcal{W}_{RF}, \forall_i$$

$$\text{tr}\{\boldsymbol{F}_{RF}\boldsymbol{F}_{BB}\boldsymbol{F}_{BB}^H\boldsymbol{F}_{RF}^H\} \leq P, \tag{5.6}$$

where P stands for the total power constraint at BS. The global optimal solution for all four variables to (5.6) is a non-convex problem due to complex nature of this expression. Thus, in 5.1, a novel hybrid beamforming design thanks to the channel characteristics in the mmWave propagation environment with low complexity and high performance will be presented.

5.1. MMSE-Based Hybrid Precoding Design

In this section, the multi-user hybrid precoding design will be investigated with three different cases – fully digital, spatially sparse and a new algorithm proposed in [3]. Different with the two-stage hybrid beamforming design presented in chapter 4, the MMSE-based hybrid precoding design allows for a joint optimization design of RF precoder and baseband precoder for each MS.

In the first stage, each MS will decide its optimal RF combiner $\boldsymbol{w}_{RF}^{opt}$ to maximize the downlink channel gain:

$$\boldsymbol{w}_{RF_i}^{opt} = \underset{\boldsymbol{w}_{RF_i} \in \mathcal{W}_{RF}}{\operatorname{argmax}} \left\| \boldsymbol{w}_{RF_i}^{H} \boldsymbol{H}_i \right\|. \tag{5.7}$$

After that, we can define the effective multiple input single output (MISO) channel from BS to each ith MS as $\widehat{h}_i^H = \boldsymbol{w}_{RF_i}^H \boldsymbol{H}_i$.

In the second stage, we shall replace the effective channel $\hat{h}_i^H$ of the original channel $\boldsymbol{H}_i$ in (5.6) to get the optimization problem.

$$\underset{\boldsymbol{F}_{RF}, \boldsymbol{f}_{RF_1}, \cdots, \boldsymbol{f}_{RF_K}}{\text{maximize}} \sum_{i=1}^{K} \log\left(1 + \frac{\left|\hat{h}_i^H \boldsymbol{F}_{RF} \boldsymbol{f}_{BB_i}\right|^2}{\sum_{j \neq i}^{K} \left|\hat{h}_i^H \boldsymbol{F}_{RF} \boldsymbol{f}_{BB_i}\right|^2 + \sigma^2}\right)$$

$$\text{subject to} \quad \boldsymbol{F}_{RF,} \in \mathcal{F}_{RF}$$

$$\text{tr}\{\boldsymbol{F}_{RF} \boldsymbol{F}_{BB} \boldsymbol{F}_{BB}^H \boldsymbol{F}_{RF}^H\} \leq P, \tag{5.8}$$

Since the RF combiner $\boldsymbol{w}_{RF}$ has been determined and baseband combiner $\boldsymbol{w}_i$ has no effect on the SINR (it only decodes the symbol), hence it can be removed from the original optimization formula in (5.6). However, the above problem is still non-convex and requires further relaxations to convert to a convex-optimization problem. Thus, three designs based on MMSE are presented in the following the address that.

5.1.1. A Fully Digital MMSE Multiuser Precoding Design

The initial motivation of using MMSE is to make the processed received signal $\tilde{\boldsymbol{y}}$ sufficiently close to the original signal $\boldsymbol{s}$. If we denote the *unnormalized* precoder at BS as $\boldsymbol{V} = [\boldsymbol{v}_1, \ldots, \boldsymbol{v}_K]$ such that $\boldsymbol{F} = \sqrt{1/\gamma}\boldsymbol{V}$, where γ is a power scaling factor. Then the power constraint condition $\text{tr}\{\boldsymbol{F}\boldsymbol{F}^{\boldsymbol{H}}\} \leq \boldsymbol{P}$ at the BS can be satisfied. Also, the power scaling factor γ needs to be multiplied at the MS side, which means $\boldsymbol{w}_{BB_i} = \sqrt{\gamma}$. Therefore, by substituting the above redefined vectors into (5.3), the reformulated received signal after combing is

$$\tilde{\boldsymbol{y}}_i = \boldsymbol{w}_i^H \boldsymbol{H}_i \boldsymbol{f}_i \boldsymbol{s}_i + \boldsymbol{w}_i^H \boldsymbol{H}_i \sum_{j \neq i}^{\boldsymbol{K}} \boldsymbol{f}_j \boldsymbol{s}_j + \boldsymbol{w}_i^{\boldsymbol{H}} \boldsymbol{n}_i \tag{5.9}$$

$$= \boldsymbol{w}_{BB_i}^H \boldsymbol{w}_{RF_i}^H \boldsymbol{H}_i \sqrt{1/\gamma}\boldsymbol{v}_i \boldsymbol{s}_i + \boldsymbol{w}_{BB_i}^H \boldsymbol{w}_{RF_i}^H \boldsymbol{H}_i \sum_{j \neq i}^{\boldsymbol{K}} \sqrt{1/\gamma}\boldsymbol{v}_j \boldsymbol{s}_j + \boldsymbol{w}_{BB_i}^H \boldsymbol{w}_{RF_i}^H \boldsymbol{n}_i$$

$$= \sqrt{\gamma}\hat{h}_i^H \sqrt{1/\gamma}\boldsymbol{v}_i \boldsymbol{s}_i + \sqrt{\gamma}\hat{h}_i^H \sum_{j \neq i}^{\boldsymbol{K}} \sqrt{1/\gamma}\boldsymbol{v}_j \boldsymbol{s}_j + \sqrt{\gamma}\boldsymbol{w}_{RF_i}^H \boldsymbol{n}_i$$

$$= \hat{h}_i^H \boldsymbol{v}_i \boldsymbol{s}_i + \hat{h}_i^H \sum_{j \neq i}^{\boldsymbol{K}} \boldsymbol{v}_j \boldsymbol{s}_j + \sqrt{\gamma}\boldsymbol{w}_{RF_i}^H \boldsymbol{n}_i$$

Given the sum rate for K data stream, if we substitute the result of $\widetilde{\boldsymbol{y}}_i$ obtained in (5.9) and the original signal $\boldsymbol{s}$ into the objective function for minimization, the MMSE precoder will then be determined from the following optimization problem:

$$\underset{\boldsymbol{V},\gamma}{\text{minimize}}\ \mathbb{E}[|\boldsymbol{s} - \widetilde{\boldsymbol{y}}|^2] \tag{5.10}$$

$$\text{subject to} \quad \text{tr}\{\boldsymbol{V}\boldsymbol{V}^{\boldsymbol{H}}\} \leq \gamma P$$

Expand (5.10) by using (5.3) and (5.9), we shall obtain the final minimization problem, where

$$\underset{\boldsymbol{V},\gamma}{\text{minimize}} \quad \text{tr}\left\{\left(\boldsymbol{I} - \widehat{\mathbf{H}}\mathbf{V}\right)\left(\boldsymbol{I} - \widehat{\mathbf{H}}\mathbf{V}\right)^H\right\} + K\gamma\sigma^2 \tag{5.11}$$

$$\text{subject to} \quad \text{tr}\{\boldsymbol{V}\boldsymbol{V}^{\boldsymbol{H}}\} \leq \gamma P$$

If $\boldsymbol{V}$ and γ satisfy the Karush-Kuhn-Tucker (KKT) [28] condition, then (5.11) is a convex problem and has a close-form solution.

Therefore, to solve it, the Lagrange function of the objective is

$$\mathcal{L} = \text{tr}\left\{\left(\boldsymbol{I} - \widehat{\mathbf{H}}\mathbf{V}\right)\left(\boldsymbol{I} - \widehat{\mathbf{H}}\mathbf{V}\right)^H\right\} + K\gamma\sigma^2 + \lambda(\text{tr}(\boldsymbol{V}\boldsymbol{V}^{\boldsymbol{H}}) - \gamma P) \tag{5.12}$$

Also, the KKT condition of $\mathcal{L}$ are

$$\begin{cases} \dfrac{\partial \mathcal{L}}{\partial \boldsymbol{V}} = 0 & (i) \\ \dfrac{\partial \mathcal{L}}{\partial \gamma} = 0 & (ii) \\ \lambda \geq 0 & (iii) \\ \lambda(\text{tr}(\boldsymbol{V}\boldsymbol{V}^{\boldsymbol{H}}) - \gamma P) = 0 & (iv) \end{cases} \tag{5.13}$$

For (*i*) in (5.13), we have

$$\frac{\partial \mathcal{L}}{\partial \boldsymbol{V}} = \frac{\partial(\mathrm{tr}\left\{\left(\boldsymbol{I} - \widehat{\mathbf{H}}\mathbf{V}\right)\left(\boldsymbol{I} - \widehat{\mathbf{H}}\mathbf{V}\right)^{H}\right\} + \lambda \mathrm{tr}(\boldsymbol{V}\boldsymbol{V}^{\boldsymbol{H}}))}{\partial \boldsymbol{V}}$$
$$= \frac{\partial(\mathrm{tr}\left\{\left(\boldsymbol{I} - \widehat{\mathbf{H}}\mathbf{V}\right)\left(\boldsymbol{I} - \mathbf{V}^{\mathrm{H}}\widehat{\mathbf{H}}^{H}\right)\right\} + \lambda \mathrm{tr}(\boldsymbol{V}\boldsymbol{V}^{\boldsymbol{H}}))}{\partial \boldsymbol{V}}$$
$$= \frac{\partial(\mathrm{tr}\left\{\boldsymbol{I} - \widehat{\mathbf{H}}\mathbf{V} - \mathbf{V}^{\mathrm{H}}\widehat{\mathbf{H}}^{H} + \widehat{\mathbf{H}}\mathbf{V}\mathbf{V}^{\mathrm{H}}\widehat{\mathbf{H}}^{H}\right\} + \lambda \mathrm{tr}(\boldsymbol{V}\boldsymbol{V}^{\boldsymbol{H}}))}{\partial \boldsymbol{V}}$$
$$= \frac{\partial(\mathrm{tr}(-\widehat{\mathbf{H}}\mathbf{V}))}{\partial \boldsymbol{V}} + \frac{\partial(\mathrm{tr}(-\mathbf{V}^{\mathrm{H}}\widehat{\mathbf{H}}^{H}))}{\partial \boldsymbol{V}} + \frac{\partial(\mathrm{tr}(\widehat{\mathbf{H}}\mathbf{V}\mathbf{V}^{\mathrm{H}}\widehat{\mathbf{H}}^{H}))}{\partial \boldsymbol{V}} + \frac{\partial(\lambda \mathrm{tr}(\boldsymbol{V}\boldsymbol{V}^{\boldsymbol{H}}))}{\partial \boldsymbol{V}}$$
$$= -\widehat{\mathbf{H}}^{H} - \widehat{\mathbf{H}}^{H} + 2\widehat{\mathbf{H}}^{H}\widehat{\mathbf{H}}\boldsymbol{V} + 2\lambda \boldsymbol{V}$$

For (ii) in (5.13), we have

$$\frac{\partial \mathcal{L}}{\partial \gamma} = \frac{\partial(K\gamma\sigma^2 - \lambda\gamma P)}{\partial \gamma} = K\sigma^2 - \lambda P$$

Thus, for the 4 conditions required in (5.13), we have the final four expressions for the requirement conditions, stated as

$$\begin{cases} \dfrac{\partial \mathcal{L}}{\partial \boldsymbol{V}} = -\widehat{\mathbf{H}}^{H} - \widehat{\mathbf{H}}^{H} + 2\widehat{\mathbf{H}}^{H}\widehat{\mathbf{H}}\boldsymbol{V} + 2\lambda \boldsymbol{V} & (v) \\ \dfrac{\partial \mathcal{L}}{\partial \gamma} = K\sigma^2 - \lambda P & (vi) \\ \lambda \geq 0 & (vii) \\ \lambda(\mathrm{tr}(\boldsymbol{V}\boldsymbol{V}^{\boldsymbol{H}}) - \gamma P) = 0 & (viii) \end{cases} \tag{5.14}$$

where (v) in (5.14) gives

$$2\boldsymbol{H}^{H} = 2\left(\widehat{\mathbf{H}}^{H}\widehat{\mathbf{H}} + \lambda \boldsymbol{I}\right)\boldsymbol{V}$$
$$\boldsymbol{V}^{opt} = \left(\widehat{\mathbf{H}}^{H}\widehat{\mathbf{H}} + \lambda \boldsymbol{I}\right)^{-\mathbf{1}}\widehat{\mathbf{H}}^{H},$$

and (vi) in (5.14) gives

$$\lambda = \frac{K\sigma^2}{P}$$

Since $K, P > 0$, and $\sigma \neq 0$, we have λ that satisfies (vii) in (5.14).

From $(viii)$ in (5.14), we get

$$\gamma^{opt} = \frac{\mathrm{tr}(\boldsymbol{V}\boldsymbol{V}^{\boldsymbol{H}})}{P} = \frac{\|\boldsymbol{V}\|_F^2}{P}$$

Therefore, the final close-form expression for optimization problem (5.11) is

$$\boldsymbol{V}^{opt} = \left(\widehat{\mathbf{H}}^H\widehat{\mathbf{H}} + \frac{K\sigma^2}{P}\boldsymbol{I}\right)^{-\mathbf{1}}\widehat{\mathbf{H}}^H, \tag{5.15}$$

where $\widehat{\mathbf{H}}^H = \left[\widehat{\boldsymbol{h}}_1, \dots, \widehat{\boldsymbol{h}}_K\right]^H$, with the optimal scaling factor $\gamma^{opt} = \frac{\|\boldsymbol{V}\|_F^2}{P}$. The normalized precoder based on MMSE is then given by $\boldsymbol{F}_{MMSE} = \sqrt{1/\gamma^{opt}}\boldsymbol{V}^{opt}$.

Although the fully digital precoder $\boldsymbol{F}_{MMSE}$ may not be decomposed into $\boldsymbol{F}_{RF}\boldsymbol{F}_{BB}$, it will be a benchmark to evaluate the performance two other practical MMSE-based precoding designs.

5.1.2. Spatially Sparse MMSE Precoding Design

Given the fully digital precoder $\boldsymbol{F}_{MMSE}$ and a pre-defined RF steering vectors from the RF codebooks, we can apply Algorithm 1 depicted in chapter 3 to reconstruct a near-optimal precoder such that $\boldsymbol{F}_{MMSE} \approx \boldsymbol{F}_{RF}\boldsymbol{F}_{BB}$ with $\boldsymbol{F}_{RF} \in \mathcal{F}_{RF}$. The main drawback of this design is that it is necessary to determine the fully digital precoder $\boldsymbol{F}_{MMSE}$ first for the rest of the design. Therefore, a new hybrid MMSE precoding design was proposed in [3] which can bypass this step.

5.1.3. Proposed Hybrid MMSE Precoding Design

To start with the design, we firstly define the *unnormalized* baseband precoder at BS as $\boldsymbol{V}_B = [\boldsymbol{v}_{B_1}, \dots, \boldsymbol{v}_{B_K}]$ such that $\boldsymbol{F} = \sqrt{1/\gamma}\boldsymbol{V}_B$, where γ is a power scaling factor. Then the power constraint condition $\text{tr}\{\boldsymbol{F}_{RF}^H\boldsymbol{F}_{RF}\boldsymbol{V}_B\boldsymbol{V}_B^H\} \le \boldsymbol{P}$ at the BS can be satisfied. By substituting $\boldsymbol{V} = \boldsymbol{F}_{RF}\boldsymbol{V}_B$ into (5.9) and expanding the sum-MSE in (5.10), we can obtain a similar optimization problem like (5.11) but to replace $\boldsymbol{V}$ by $\boldsymbol{F}_{RF}\boldsymbol{V}_B$.

$$\underset{\boldsymbol{F}_{RF},\boldsymbol{V}_B,\gamma}{\text{minimize}} \quad \text{tr}\left\{\left(\boldsymbol{I} - \widehat{\mathbf{H}}\,\boldsymbol{F}_{RF}\boldsymbol{V}_B\right)\left(\boldsymbol{I} - \widehat{\mathbf{H}}\,\boldsymbol{F}_{RF}\boldsymbol{V}_B\right)^H\right\} + K\gamma\sigma^2 \tag{5.16}$$

$$\text{subject to} \quad \boldsymbol{F}_{RF} \in \mathcal{F}_{RF} \text{ and } \text{tr}\{\boldsymbol{F}_{RF}^H\boldsymbol{F}_{RF}\boldsymbol{V}_B\boldsymbol{V}_B^H\} \le \gamma P$$

Since the cost function contains a multiplication of $\boldsymbol{F}_{RF}$ and $\boldsymbol{V}_B$, thus it is non-convex and very difficult to solve. However, if the RF precoder $\boldsymbol{F}_{RF}$ is pre-determined form a RF codebook, we can remove the effect of $\boldsymbol{F}_{RF}$ in (5.16) and simplify it to become

$$\underset{\boldsymbol{V}_B,\gamma}{\text{minimize}} \quad \text{tr}\left\{\left(\boldsymbol{I} - \widehat{\mathbf{H}}\,\boldsymbol{F}_{RF}\boldsymbol{V}_B\right)\left(\boldsymbol{I} - \widehat{\mathbf{H}}\,\boldsymbol{F}_{RF}\boldsymbol{V}_B\right)^H\right\} + K\gamma\sigma^2 \tag{5.17}$$

$$\text{subject to} \quad \text{tr}\{\boldsymbol{F}_{RF}^H\boldsymbol{F}_{RF}\boldsymbol{V}_B\boldsymbol{V}_B^H\} \le \gamma P$$

If $\boldsymbol{V}_B$ and γ satisfy the Karush-Kuhn-Tucker (KKT) [28] condition, then (5.17) is a convex problem and has a close-form solution.

Therefore, to solve it, the Lagrange function of the objective is

$$\mathcal{L} = \mathrm{tr}\left\{\left(\boldsymbol{I} - \widehat{\mathbf{H}}\,\boldsymbol{F}_{RF}\boldsymbol{V}_B\right)\left(\boldsymbol{I} - \widehat{\mathbf{H}}\,\boldsymbol{F}_{RF}\boldsymbol{V}_B\right)^H\right\} + K\gamma\sigma^2 + \lambda(\mathrm{tr}(\boldsymbol{F}_{RF}^H\boldsymbol{F}_{RF}\boldsymbol{V}_B\boldsymbol{V}_B^H) - \gamma P) \qquad (5.18)$$

Also, the KKT condition of $\mathcal{L}$ are

$$\begin{cases} \dfrac{\partial \mathcal{L}}{\partial \boldsymbol{V}_B} = 0 & (i) \\ \dfrac{\partial \mathcal{L}}{\partial \gamma} = 0 & (ii) \\ \lambda \geq 0 & (iii) \\ \lambda(\mathrm{tr}(\boldsymbol{F}_{RF}^H\boldsymbol{F}_{RF}\boldsymbol{V}_B\boldsymbol{V}_B^H) - \gamma P) = 0 & (iv) \end{cases} \qquad (5.19)$$

For (*i*) in (5.19), we have

$$\begin{aligned} \frac{\partial \mathcal{L}}{\partial \boldsymbol{V}} &= \frac{\partial\left(\mathrm{tr}\left\{\left(\boldsymbol{I} - \widehat{\mathbf{H}}\,\boldsymbol{F}_{RF}\boldsymbol{V}_B\right)\left(\boldsymbol{I} - \widehat{\mathbf{H}}\,\boldsymbol{F}_{RF}\boldsymbol{V}_B\right)^H\right\} + \lambda(\mathrm{tr}(\boldsymbol{F}_{RF}^H\boldsymbol{F}_{RF}\boldsymbol{V}_B\boldsymbol{V}_B^H) - \gamma P)\right)}{\partial \boldsymbol{V}} \\ &= \frac{\partial(\mathrm{tr}\{\left(\boldsymbol{I} - \widehat{\mathbf{H}}\mathbf{V}\right)\left(\boldsymbol{I} - \mathbf{V}_\mathrm{B}^\mathrm{H}\,\boldsymbol{F}_{RF}^H\widehat{\mathbf{H}}^H\right)\} + \lambda(\mathrm{tr}(\boldsymbol{F}_{RF}^H\boldsymbol{F}_{RF}\boldsymbol{V}_B\boldsymbol{V}_B^H) - \gamma P))}{\partial \boldsymbol{V}} \\ &= \frac{\partial(\mathrm{tr}\{\boldsymbol{I} - \widehat{\mathbf{H}}\,\boldsymbol{F}_{RF}\mathbf{V} - \mathbf{V}_\mathrm{B}^\mathrm{H}\,\boldsymbol{F}_{RF}^H\widehat{\mathbf{H}}^H + \widehat{\mathbf{H}}\,\boldsymbol{F}_{RF}\mathbf{V}_\mathrm{B}\mathbf{V}_\mathrm{B}^\mathrm{H}\,\boldsymbol{F}_{RF}^H\widehat{\mathbf{H}}^H\} + \lambda\mathrm{tr}(\boldsymbol{F}_{RF}^H\boldsymbol{F}_{RF}\boldsymbol{V}_B\boldsymbol{V}_B^H))}{\partial \boldsymbol{V}} \\ &= \frac{\partial(\mathrm{tr}(-\widehat{\mathbf{H}}\,\boldsymbol{F}_{RF}\mathbf{V}))}{\partial \boldsymbol{V}} + \frac{\partial(\mathrm{tr}(-\mathbf{V}_\mathrm{B}^\mathrm{H}\,\boldsymbol{F}_{RF}^H\widehat{\mathbf{H}}^H))}{\partial \boldsymbol{V}} + \frac{\partial(\mathrm{tr}(\widehat{\mathbf{H}}\,\boldsymbol{F}_{RF}\mathbf{V}_\mathrm{B}\mathbf{V}_\mathrm{B}^\mathrm{H}\,\boldsymbol{F}_{RF}^H\widehat{\mathbf{H}}^H))}{\partial \boldsymbol{V}} \\ &\qquad + \frac{\partial(\lambda\mathrm{tr}(\boldsymbol{F}_{RF}^H\boldsymbol{F}_{RF}\boldsymbol{V}_B\boldsymbol{V}_B^H))}{\partial \boldsymbol{V}} \\ &= -(\widehat{\mathbf{H}}\,\boldsymbol{F}_{RF})^H - (\widehat{\mathbf{H}}\,\boldsymbol{F}_{RF})^H + 2\,\boldsymbol{F}_{RF}^H\widehat{\mathbf{H}}^H\widehat{\mathbf{H}}\,\boldsymbol{F}_{RF}\boldsymbol{V}_B + 2\lambda\,\boldsymbol{F}_{RF}^H\boldsymbol{F}_{RF}\boldsymbol{V} \end{aligned}$$

For (*ii*) in (5.19), we have

$$\frac{\partial \mathcal{L}}{\partial \gamma} = \frac{\partial(K\gamma\sigma^2 - \lambda\gamma P)}{\partial \gamma} = K\sigma^2 - \lambda P$$

Thus, for the 4 conditions required in (5.19), we have the final four expressions for the requirement conditions, stated as

$$\begin{cases} \dfrac{\partial \mathcal{L}}{\partial \boldsymbol{V}} = -(\widehat{\mathbf{H}}\,\boldsymbol{F}_{RF})^H - (\widehat{\mathbf{H}}\,\boldsymbol{F}_{RF})^H + 2\,\boldsymbol{F}_{RF}^H\widehat{\mathbf{H}}^H\widehat{\mathbf{H}}\,\boldsymbol{F}_{RF}\boldsymbol{V}_B + 2\lambda\,\boldsymbol{F}_{RF}^H\boldsymbol{F}_{RF}\boldsymbol{V} & (v) \\ \dfrac{\partial \mathcal{L}}{\partial \gamma} = K\sigma^2 - \lambda P & (vi) \\ \lambda \geq 0 & (vii) \\ \lambda(\mathrm{tr}(\,\boldsymbol{F}_{RF}^H\boldsymbol{F}_{RF}\boldsymbol{V}_B\boldsymbol{V}_B^H) - \gamma P) = 0 & (viii) \end{cases} \tag{5.20}$$

where (v) in (5.20) gives

$$\begin{aligned} 2(\widehat{\mathbf{H}}\,\boldsymbol{F}_{RF})^H &= 2(\,\boldsymbol{F}_{RF}^H\widehat{\mathbf{H}}^H\widehat{\mathbf{H}}\,\boldsymbol{F}_{RF}\boldsymbol{V}_B + \lambda\,\boldsymbol{F}_{RF}^H\boldsymbol{F}_{RF}\boldsymbol{V}_B) \\ (\widehat{\mathbf{H}}\,\boldsymbol{F}_{RF})^H &= \boldsymbol{V}_B(\,\boldsymbol{F}_{RF}^H\widehat{\mathbf{H}}^H\widehat{\mathbf{H}}\,\boldsymbol{F}_{RF} + \lambda\boldsymbol{F}_{RF}^H\boldsymbol{F}_{RF}) \\ \boldsymbol{V}_B^{opt} &= \left(\,\boldsymbol{F}_{RF}^H\widehat{\mathbf{H}}^H\widehat{\mathbf{H}}\,\boldsymbol{F}_{RF} + \lambda\,\boldsymbol{F}_{RF}^H\boldsymbol{F}_{RF}\right)^{-\mathbf{1}}\boldsymbol{F}_{RF}^H\widehat{\mathbf{H}}^H, \end{aligned}$$

and (vi) in (5.20) gives

$$\lambda = \frac{K\sigma^2}{P}$$

Since $K, P > 0$, and $\sigma \neq 0$, we have λ that satisfies (vii) in (5.20).

From $(viii)$ in (5.20), we get

$$\gamma^{opt} = \frac{\mathrm{tr}(\,\boldsymbol{F}_{RF}^H\boldsymbol{F}_{RF}\boldsymbol{V}_B\boldsymbol{V}_B^H)}{P} = \frac{\|\boldsymbol{F}_{RF}\boldsymbol{V}_B\|_F^2}{P}$$

Therefore, the final close-form expression for optimization problem (5.17) is

$$\boldsymbol{V}_B^{opt} = \left(\,\boldsymbol{F}_{RF}^H\widehat{\mathbf{H}}^H\widehat{\mathbf{H}}\,\boldsymbol{F}_{RF} + \frac{K\sigma^2}{P}\boldsymbol{F}_{RF}^H\boldsymbol{F}_{RF}\right)^{-\mathbf{1}}\boldsymbol{F}_{RF}^H\widehat{\mathbf{H}}^H, \tag{5.21}$$

where $\widehat{\mathbf{H}}^H = \left[\widehat{\boldsymbol{h}}_1, \ldots, \widehat{\boldsymbol{h}}_K\right]^H$, with the optimal scaling factor $\gamma^{opt} = \frac{\|\boldsymbol{F}_{RF}\boldsymbol{V}_B\|_F^2}{P}$. The optimal baseband precoder is finally determined as by $\boldsymbol{F}_{BB}^{opt} = \sqrt{1/\gamma^{opt}}\boldsymbol{V}_B^{opt}$.

For the RF precoder $\boldsymbol{F}_{RF}$, similar assumption is adopted here as previously mentioned in chapter 3. Specifically, each column of $\boldsymbol{F}_{RF}$ is restricted in the basis vectors from the array response vector $\mathbf{A} = [\mathbf{a}_1, \ldots, \mathbf{a}_\mathrm{L}]$. Therefore, an extra sparsity constraint $\|\mathrm{diag}\{\boldsymbol{V}_B\boldsymbol{V}_B^H\}\|_0 = N_t^{RF}$ to restrict the number of selected basis should be added on (5.17). In other words, only N_t^{RF} basis from $\mathbf{A}$ will be selected to reconstruct the optimal precoder. The detailed practical meanings of this constraint are explained in 3.3. Accordingly, the complete algorithm which directly reflections this procedure is stated as follows.

Algorithm 4 Proposed [3] Hybrid MMSE Precoding via Orthogonal Matching Pursuit

Input: $\widehat{\mathbf{H}}$, **A**

Output: $\boldsymbol{F}_{RF}, \boldsymbol{F}_{BB}$

1. $\boldsymbol{F}_{RF} = Empty\ Matrix$
2. $\boldsymbol{V}_{res} = \boldsymbol{I}$
3. **For** $i \leq N_t^{RF}$ **do**
4. $\boldsymbol{\psi} = \boldsymbol{A}^H \widehat{\mathbf{H}} \boldsymbol{V}_{res}$
5. $k = argmax_{l=1,\ldots,N_{cl}N_{ray}} (\boldsymbol{\psi}\boldsymbol{\psi}^{\boldsymbol{H}})_{l,l}$
6. $\boldsymbol{F}_{RF} = [\, \boldsymbol{F}_{RF} | \boldsymbol{A}^{(k)}]$
7. $\boldsymbol{V}_B = \left(\boldsymbol{F}_{RF}^H \widehat{\mathbf{H}}^H \widehat{\mathbf{H}}\, \boldsymbol{F}_{RF} + \frac{K\sigma^2}{P} \boldsymbol{F}_{RF}^H \boldsymbol{F}_{RF} \right)^{-1} \boldsymbol{F}_{RF}^H \widehat{\mathbf{H}}^H$
8. $\boldsymbol{V}_{res} = \frac{\boldsymbol{I} - \widehat{\mathbf{H}} \boldsymbol{F}_{RF} \boldsymbol{V}_{BB}}{\left\| \boldsymbol{I} - \widehat{\mathbf{H}} \boldsymbol{F}_{RF} \boldsymbol{V}_{BB} \right\|_F}$
9. **End for**
10. $\gamma = \frac{\mathrm{tr}\left(\boldsymbol{F}_{RF}^H \boldsymbol{F}_{RF} \boldsymbol{V}_B \boldsymbol{V}_B^H \right)}{P}$
11. $\boldsymbol{F}_{BB} = \sqrt{N_s} \frac{\boldsymbol{F}_{BB}}{\| \boldsymbol{F}_{RF} \boldsymbol{F}_{BB} \|_F}$
12. **Return** $\boldsymbol{F}_{RF}, \boldsymbol{F}_{BB}$

It is noted that in this algorithm, different from **Algorithm 1**, the optimal precoder $\boldsymbol{F}_{opt}$ is not required. Another main difference between this algorithm and **Algorithm 1** is that this proposed algorithm uses a MSE minimization solution for the *unnormalized* baseband precoder $\boldsymbol{V}_B$ in step 7 while **Algorithm 1** applies a least square solution for the baseband precoder $\boldsymbol{F}_{BB}$.

For quantization for RF precoder and combiner use the same approach depicted in 3.3.

5.2. Simulation Results and Performance Analysis

In this section, the simulation results for the three MMSE-based hybrid precoding designs discussed in 5.1 will be shown. The system parameters are setup as follows.

A massive MIMO system with 8×8 UPA ($N_t = 64$) for BS and 4×4 UPA ($N_r = 16$) for each MS is assumed. There are $K = 8$ MSs in the system and each MS is equipped with only one RF chain. The number of RF chain in BS is set to be equal to the number of MSs. The channel for each user contains 10 paths ($N_{cl} = 2, N_{ray} = 5$). The azimuth and elevation AOA/AODs of the rays within a cluster are assumed to be randomly Laplacian distributed with an angle spread of 5°. The means of azimuth and elevation at both BS and MS are set to be uniformly distributed in $[0,2\pi]$ and $[-\frac{\pi}{2}, \frac{\pi}{2}]$ respectively. Perfect AOA/AOD codebooks are assumed, meaning that both BS and MS possess the full channel state information. All the channel path gains $\alpha_{i,l}{}'s$ are i.i.d. Gaussian distribution with variance $\sigma_\alpha^2 = 1$. The SNR is defined as $SNR = \frac{P\sigma_\alpha^2}{K}$. The parameters above all adopted for all scenarios unless stated otherwise. All plots are the averaged outcome for 500 times simulation trials.

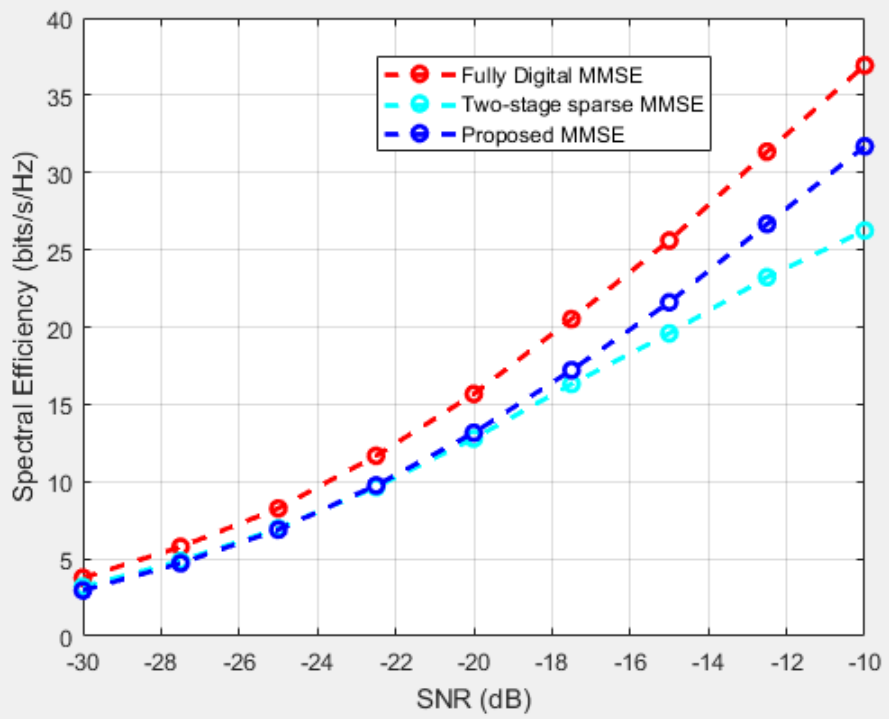

Figure 24: System sum-rate vs. SNR for three MMSE-based hybrid beamforming design for a 64×16 massive MIMO system with square planar arrays at transmitter and receiver.

Figure 24 shows the performances of three MMSE-based hybrid beamforming design. As observed from the figure, the proposed MMSE beamforming design by Nguyen [3] described in **Algorithm 4** outperforms two-stage sparse MMSE beamforming design obtained from **Algorithm 1** and **Algorithm 2**, especially at large SNR. This is because the hybrid precoder derived from **Algorithm 1** is not necessarily a good choice for multi-user system although it achieves a near-optimal performance in single user scenario. Also, the MMSE solution is usually superior to the least square solution for obtaining the baseband precoder.

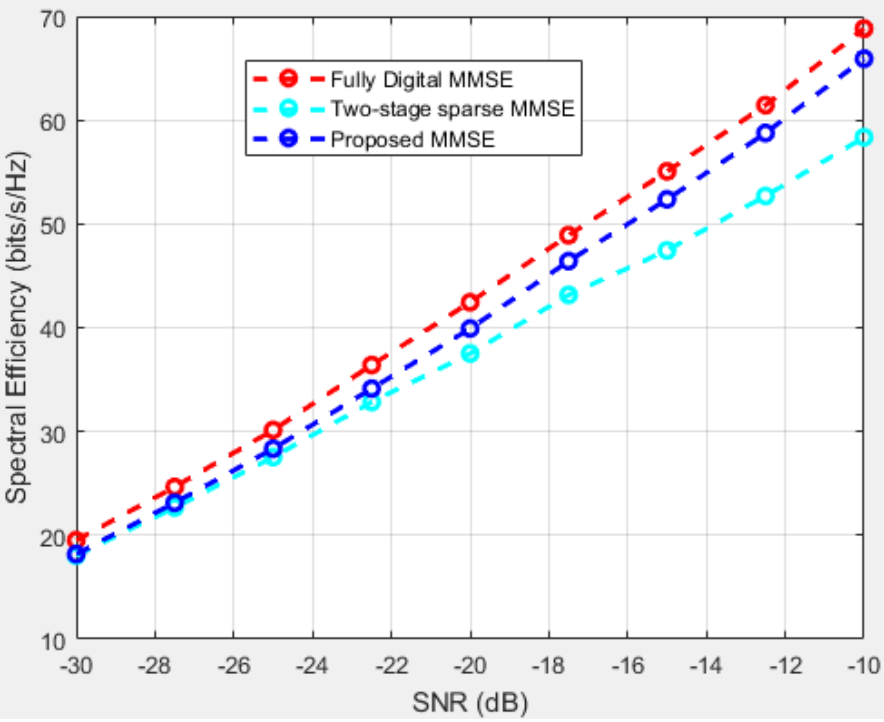

Figure 25: System sum-rate vs. SNR for three MMSE-based hybrid beamforming design for a 256×64 *massive MIMO system with square planar arrays at transmitter and receiver.*

Figure 25 uses the same setup with Figure 24 but replace the antenna arrays with a much larger configuration. In this case, 256 antennas are employed at BS and 64 antennas are employed at each MS. Similar with the findings in Figure 24, the proposed MMSE beamformer still outperforms two-stage sparse MMSE beamformer around by approximately 2.5 dB. However, the rate difference between fully digital MMSE and proposed MMSE shrinks. This is because for a larger massive MIMO system, the asymptotic orthogonality principle is more effective such that the multi-user interference at mmWave system can be improved. Therefore, the performance obtained by hybrid beamforming is closer to the optimal unconstrained beamformer.

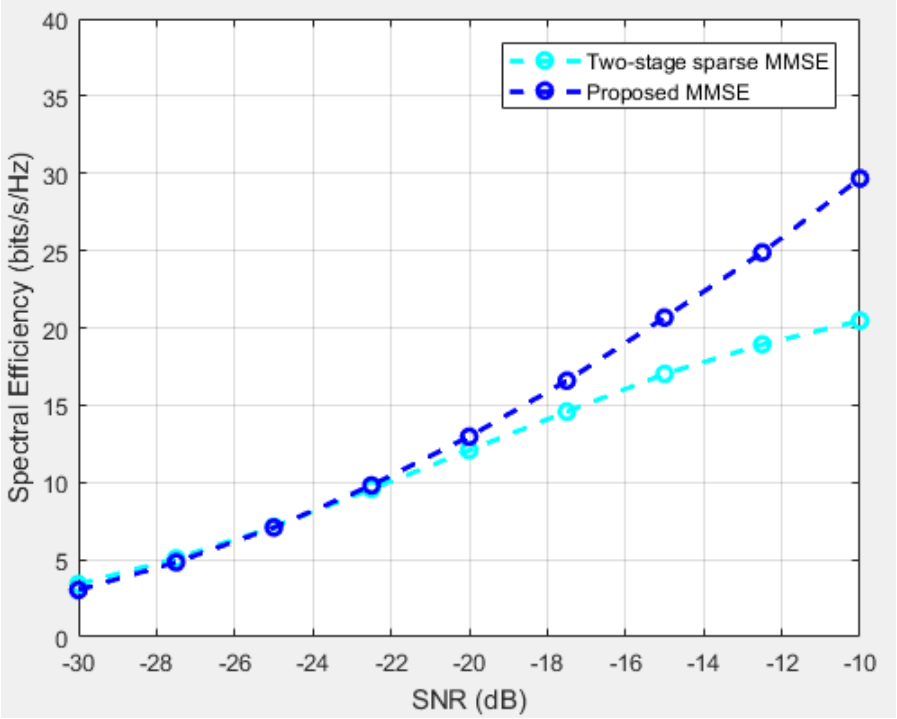

Figure 26: System sum-rate vs. SNR for three MMSE-based hybrid beamforming design for a 64 × 16 massive MIMO system with square planar arrays at transmitter and receiver. The number of quantization bits per azimuth/elevation angle is 5.

Figure 26 uses the same setup with Figure 24 while applying a quantized bits for all azimuth and elevation angle. Compared with the result shown in Figure 24, the performance for proposed and two-stage sparse MMSE beamforming design both degrades but with different magnitudes. For example, when $SNR = -10$, the degradation of proposed MMSE is only around 2 bits/s/Hz. However, for two-stage hybrid MMSE design, the degradation becomes around 5.5 bits/s/Hz, which is much higher. This is because in two-stage sparse beamforming, a quantization for the baseband precoder is required while for the proposed MMSE beamforming design as stated in **Algorithm 4**, quantizing the baseband precoder is not needed. Thus, since the author only applies quantization for RF precoder, the performance degradation of two-stage sparse beamforming comes from both RF precoder quantization and the lack of quantization process for baseband precoder. However, by comparing Figure 24 and Figure 26, even if we quantize all azimuth and elevation angles by 5 bits, the rate loss of proposed MMSE is negligible such that this hybrid beamforming design can be utilized in practice mmWave Massive MIMO systems.

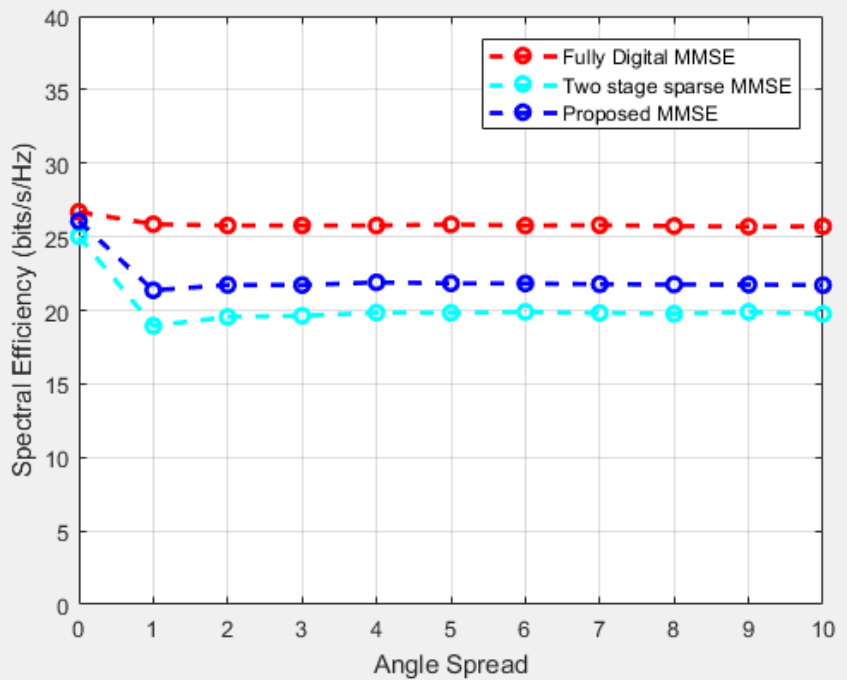

Figure 27: System sum-rate vs. angle spread for three MMSE-based hybrid beamforming design for a 64×16 *massive MIMO system with square planar arrays at transmitter and receiver.*

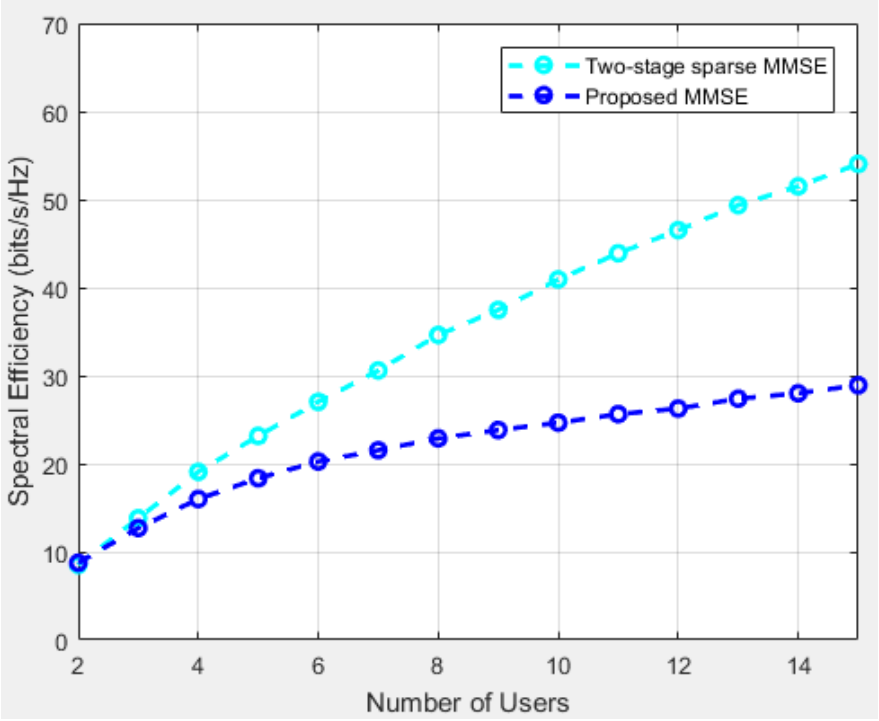

Figure 28: System sum-rate vs. Number of users for three MMSE-based hybrid beamforming design for a 64×16 *massive MIMO system with square planar arrays at transmitter and receiver.*

Figure 27 investigates the impact of angle spread on the system sum-rate by changing it from 0 to 10 degrees. When the angle spread increases, the levels of scattering become richer, leading to the decrease of system performance. However, the sum-rate remains almost unchanged once the angle spread reaches to 1. A clear performance advantage of proposed hybrid MMSE beamforming design over the two-stage sparse MMSE design can be observed at all levels of scattering. This figure basically coincides with the plot of the outcome in [17].

In Figure 28, the sum-rate performances of two different MMSE beamforming designs are compared regarding to the number of users K. Also, the number of RF chains at BS are equal to the number of users. The SNR is set at -20 dB. As observed from the figure, the sum-rate increases almost linearly with the increase of number of users for propose MMSE hybrid beamforming. However, the growth rate of two-stage sparse MMSE is much slower compared with the proposed MMSE.

5.3. Summary

In this chapter, three MMSE based hybrid beamforming designs are investigated and simulated. Different from the algorithms described in chapter 3 and 4, the proposed hybrid beamforming algorithm by Nguyen [3] mainly aims to minimize the sum Mean Square Error (MSE) in receiving the data streams at the users. It has shown its performance advantage for multi-user mmWave massive MIMO system over the extended two-stage single user spatially sparse beamforming design. A future work which involves jointly design the hybrid precoding and combining across both BS and MSs is expected.

Chapter 6

6. Conclusions and Future Works

In conclusion, this thesis reviewed and presented some solutions to the challenges in designing narrowband hybrid beamforming algorithms for mmWave-enabled massive MIMO systems. In the following a brief summary in terms of every chapter will be shown. After that, some future research directions will be introduced.

6.1. Summary of the Thesis

Chapter 1 gives a brief introduction to this project and poses the motivation and main objectives of this project. Chapter 2 presents the general background of massive MIMO, mmWave, and different types of beamforming strategies. A brief literature survey of hybrid beamforming design is also summarized. Chapter 3 illustrates a state-of-art hybrid beamforming algorithm for single-user mmWave system with a closed form expression. The spatially sparse beamforming design demonstrated in this chapter shows a near-optimal performance. Chapter 4 investigates a multi-user hybrid beamforming strategy with limited feedback called two-stage multi-user hybrid beamforming design. It has low-complexity and good achievable rates. The performance advantage over analog-only beamforming at large dimensional regime and single path scenarios are demonstrated. Chapter 5 illustrates three MMSE-based hybrid beamforming designs for multi-user system. The result shows that the proposed MMSE design by Nguyen [3] achieves higher rate than two-stage sparse MMSE design especially at high signal to noise ratios. The performance of proposed MMSE is close to the fully digital MMSE design.

The influence of different system parameters are also investigated through all system models in chapter 3, 4, and 5.

6.2. Future Works

The future works based on the current project achievement is proposed as follows.

(1) **Channel estimation of mmWave:** The performance of a massive MIMO system is quite dependent on the knowledge of channel state information (CSI). In this thesis, all the work is conducted with a perfect channel knowledge assumption at both transmitter and receiver side. When the channel information is not provide, an algorithm to estimate the mmWave channel parameters is required. Thus, how to estimate the channel is one of the most important works in future research for this project.

(2) **Quantization of baseband precoder:** In chapter 3, an infinite-resolution codebook for baseband precoder is assumed. However, in practice, a finite-resolution codebook is required to quantize the baseband precoder. Thus, the impact of this quantization effect needs to be investigated in future works.

(3) **RVQ of effective channels:** In chapter 4, a quantization for effective channels is required in **Algorithm 3**. However, the author omitted this step and used a higher RF quantization bits to compensate its potential degradation. Therefore, the construction of a RVQ codebook for effective channels are one of the key concerns in future works of this project.

(4) **More hybrid beamforming algorithms:** The design of the optimal hybrid beamforming scheme is a challenging task due to the non-convex constraint imposed by phase shifters. These constraints lead to the optimization search of hybrid beamforming designs to a difficult non-convex and combinatorial problem and have no closed-for solutions. However, more and more recent research focusing on finding the sub-optimal solutions are worth studying and investigating. The author is preferred to study, understand and gain insight from the latest algorithms to create innovative and effective designs for this problem.

Bibliography

[1] S. Payami, "Hybrid beamforming for massive MIMO systems," University of Surrey, 2017.

[2] R. W. Heath, N. Gonzalez-Prelcic, S. Rangan, W. Roh, and A. M. Sayeed, "An overview of signal processing techniques for millimeter wave MIMO systems," *IEEE journal of selected topics in signal processing*, vol. 10, no. 3, pp. 436-453, 2016.

[3] D. H. Nguyen, L. B. Le, and T. Le-Ngoc, "Hybrid MMSE precoding for mmWave multiuser MIMO systems," in *Communications (ICC), 2016 IEEE International Conference on*, 2016, pp. 1-6: IEEE.

[4] E. Björnson, J. Hoydis, and L. Sanguinetti, "Massive MIMO networks: Spectral, energy, and hardware efficiency," *Foundations and Trends® in Signal Processing*, vol. 11, no. 3-4, pp. 154-655, 2017.

[5] E. Björnson. (2017, Nov 17). *Massive MIMO for 5G: How Big Can it Get?* Available: http://www.commsys.isy.liu.se/~ebjornson/webinar_how_big_can_it_get.pdf

[6] P. Fan, J. Zhao, and I. Chih-Lin, "5G high mobility wireless communications: Challenges and solutions," *China Communications*, vol. 13, no. Supplement2, pp. 1-13, 2016.

[7] C. E. Shannon, "A mathematical theory of communication," *Bell system technical journal*, vol. 27, no. 3, pp. 379-423, 1948.

[8] T. L. Marzetta, "Noncooperative cellular wireless with unlimited numbers of base station antennas," *IEEE Transactions on Wireless Communications*, vol. 9, no. 11, pp. 3590-3600, 2010.

[9] J. Vieira *et al.*, "A flexible 100-antenna testbed for massive MIMO," in *Globecom Workshops (GC Wkshps), 2014*, 2014, pp. 287-293: IEEE.

[10] T. Kashima *et al.*, "Large scale massive MIMO field trial for 5G mobile communications system," in *Antennas and Propagation (ISAP), 2016 International Symposium on*, 2016, pp. 602-603: IEEE.

[11] E. G. Larsson, O. Edfors, F. Tufvesson, and T. L. Marzetta, "Massive MIMO for next generation wireless systems," *IEEE communications magazine*, vol. 52, no. 2, pp. 186-195, 2014.

[12] A. Alkhateeb, G. Leus, and R. W. Heath, "Limited feedback hybrid precoding for multi-user millimeter wave systems," *IEEE transactions on wireless communications*, vol. 14, no. 11, pp. 6481-6494, 2015.

[13] A. M. Sayeed, "Deconstructing multiantenna fading channels," *IEEE Transactions on Signal Processing*, vol. 50, no. 10, pp. 2563-2579, 2002.

[14] H. Xu, V. Kukshya, and T. S. Rappaport, "Spatial and temporal characteristics of 60-GHz indoor channels," *IEEE Journal on selected areas in communications*, vol. 20, no. 3, pp. 620-630, 2002.

[15] O. El Ayach, S. Rajagopal, S. Abu-Surra, Z. Pi, and R. W. Heath, "Spatially sparse precoding in millimeter wave MIMO systems," *IEEE transactions on wireless communications*, vol. 13, no. 3, pp. 1499-1513, 2014.

[16] I. W. Group, "IEEE Standard for Information Technology–Telecommunications and information exchange between systems–Local and metropolitan area networks–Specific requirements–Part 11: Wireless LAN Medium Access Control (MAC) and Physical Layer (PHY) specifications Amendment 6: Wireless Access in Vehicular Environments," *IEEE Std*, vol. 802, no. 11, 2010.

[17] D. H. Nguyen, L. B. Le, T. Le-Ngoc, and R. W. Heath, "Hybrid mmse precoding and combining designs for mmwave multiuser systems," *IEEE Access,* vol. 5, pp. 19167-19181, 2017.
[18] C.-B. Chae, D. Mazzarese, T. Inoue, and R. W. Heath, "Coordinated beamforming for the multiuser MIMO broadcast channel with limited feedforward," *IEEE Transactions on Signal Processing,* vol. 56, no. 12, pp. 6044-6056, 2008.
[19] C.-B. Chae, D. Mazzarese, N. Jindal, and R. W. Heath, "Coordinated beamforming with limited feedback in the MIMO broadcast channel," *IEEE Journal on Selected Areas in Communications,* vol. 26, no. 8, 2008.
[20] X. Yu, J.-C. Shen, J. Zhang, and K. B. Letaief, "Alternating Minimization Algorithms for Hybrid Precoding in Millimeter Wave MIMO Systems," *J. Sel. Topics Signal Processing,* vol. 10, no. 3, pp. 485-500, 2016.
[21] A. Alkhateeb, O. El Ayach, G. Leus, and R. W. Heath, "Channel estimation and hybrid precoding for millimeter wave cellular systems," *IEEE Journal of Selected Topics in Signal Processing,* vol. 8, no. 5, pp. 831-846, 2014.
[22] F. Zhang, *The Schur complement and its applications*. Springer Science & Business Media, 2006.
[23] J. M. Lee, *Riemannian manifolds: an introduction to curvature*. Springer Science & Business Media, 2006.
[24] D. J. Love and R. W. Heath, "Limited feedback unitary precoding for spatial multiplexing systems," *IEEE Transactions on Information theory,* vol. 51, no. 8, pp. 2967-2976, 2005.
[25] D. J. Love, R. W. Heath, and T. Strohmer, "Grassmannian beamforming for multiple-input multiple-output wireless systems," in *Communications, 2003. ICC'03. IEEE International Conference on,* 2003, vol. 4, pp. 2618-2622: IEEE.
[26] R. Gray, "Vector quantization," *IEEE Assp Magazine,* vol. 1, no. 2, pp. 4-29, 1984.
[27] A. Forenza, D. J. Love, and R. W. Heath, "Simplified spatial correlation models for clustered MIMO channels with different array configurations," *IEEE Transactions on Vehicular Technology,* vol. 56, no. 4, pp. 1924-1934, 2007.
[28] G. Gordon and R. Tibshirani, "Karush-kuhn-tucker conditions," *Optimization,* vol. 10, no. 725/36, p. 725, 2012.